PHYTOPLANKTON COMMUNITY STRUCTURE, PRODUCTIVITY AND NITROGEN METABOLISM AS A FUNCTION OF LIGHT AVAILABILITY IN THE ATLANTIC SECTOR OF THE SOUTHERN OCEAN

By

Erika Anne Kean
Zoology Department
University of Cape Town

Dissertation submitted in fulfilment of the requirement for the degree of Master of Science in the Department of Zoology, University Cape Town,
July 2012

Plagiarism declaration

I know the meaning of plagiarism and declare that all of the work in the dissertation, save for that which is properly acknowledged, is my own.

…….

Erika Anne Kean

Abstract

The use of photosynthesis vs. irradiance experiments to determine light controls on nitrogen assimilation is sparse in the Southern Ocean. More attention has been given to iron and light limitation of photosynthesis, while we know that iron and light co-limitation play a role in nitrogen metabolism, particularly in regard to ρNO_3^-, which is known to be more energetically expensive than reduced N (NH_4^+) assimilation. The use of this approach is important because we suspect that at depth ρNO_3^- becomes light-limited with respect to reduced N uptake, as usually revealed by a declining *f*-ratio with depth. However, the only real way to rigorously test this is by using a P-E approach combined with ^{15}N tracer studies on light-dependent uptake of both oxidised and reduced N species. This study covered six oceanic regions within the south Atlantic sector of the Southern Ocean during austral summer 2008/2009. Four transects from Cape Town to Antarctica, Antarctica to South Georgia Island and the return reciprocal legs surveyed the following regions, the Subtropical zone (STZ) north of the Subtropical Front (STF), the Northern Antarctic Circumpolar Current zone (N-ACC) from the STF to the Antarctic Polar Front (APF), the Antarctic zone (AAZ) from the APF to the Southern Boundary (SBdy) of the ACC, the Weddell Gyre zone south of the SBdy to 68°S, the Subantarctic Islands and Shallow Bathymetry zone (SAISB) and finally the Antarctic Continental Shelf zone (ACS), each providing a natural laboratory to test light-dependent uptake of both oxidised and reduced N species. Productivity and nitrogen metabolism experiments were performed at 11 'productivity' stations to determine the potential for carbon (C) export using the *f*-ratio. Additionally, phytoplankton chlorophyll-*a* (chl-*a*) biomass, community structure using High Performance Liquid Chromatography (HPLC) pigments and the macronutrient environment were measured to give some indication of the effectiveness of the biological carbon pump. Biomass was high in the ACS (mean 1.57 ±0.37 mg Chl-*a* m^{-3}) and SAISB (mean 1.17±0.59 mg Chl-*a* m^{-3}) regions as well as along one leg of four in the WG region (mean 1.12±0.71 mg Chl-*a* m^{-3}). All other regions exhibited low to moderate chl-*a* biomass. Areas of high biomass were associated with shallow bathymetric features and land masses or ice melt from various forms, each related to relief from Fe stress. In most regions phytoplankton in the >20 µm size class dominated, except for in oligotrophic waters in the STZ where pico plankton dominated and at one station in the N-ACC and one in the WG where nano plankton replaced micro plankton's dominant role. Low *f*-ratios were recorded for all regions (mean f = 0.18±0.1) and were characteristic of a N recycling community where new production and carbon export is reduced. However, the SAISB proved to be an exception where high productivity and large diatoms exhibited potential for significant C sequestration. P^B_{max} for C-fixation, NH_4^+ and NO_3^- uptake was variable between regions. NH_4^+ assimilation (mean 0.16±0.2 mgN mgChl$a^{-1}h^{-1}$) always exceeded NO_3^- uptake (0.02±.02 mgN mgChl$a^{-1}h^{-1}$) which supports preferential utilisation of NH_4^+ over NO_3^-, a more metabolically efficient means of production when Fe is limiting. Relatively low irradiances were required to saturate NO_3^- and NH_4^+ uptake and C fixation at all stations where E_k values (mean for all substrates 177±20.5 µEm^{-2}s^{-1}) were generally 50% or less of surface irradiance values (regional PAR mean 362 µEm^{-2}s^{-1}) indicating communities were well adapted to low light conditions. Even still light was not a limiting factor and presumably Fe, microzooplankton grazing, and or deep vertical mixing restrained productivity and biomass at 4 out of 6 regions in this study.

Acknowledgements

This research was made possible through funding from the Southern Ocean Carbon and Climate Observatory Programme at the Council for Scientific and Industrial Research (CSIR). I wish to acknowledge and thank the CSIR for providing my postgraduate fellowship over the course of this study.

I would like to thank my supervisors, Dr. Mike Lucas and Dr. Sandy Thomalla, both of whom have been instrumental and inspiring in my development as a scientist and the completion of this dissertation. I discovered Mike's area of expertise in the Southern Ocean while still living in the State's and consider the opportunity to learn from him and more recently to work with him a dream realized, indeed an opportunity of a lifetime. Sandy was the chief scientist aboard the cruise to Antarctica and has been a constant source of inspiration in work and in life since our 10 week journey across the rolling Southern Ocean seas.

Thanks are also due to Captain 'Freddie' Ligthelm and the crew of the *SA Agulhas* for the safe trip to the ice and back. I often thought of the *Agulhas* as this incredible steel Mama sheltering us from the harsh conditions down south and, of course, she was continually guided by an amazing and hard working crew of people. Thanks to the research team, Stephan Woodbourne, Zoe Gebhardt, Stephanie Rainer, Marie Smith and last, but certainly not least MJ Gibberd, whom without his valuable insight and feedback, I imagine this project would have been more difficult to complete to say the least! If I didn't have someone to make coffee for, wake up in the wee hours of the morning, play the right music at the right time, keep cool, listen to my bantering or witness my 'borderline silly' ways while at sea I might have abandoned ship, so special thanks MJ, my great friend and fellow MSc. student.

Thanks to Ray Barlow for running the HPLC data as well as comments and advice on interpreting the data, Ian Newton for running the ^{15}N and ^{13}C samples and giving lessons in mass spectrometry, Sebastian Swart for determining the fronts from the MADT data and providing the SeaWiFS chlorophyll satellite composite image, and Nicholas Fauchereau for assisting with the PAR satellite images.

Finally I would like to thank my husband, Gareth for simply being himself and always inspiring my days, my son Sylvan for being born in the midst of this project! and my parents, family and friends for their love, love, love and eternal support and motivation throughout this Masters degree. It has been a fortunate, challenging and satisfying experience.

Contents

List of figures

List of tables

List of abbreviations

AABW	Antarctic Bottom Water
AAIW	Antarctic Intermediate Water
AASW	Antarctic Surface Water
AAZ	Antarctic Zone
ACC	Antarctic Circumpolar Current
ACS	Antarctic Continental Shelf
allo	alloxanthin
AMSR-E	Advanced Microwave Scanning Radiometer-Earth Observing System
APF	Antarctic Polar Front
ATP	adenosine triphosphate
but	19'-butanoyloxyfucoxanthin
BSi	biogenic silica
C	carbon
CDW	Circumpolar Deep Water
chl-*a*	chlorophyll-*a*
CO_2	carbon dioxide
DD+DT	diadinoxanthin + diatoxanthin
dFe	dissolved iron
diad	diadinoxanthin
DIC	dissolved inorganic carbon
DMSP	dimethylsulfoniopropionate
DOC	dissolved organic carbon
DP	diagnostic pigments
DPw	weighted diagnostic pigments
Fe	iron
Fd	ferredoxin
fuco	fucoxanthin
hex	19'-hexanoyloxyfucoxanthin
HNLC	high nutrient low chlorophyll

HPLC	High Performance Liquid Chromatography
lut	lutein
MADT	Maps of Absolute Dynamic Topography
MIZ	marginal ice zone
MLD	mixed layer depth
N	nitrogen
N-ACC	Northern Antarctic Circumpolar Current region
NADW	North Atlantic Deep Water
$NADP^+$	nicotinamide adenine dinucleotide phosphate
NADPH	reduced nicotinamide adenine dinucleotide phosphate
NH_4^+	ammonium
NO_3^-	nitrate
NPP	net primary production
NSIDC	National Snow and Ice Data Center
O_2	oxygen
PAR	photosynthetic available radiation
P-E	photosynthesis versus irradiance
pCO_2	partial pressure of CO_2
perid	peridinin
PFZ	Polar Frontal Zone
PIC	particulate inorganic carbon
POC	particulate organic carbon
POM	particulate organic matter
PON	particulate organic nitrogen
PPC	photoprotective carotenoids
pras	prasinoxanthin
PSC	photosynthetic carotenoids
PSI	photosystem I
PSII	photosystem II
sACCf	Southern Antarctic Circumpolar Front
SACCZ	South of the Antarctic Circumpolar Current Zone

SAF	Subantarctic Front
SAISB	Subantarctic Island and Shallow Bathymetry
SAMW	Subantarctic Mode Water
SAZ	Subantarctic Zone
SBdy	Southern Boundary of the Antarctic Circumpolar Current
Si	silicic acid ($Si(OH)_4$)
SSH	sea surface height
STF	Subtropical Front
STZ	Subtropical Zone
TP	total pigments
UCT	University of Cape Town
viol	violaxanthin
WG	Weddell Gyre
XBT	Expendable Bathythermograph
zea	zeaxanthin

Chapter 1. General Introduction

1.1 The Global Carbon Cycle

The Earth's radiative energy balance is undergoing change due to the increase in greenhouse gases, primarily CO_2 from fossil fuel combustion, and from anthropogenic aerosols. Basic laws of physics dictate this, however what is uncertain is how the Earth's climate is responding to this change and how quickly that response will happen (Bengtsson 2010). The long term trend of increasing atmospheric CO_2 has become a focal point in current research across atmospheric, terrestrial, and marine science disciplines. An evolved understanding of how our current global climate is being and will be influenced by continuing increases in CO_2 emissions and subsequent global warming is required to predict how climate change will impact our livelihood and the future health of all ecosystems.

The concentration of atmospheric CO_2 is a critical component of the 'Earth System' and plays many roles in its functioning (Watson & Orr 2003). For example, it provides an inorganic carbon source to support photosynthesis and thus in turn the oxygen to support life. It also contributes to carbonic acid formation for weathering rocks that form the basis of soil and nutrient formation and delivery to soils, rivers, and the sea. Lastly, it is an important greenhouse gas that critically helps to balance Earth's climate.

It is now well documented that the anthropogenic CO_2 concentration in the atmosphere is increasing and that as a result, the delicate balance of Earth's climate is undergoing change. For 5,000 years prior to the industrial revolution (1750), global atmospheric CO_2 variability was slight, varying less than 10 parts per million (ppm) from a concentration of ~280 ppm. But since the post-industrial revolution, CO_2 has increased by 90 ppm in the last 150 years (Indermuhle et al. 1999, Watson & Orr 2003, Feely 2004) bringing it to 383 ppm in 2007 (Le Quéré et al. 2009). Under current practices, anthropogenic CO_2 is expected to double over the next century from pre-industrial concentrations (Watson & Orr 2003). In 2008 total human CO_2 emissions were 10 billion tons of carbon per year (1 billion tons = 1 Pg = 1 x 10^{15} g) (Doney et al. 2009a). Of this total, 8.7 ±0.5 billion tons comes from fossil fuel burning and cement production and an additional 1.2 ±0.7 billion tons from deforestation (Doney et al. 2009a, Le Quéré et al. 2009). Slightly less than half of this amount remains in the atmosphere as a greenhouse gas, inducing changes in the Earth's

climate that are not fully understood. The remainder is taken up by the global ocean and terrestrial vegetation (~30% and 20% of the total respectively, Feely et al. 2004) (Figure 1.1).

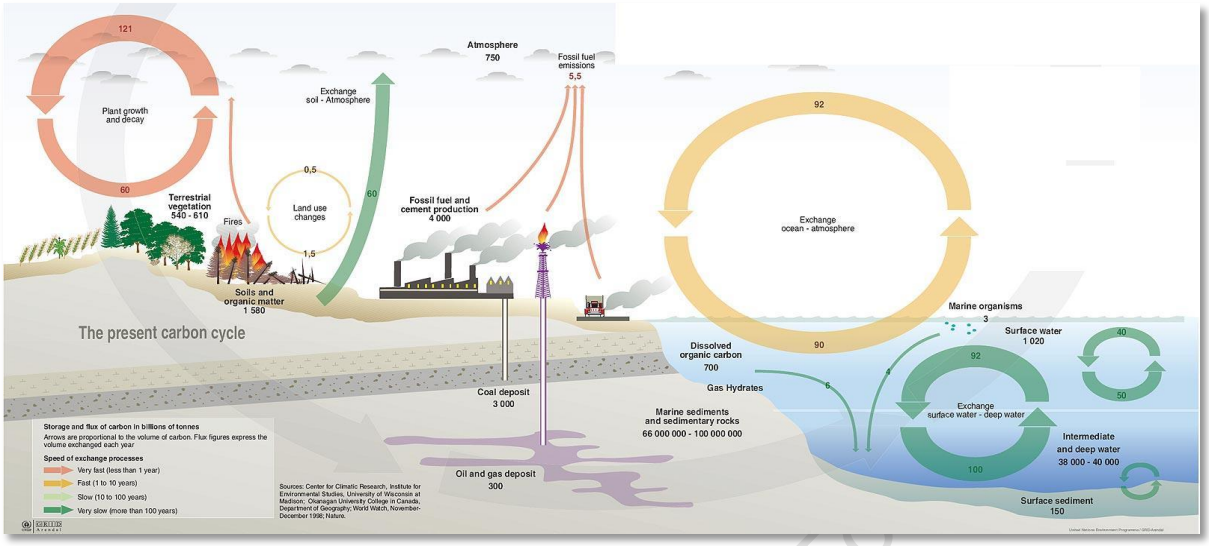

Figure 1.1 The global carbon cycle. Carbon storage and flux given in billions of tonnes. Rate of exchange processes indicated by coloured arrows: Red is less than 1 year, Yellow is 1 to 10 years, pale Green is 10 to 100 years, and dark green is more than 100 years. Image courtesy of Centre for Climatic Research, University of Wisconsin at Madison & Department of Geography, Okanagan University College in Canada, December 1998, Nature.

This rapid, unprecedented increase in atmospheric CO_2, not seen for at least 650,000 and over 6 glacial-interglacial cycles, effects the Earth's climate, terrestrial and marine ecosystems as well as biogeochemical cycles (IPCC 2007). For example, decreased ocean pH, 'ocean acidification', is leading to undersaturation of $CaCO_3$ in polar oceans (Feely et al. 2004, Orr et al. 2005, Doney et al. 2009a). Changing pH gradients and calcification processes can impact photosynthesis, nutrient transport, respiratory metabolism, phytoplankton growth, shellfish and benthic calcifier development, marine ecosystems and local marine fisheries (Doney et al. 2009a). Other observations relating to increased concentrations of atmospheric CO_2 include temporal shifts in the onset of spring, glacial melting and changes in sea ice extent in polar regions (Denman et al. 2007).

1.2 The solubility and biological carbon pumps

The global ocean serves as a buffer to human induced climate change by absorbing ~30% of anthropogenic CO_2 through two mechanisms which recycle CO_2, termed the 'solubility pump' and the 'biological pump' (Figure 1.2). In the North Atlantic near Greenland and Iceland (and in the Southern Ocean Weddell Gyre region), cold, dense (i.e. salty), CO_2

enriched waters (because of the improved solubility of gases in cold water) at high latitudes sink from the sea surface layer to depths of 1000-3000 m where the residence time is on the scale of thousands of years (Ito & Follows 2003). This localised sinking, affiliated with Meridional Overturning Circulation and thermohaline circulation on a larger scale, is termed the 'solubility pump' (see Figure 1.2). This means of exporting carbon from surface waters to abyssal depths is ultimately driven by differences in temperature and water density, so that cold polar oceans are predominantly sinks, while warm equatorial oceans are predominantly sources (Volk & Hoffert 1985) (Figure 1.3). Over long periods of time (100's to 1000's of years) these sinks are approximately balanced by the upward transport of dissolved inorganic carbon (DIC) into mainly warm surface waters (Ito & Follows 2003, Denman et al. 2007). While the physico-chemical processes respond on relatively short time scales of years to decades, the feedbacks on biological processes, mediated largely by deep ocean circulation, operate on much greater time scales of centuries to millennia (Sarmiento and Bender 1994, Raven and Falkowski 1999). Because of these varying timescales between the different mechanisms of exchange and the much longer response time of biological systems, it is more important than ever to gain a better understanding of how they work and how they will change.

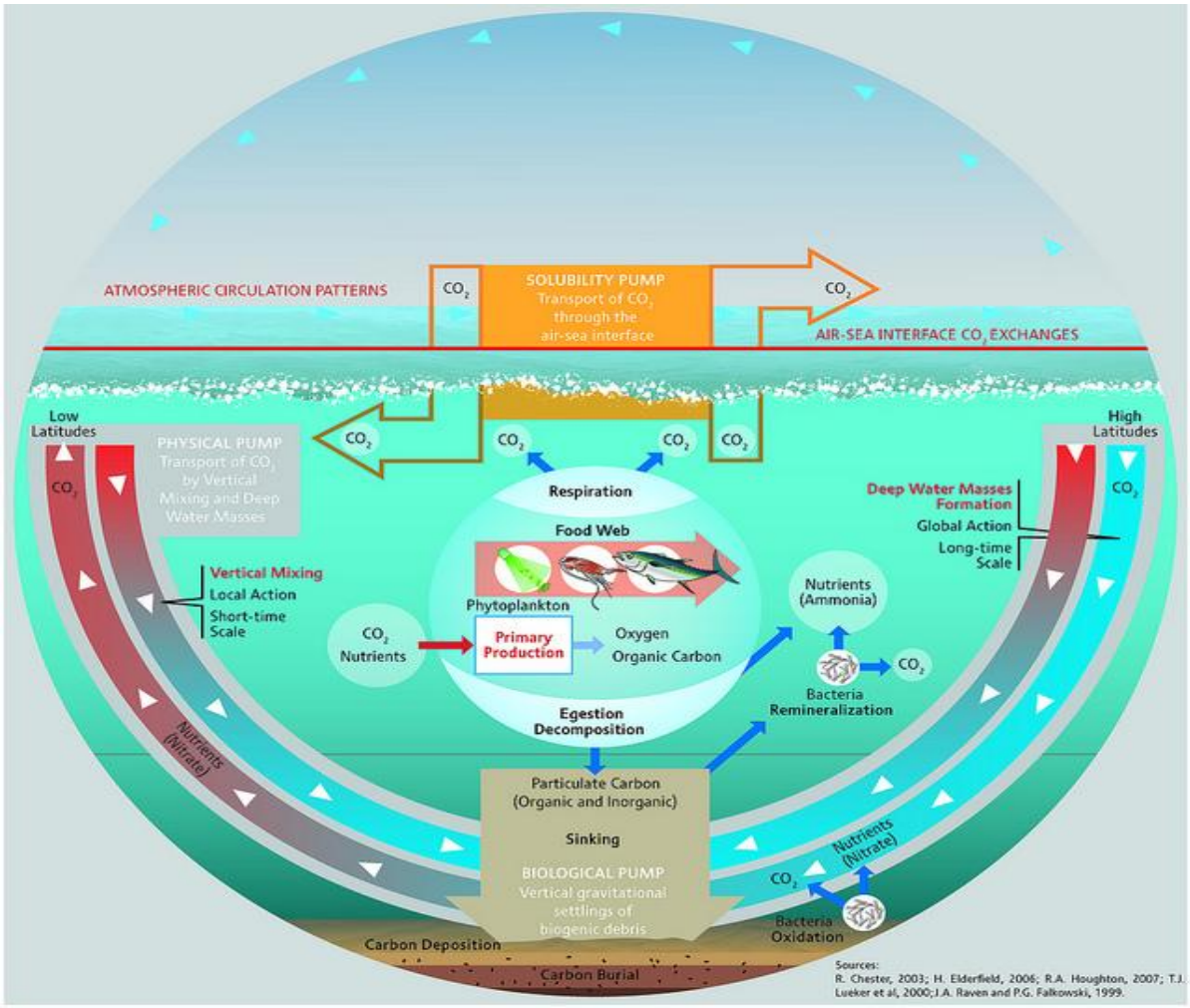

Figure 1.2 Schematic of the biological (centre), physical (left and right) and solubility (air-sea interface) carbon pumps. The multi-faceted biological process ultimately draws CO_2 to the sea floor through the settling of particulate organic and inorganic carbon. The physical and solubility processes recycle CO_2 from the air to the sea surface to the deep sea. The schematic was reproduced from R. Chester 2003, H. Elderfield 2006, R. A. Houghton 2007, T. J. Lueker et al. 2000, J. A. Raven & P. G. Falkowski 1999.

Marine phytoplankton in the euphotic layer incorporate inorganic carbon through the process of photosynthesis thus, lowering the partial pressure of CO_2 (ρCO_2) in the upper ocean (Falkowski et al. 2008). These organisms provide the foundation of all marine food chains and when they die, the sinking organic matter facilitates the diffusive sequestration of atmospheric CO_2 into surface waters in a process that is termed the 'biological pump' (Ito & Follows 2003, Falkowski et al. 2008) (see Figure 1.2). The biological and solubility pump work together to create a vertical concentration gradient of dissolved inorganic carbon that increases with depth. Globally, natural CO_2 fluxes are practically balanced (except for a small net outgassing from the input of carbon by rivers and from volcanic activity), whereas anthropogenic CO_2 has a global integral uptake of 2.2± 0.5 GtC yr^{-1}. This net positive uptake by the global ocean is divided into a mosaic of regional sources and sinks for natural and

anthropogenic CO_2 (see Figure 1.3). Most tropical oceans outgas CO_2 to the atmosphere with a combined mean flux of 0.7 GtC yr^{-1}, whereas the extra-tropical northern hemisphere is a net sink for natural and anthropogenic CO_2 at 1.2 GtC yr^{-1}. Of all the world's oceans, the Southern Ocean is the largest sink of both natural and anthropogenic CO_2, taking up an estimated 1.5 GtC yr^{-1} (Gurney et al. 2002, Takahashi et al. 2002, Gloor et al. 2003, Roy et al. 2003, Mikaloff et al. 2006, Denman et al. 2007).

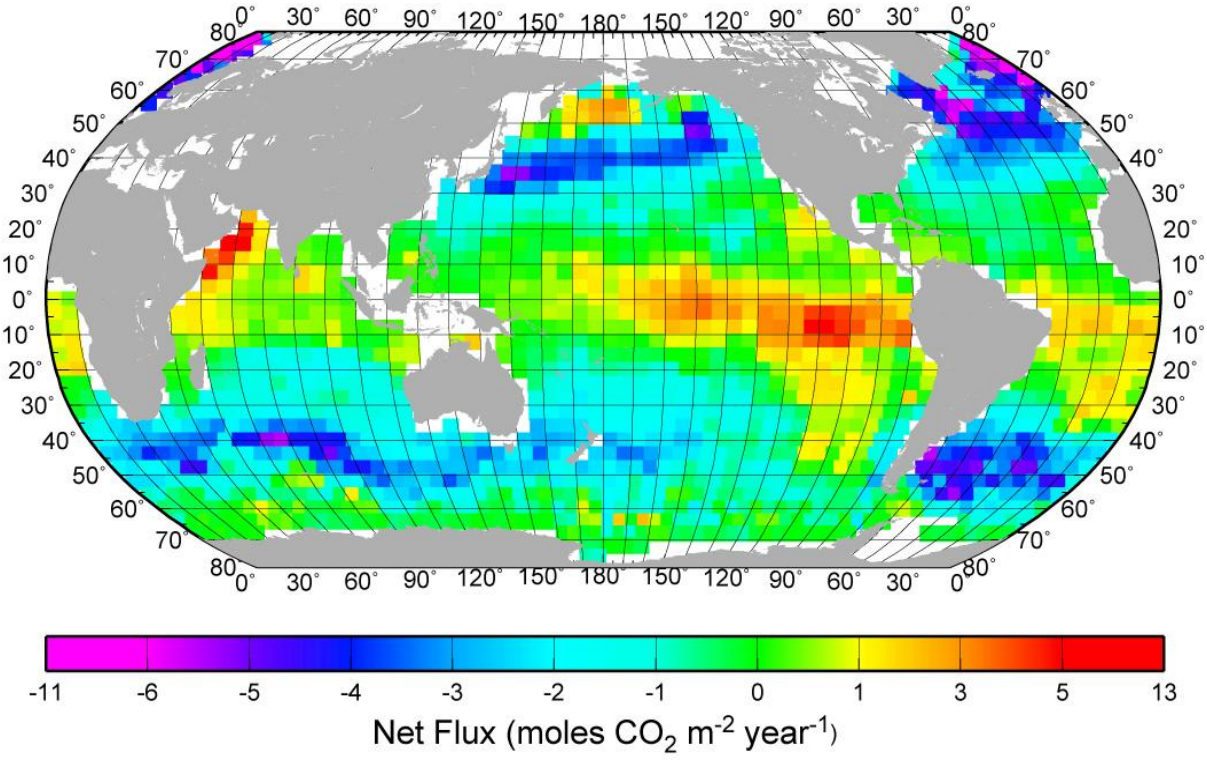

Figure 1.3 Annual sea-air fluxes for a nominal year of 1995. Positive values indicate a flux of CO_2 out of the ocean (Takahashi, 2002).

1.3 The Southern Ocean CO_2 Sink

When contemplating the fate of the Earth's future climate, a critical component to elucidate is the ocean's role in balancing climate over long periods of time, particularly in the Southern Ocean, which stores approximately 60% of the total oceanic anthropogenic CO_2 inventory (Sabine et al. 2004). In addition, the Southern Ocean is potentially one of the more sensitive regions on the planet to climate variability and change, provoking in depth studies into understanding how it functions and is likely to respond in terms of CO_2 flux in the future (Busalacchi 2004, Le Quere et al. 2007, Lovenduski et al. 2007).

The Southern Ocean plays a major role in regulating global CO_2 variability, controlled by physical and chemical oceanographic processes and by biological primary production (Sigman & Boyle 2000). Both these mechanisms have a bearing on global warming and on global efforts to mitigate climate change. Firstly, the Southern Ocean is the only part of the global ocean where CO_2 rich deep waters (> 1000 m & pCO_2 > 450 µatm) exchange CO_2 directly with the atmosphere. This means that despite storing ~60% of industrial CO_2 emissions, it has the potential capacity to become a CO_2 source (Le Quere et al. 2007, Lovenduski et al. 2007, Le Quere et al. 2009). Secondly, surface nutrient concentrations in the Southern Ocean are predominantly high (>20 µmols NO_3, >60 µmols Si) and under-utilized, which together with the physics of Mode Water formation and flow into low latitudes (Figure 1.4) is responsible for supplying the nutrients that drive > 75% of ocean productivity. Both mechanisms are connected to surface ocean physics that are likely to respond sensitively to climate change.

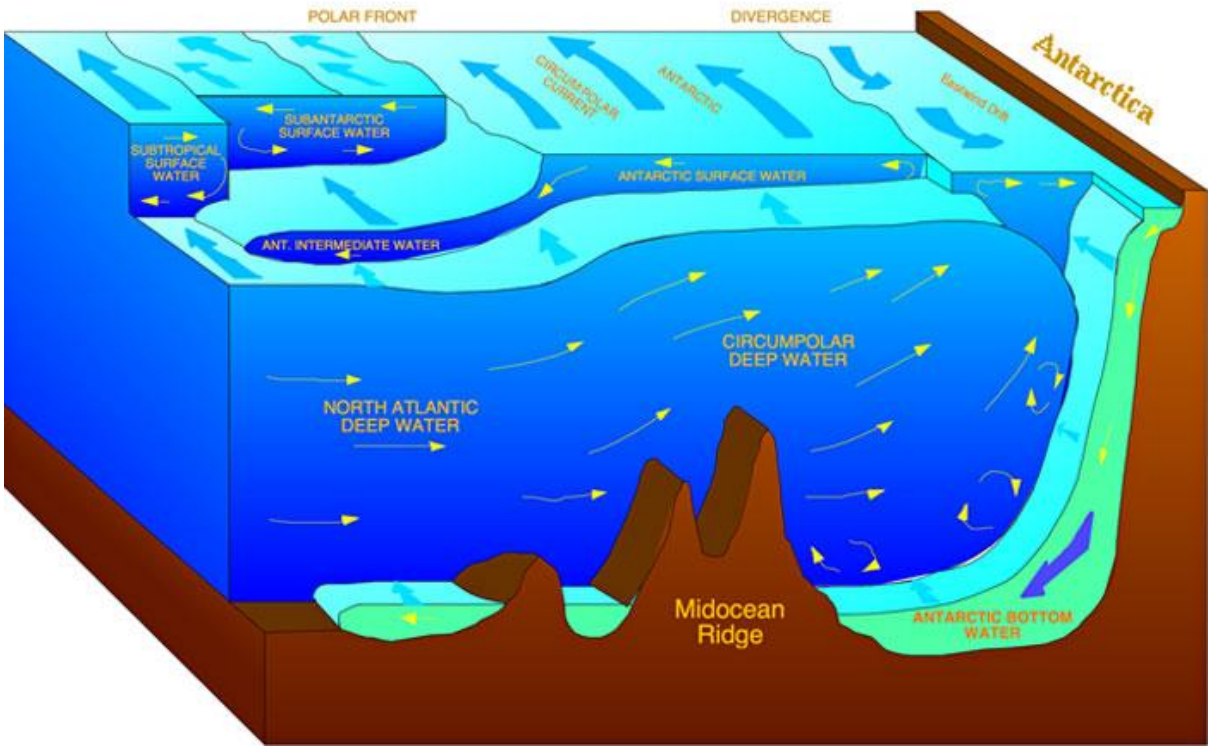

Figure 1.4 Typical water masses found in the Southern Ocean and their generalised circulation pattern (Hannes Grobe, Alfred Wegener Institute for Polar and Marine Research, Bremerhaven, Germany).

1.4 Factors influencing the physical solubility pump

Over timescales of hundreds to thousands of years, the unique climatology and physical structure of the Southern Ocean dictates its role in the carbon cycle. The Southern Ocean makes up 10-20% of the world ocean and is central to global thermohaline circulation (Cochlan 2008) (Figure 1.5). It consists of two major current systems: the very strong eastward flowing Antarctic Circumpolar Current (ACC) and the westward flowing Antarctic Coastal Current, through which indirect and direct connections are made with all other oceans on Earth. It plays a role in the formation or transformation of all major water masses that make up the thermohaline circuit. For example Subantarctic Mode Water (SAMW) and Antarctic Intermediate Water (AAIW) formation both have a major impact on the oceanic sink for anthropogenic CO_2 (Talley et al. 2008).

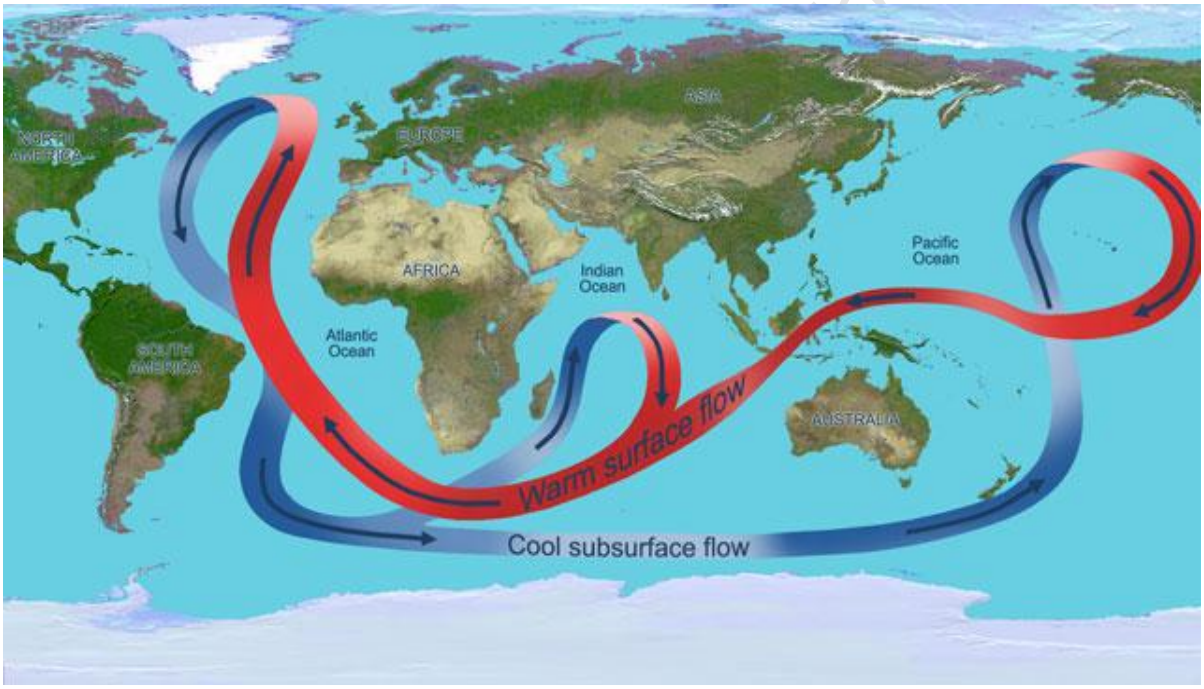

Figure 1.5 A simplified schematic of the global thermohaline circulation pattern, the overturning circulation of the global ocean. Throughout the Atlantic Ocean, the circulation carries warm waters (red arrows) northward near the surface and cold deep waters (blue arrows) southward into the Southern Ocean. Image credit: NASA/JPL

One of the most influential climatic features of the Antarctic is the Southern Hemisphere westerly wind field (Sigman & Boyle 2000). Southern Ocean hydrography, sea ice distribution and biological productivity, all of which regulate atmospheric CO_2, are greatly impacted by these westerly winds. Constrained primarily between ~40°S and ~65°S, the westerly's set-up the dominant easterly surface current and the subsequent northwardly steered Ekman flow that contributes to the creation of Antarctic Intermediate

Water (AIW), a main driver of the solubility pump (Sigman & Boyle 2000, Lovenduski & Gruber 2005). The latitudinal position and intensity of the westerlies is established by the pressure gradient between Antarctic low pressure systems and subtropical high pressure systems centred over the South Atlantic and Pacific Oceans (Kreutz et al. 1997, Sigman & Boyle 2000, Pendall et al. 2001). The position and intensity of these westerlies has a pulse termed the Southern Annular Mode (SAM). During positive phases of the SAM, the westerly wind belt contracts and moves poleward, resulting in more intense westerly winds between 50°S and 65°S. During negative phases of the SAM, the reverse happens, and the westerly wind belt expands equatorwards, causing winds to decrease at high latitudes. In recent decades, researchers have recorded a tendency towards increasing frequencies of the positive phase of the SAM that results from man induced climate change. This trend towards more positive phases of the SAM increases the amount of upwelling of CO_2 rich deep water south of 50°S, thereby suppressing the effectiveness of the Southern Ocean's CO_2 sink (Boning et al. 2008, Gille 2008, Le Quere et al. 2009). While the trend in a positive SAM is thought to reduce the Southern Ocean CO_2 sink through modification of the solubility pump, its impact on biology is still unclear. Lovenduski and Gruber (2005) suggest that a positive SAM is on average related to an increase in primary production south of the Antarctic Polar Front (APF).

In addition to changes in the SAM, model data as well as in situ observations over the past 30 years indicate that long term trends are developing in surface mixed layer (SML) characteristics of the Southern Ocean that are consistent with the expected outcomes of global warming driven climate change. Mixed layer stratification of the Southern Ocean is said to increase through increased freshening and an increase in atmosphere to ocean heat fluxes. Greater stratification may reduce the vertical supply of nutrients and hinder phytoplankton growth (e.g. Bopp et al. 2001). With caution in mind when interpreting basin scale model predictions, Bopp et al. (2001) speculate that increased stratification will reduce vertical nutrient and trace element fluxes by up to 10%, whereas a shoaling of the mixed layer will elevate mean underwater irradiances (Boyd et al. 2002). Although such increases in mean underwater irradiances will lower iron (Fe) demands, the reduced Fe pool available in a shallower mixed layer may ultimately limit production despite an improved light environment (Boyd et al. 2002). However, such developments may be counteracted by a

reduction in the vertical fluxes of Fe, the primary mechanism by which Fe is supplied to these waters (Boyd et al. 2002). Future implications of density stratification under surface ocean warming conditions thus remain uncertain (Behrenhfeld 2011). The uncertainties involved in understanding the complex feedback mechanisms associated with such predicted changes highlights gaps in our knowledge of the response of the Southern Oceans carbon sink to anticipated climate change.

1.5 Factors influencing the biological carbon pump

Takahashi et al. (2002) suggest that CO_2 drawdown in the Southern Ocean is driven primarily by biogeochemical processes ('biological pump') rather than by sea surface temperature (SST) and physical solubility processes ('solubility pump'). These findings prompt the current raft of comprehensive investigations into Southern Ocean biology that drive the carbon cycle there. Often referred to as the 'Antarctic Paradox' (Tréguer and Jaques 1992, Priddle et al. 1992), the Southern Ocean's defining biogeochemical characteristic is a water body high in macro-nutrients Nitrogen (N), Phosphorous (P), and Silicate (Si), but low in chlorophyll-*a* (mostly <0.5 mg m^{-3}), making it a high nutrient low-chlorophyll (HNLC) ecosystem (Moore and Abbott 2000). More than 75 years ago Hart (1934) identified irradiance, stratification, mixing, macronutrients, micronutrients, and grazing as factors that regulate algal biomass and productivity in the Southern Ocean, preventing utilisation of all available nutrients at various locations and times. However, how these various regulating factors operate in combination in the complex spatial domain of the Southern Ocean is still poorly understood (Hiscock et al. 2007). Equally, how they may respond to significant temperature change is difficult to predict. Model simulations by Taucher and Oschilies (2011) show two opposing results for simulated marine net primary production (NPP) depending on whether biological processes are deemed temperature sensitive or not. This infers that indirect temperature effects like shifts in nutrient supply and light are not the only relevant factors to include when modelling the response of marine ecosystems to climate change and highlights the need for a better understanding of all relevant factors (Taucher and Oschilies 2011).

The Southern Ocean HNLC environment is generally described as being controlled by "top-down" (ecological) or by "bottom-up" (physiological) mechanisms, or in other words, "yield" versus "rate" (Smith and Lancelot 2004, Cochlan 2008). Some of the bottom up controls on phytoplankton processes in the Southern Ocean include light availability (regulated by changes in MLD and low PAR), low temperatures (Boyd 2002, Cochlan 2008), and UV inhibition of photosynthesis. In addition, phytoplankton productivity is controlled by macro-nutrient availability such as silicic (Si) acid required by diatoms (Boyd 2002), and the form of nitrogen available. Si is non-limiting south of the Antarctic Polar front (APF), but may approach limitation in sub-Antarctic waters, particularly between the Subtropical front (STF) and the Sub-Antarctic front (SAF). Although nitrate (NO_3^-) is abundant south of the SAF, nitrate uptake (ρNO_3^-) may be Fe-limited, while ammonium (NH_4^+) accumulation may also suppress ρNO_3^- (Cochlan 2008). Many studies have demonstrated iron-light (and zinc) co-limitation of both ρNO_3^- and photosynthesis (Cullen 1991, De Mora et al. 2000, Boyd 2002, Sunda & Huntsman, 2005, Moore et al., 2007a,b, Cochlan 2008, Pollard et al., 2009). A well known, but understudied top down control on phytoplankton production in the Southern Ocean is grazing (Fronenman et al. 1996, Irigoien et al. 2005, Smetacek et al. 2004). A more detailed discussion on the top down and bottom up controls on phytoplankton production in the Southern Ocean follows below.

1.5.1 Light

The light environment experienced by phytoplankton in the Southern Ocean has three main controlling variables 1) the time of year (and thus photoperiod and solar angle), 2) the vertical mixing depth, and 3) the amount of ice cover, including both thickness and overlying snow cover (Cochaln 2008). Photosynthetically available radiation (PAR) at the sea surface also varies with latitude, diurnal effects and sea state (angle of reflection and absorption relative to wave height and direction). Underwater irradiance is defined by its attenuation coefficient in sea-water (K_d). The depth of light penetration defines the euphotic zone (1% or 0.1% of surface light) where light is sufficient to support phytoplankton growth and reproduction by photosynthesis. Wind stress at the surface will either deepen or shallow the surface mixed layer (SML) and thus also control the depth to which phytoplankton cells are mixed through the euphotic zone. When deep mixing occurs, phytoplankton may be

forced into the aphotic layer and productivity decreases. Critical depth models of photosynthesis are built on this concept (Nelson and Smith, 1991). The compensation depth (Dc) is defined as the depth at which a cell's respiration (CO_2 production) during 24 hours exactly balances CO_2 fixed by photosynthesis during the same period (i.e. Pc=Rc) – a depth which varies from 20-100 m over much of the Southern Ocean (Jaques 1983, Knox 1994). The depth at which photosynthesis throughout the water column is balanced by phytoplankton respiration throughout the water column (Pw=Rw) is called the critical depth (Dcr). Sverdrup (1953) theorized that when the critical depth is shallower than the mixed layer depth (MLD), no net production takes place since Rw>Pw over 24 hours. Net production (Pw>Rw) only occurs when the critical depth lies below the mixing depth.

The Southern Ocean is well known for its inclement weather and tempestuous seas. Wind stress is frequently so great that a homogeneous (isothermal and isohaline) water column develops which reaches depths of 50 – 100 m (Nelson and Smith 1991, Knox 1994). Under this scenario, free-floating or slightly motile phytoplankton cells are likely to be mixed well below the Dcr, so that Pw<Rw. In this way, light limitation through deep mixed layers is considered to hinder the development of blooms and contribute to the low primary productivity of Antarctic waters. A recent study by Venables and Moore (2011) using data on MLD from Argo float profiles and chlorophyll concentrations and PAR from SeaWiFS concluded, however, that light limitation did not significantly constrain the annual integrated standing stock of chl-a in the HNLC Southern Ocean. An increase in water column stability and a shallowing of the mixed layer is conversely expected to help maintain phytoplankton in the euphotic zone, thus promoting growth and subsequent biomass accumulation (Bidigare et al. 1986). This is thought to occur at the ice edge, at the Sub Tropical Front (STF) and around Subantarctic islands, where local water or thermal stabilisation of the upper water may reduce the critical depth and therefore permit high phytoplankton productivity and biomass accumulation (Allanson et al. 1981, Lutjerharms et al. 1985, Nelson and Smith 1991, Dower and Lucas 1993).

More recent work on light availability in the mixed layer and its influence on bloom initiation in the North Atlantic (see Behrenfield 2010 & Venables & Moore 2011) however, challenges Sveredrup's classical Critical Depth Hypothesis. Behernfield's (2010), Dilution-

Recoupling Hypothesis describes how changes in MLD affect the balance between net phytoplankton growth rates and losses (from grazing, sinking, parasitism or viral infection and physical flushing losses, such as dilution) in two distinct ways. Firstly, 'dilution' of predator-prey interactions through a deepening MLD leads to a decrease in loss terms relative to phytoplankton growth and secondly, when the mixed layer shallows 'decoupling' begins whereby mobile predators are concentrated into a decreasing volume and grazing increases relative to phytoplankton growth. According to Behernfield's Dilution-Recoupling Hypothesis, bloom initiation occurs in mid-winter when light levels are minimal and near surface mixing is deepest. However, given that the North Atlantic is a considerably different environment, a similar study would need to be addressed in the Southern Ocean before abandoning Sveredrup's age-old theories completely.

Furthermore, the current raft of Fe limitation theory suggests that improved stability is not the most important trigger of bloom formation, but rather a combination of extended day-length and Fe availability. After all, in late summer (i.e. late December onwards) when the water column shows the greatest degree of stratification and light is often greatest, blooms actually crash. Why? Fe limitation and an increase in grazing pressure (Lucas et al. 2007, Fielding et al. 2007).

1.5.2 Temperature

A dramatic shift in temperature occurs across the APF, where warmer Subantarctic waters are left behind for cold polar waters that can range between ~5°C and -1.8°C, the temperature at which sea water freezes. Phytoplankton physiology is directly impacted by changes in the latitudinal temperature gradient. In classical terms, the maximal rate of growth (μmax) is a function of temperature, where for every 10°C rise in temperature, μmax doubles (Eppley 1972, Goldman & Carpenter 1974). However, a subsequent study found temperature to have opposing effects on cell division and nutrient uptake, calling attention to diverse and species-dependent responses to temperature (Goldman 1977a & b). While not a dominant controlling factor, temperature is thought to set an upper limit on phytoplankton growth rates, with the understanding that growth rates can be altered by other environmental factors (Tilzer et al. 1986, Smith & Sakshaug 1990, Wiencke et al. 1993, Boyd 2002). In Addition, low temperatures are known to hinder phytoplankton's utilization

efficiency of incident irradiation (Tilzer et al. 1986) and their ability to enlist the metabolically expensive damage-repair cycle for a damaged photo-system II (PSII) reaction centre when recovering from photoinhibition (Alderkamp et al. 2010).

1.5.3 Macronutrients

Diatoms make up the most abundant group of phytoplankton in the Southern Ocean. They are the greatest contributors to bio-silicification and require the macronutrient $SiOH_4$ to form their frustules (Boyd 2002). Subsequently they are also the most affected by silicic acid limitation. Surface silicate concentrations in the Southern Ocean decrease northwards from high concentrations (~60 µM) in the Southern Antarctic Circumpolar Current Zone (SACCZ) to low concentrations (~4 µM) in the sub-Antarctic zone (SAZ) (Boyd 2002, Pollard et al. 2002). Diatoms are believed responsible for much of the carbon export from the surface to the deep-sea due to the increase in ballast form their opaline frustules (Armstrong et al. 2002). Limitation of diatom growth by low Si waters (such as those of the Subantarctic) can result in a physiological cascade that affects diatom /non-diatom community succession, with implications for food chains, export rates and CO_2 sequestration (Brzezinski et al. 2003, Sarmiento et al. 2004).

Also important to consider when determining limitations to production is the type of N substrate available for uptake and growth. Evidence suggests that both NH_4^+ and urea can inhibit NO_3^- uptake by phytoplankton, especially in areas of low dissolved Fe concentrations (Cochlan 2008). Furthermore, it is important to note that varying concentrations of NH_4^+ (0.1 to 1.0 µM) have been found to suppress NO_3^- uptake rates (see review Cochlan 2008). Observed variations depend upon factors such as nutrient history, light, and the species composition of the phytoplankton community. For example, while complete inhibition of NO_3^- uptake in Subantarctic Pacific assemblages, primarily consisting of autotrophic flagellates, occurred with NH_4^+ concentrations as low as 0.1 – 0.3 µM (Booth 1987, Wheeler and Kokkinakis 1990, Cochlan 2008), in a diatom-dominated assemblage of newly upwelled waters off the coast of Oregon NH_4^+concentrations of 0.6 µM had little effect on NO_3^- uptake (Kokkinakis and Wheeler 1987, Cochlan 2008). In a more comprehensive look at the potential for NH_4^+ inhibition of NO_3^- uptake Lucas et al. (2007) found that at low concentrations of (<~0.25 µmol l^{-1}) specific uptake rates of NO_3^- were highest, indicating no inhibition, while at high concentrations (>~0.6 µmol l^{-1}) specific nitrate uptake is greatly

inhibited. However, this is only so at the 1% light depth in both the North and South regions of the Crozet Island study. Areas sampled outside of this light depth showed no correlation with depth or region when concentrations were between 0.25 µmol l^{-1} and 0.6 µmol l^{-1}, thus implying NH_4^+inhibition of NO_3^- uptake at mid-range concentrations is weak.

1.5.4 Iron

The nitrogenous nutrition of phytoplankton in HNLC regions is compromised when Fe is scarce because phytoplankton are unable to fully utilize the abundant NO_3^- reserves during the growth season. Fe plays a critical role in the bioenergetics of C and N metabolism. Both photosynthetic and respiratory electron transport chains, the synthesis of chlorophyll, and the assimilation of NO_3^- require substantial amounts of Fe (Cochlan 2008). In terms of Fe utilisation efficiency, theoretical calculations and experimental observations indicate that NO_3^- based 'new' production (Eppley and Petersen 1979) requires 60% more Fe than 'regenerated' production based on NH_4^+ or urea uptake (Cochlan 2008). More Fe is needed to reduce NO_3^- to NH_4^+ at which point it can be assimilated into amino acids. This requires the enzymes nitrate reductase (requires one atom of Fe) and nitrite reductase (requires five atoms of Fe) plus, either ferredoxin (an Fe containing electron [e-] donor) or flavodoxin (a non-ferrous e- donor) in addition to the need for a larger amount of reducing power (8 mol e-/mol N) gained from Fe-dependent redox reactions (Cochlan 2008). Thus in HNLC regions of the Southern Ocean a more energetically efficient means of harvesting N is realized through the utilization of NH_4^+ over NO_3^- when Fe is limited.

The absence of a continental land mass makes the Southern Ocean one of the most Fe impoverished of the world's oceans (Wagener et al. 2008). Iron limited phytoplankton production in the Southern Ocean is now unequivocally established through a number of artificial iron fertilisation experiments (De Baar et al. 2005, Boyd et al. 2007) while two natural iron fertilization experiments (KEOPS: Blain et al. 2001 and CROZEX: Pollard et al. 2007, 2009) have further assessed the impact of Fe-fertilisation on carbon export and the carbon to iron (C:Fe) export efficiency, which is highly variable. Regions of relative iron availability are characterized by larger average cell sizes, dominance by diatoms, higher *f*-ratios, faster rates of specific nitrate uptake (V_{NO3} d^{-1}), lower particulate organic carbon to chlorophyll-a (POC:chl-a) ratios (Lucas et al., 2007) and improved photo-physiological

competency (Moore et al., 2007a,b). All these parameters provide physiological and taxonomic evidence for the impact of Fe availability which increases with proximity to sub-Antarctic Islands such as the Crozet and Kerguelen archipelagos (Blain et al. 2001, Lucas et al. 2007, Moore et al. 2007a,b, Pollard et al. 2007, Poulton et al. 2007, Seeyave et al. 2007). Indeed, ocean colour satellite imagery demonstrates perennial blooms around all the Subantarctic Islands, including the Prince Edward Islands (Pollard et al., 2007).

1.5.5 Grazing

Grazing, in the form of herbivorous meso- and microzooplankton predation pressure is an important 'top down' control on primary production. Size selectivity during grazing also impacts on the efficiency of the biological carbon pump. When larger cells eclipse other sizes in phytoplankton biomass, the majority of photosynthetically fixed carbon is transferred to the meso- and macrozooplankton fractions (Fronenman et al. 1996a, Irigoien et al. 2005). This promotes a rapid more efficient transfer of organic carbon out of the euphotic zone into the deep ocean via vertical migration and large faecal pellet production. In contrast, when the smaller size fractions dominate the phytoplankton population, a greater proportion of the photosynthetically fixed carbon is transported to the microzooplankton fraction (Fronenman et al. 1996a). In this instance the carbon pump is less efficient as most of the carbon is recycled within the microbial loop in the upper mixed layer, leaving little carbon to be transferred to the deep ocean (Fronenman et al. 1996a, Fielding et al. 2007).

1.6 Distribution of Phytoplankton Biomass in the Southern Ocean

While the annual average net primary production rate in the Southern Ocean is low, relative to the supply of macronutrients, very intense phytoplankton blooms do occur locally and contribute to high temporal and spatial variability in Southern Ocean productivity (e.g. Seeyave et al. 2007). Low production rates are associated with permanent open ocean zones north of the extent of the sea ice, while high production rates are correlated with divergent frontal zones (Moore and Abbott 2000). Elevated chlorophyll concentrations correlated with the major fronts of the ACC have been substantiated and ascribed to many processes such as cross-frontal mixing of macronutrients, an improved

light environment through enhanced stratification and increased Fe concentrations through upwelling and interaction of the fronts with shallow topography (e.g. Lutjerharms et al.1985, Laubscher et al. 1993, Moore and Abbott 2002). Other areas of high production in Southern Ocean waters are found over regions of shallow bathymetry; around and downstream of Subantarctic islands, the continental shelf, over mid-ocean ridges and large plateaus. In these regions of shallow bathymetry, current flow through relative vorticity (Moore et al. 1999, Hogg and Blundell 2006) and/or bottom pressure torque (Sokolov and Rintoul 2007a) is believed to enhance the flux of Fe into surface waters (Park et al. 2010, Venables and Moore 2010) governing the typical inverse relationship found between depth and chlorophyll in the Southern Ocean (Comiso et al. 1993). Highest chlorophyll concentrations are generally correlated with the marginal ice zone (MIZ) (Arrigo and Van Dijken 2004), through enhanced irradiance from increased vertical stratification when ice melts (Smith and Nelson 1986), through Fe injections from melting ice (Sedwick and DiTullio 1997, Gao et al. 2003, Grotti et al. 2005) and mixing of Fe rich sediments along the continental shelf (Schoemann et al. 1998, Johnson et al. 1999). Additionally, downwind of dry continental areas (e.g. Patagonia, south and south west of Australia, New Zealand and Africa) regular deposits of atmospheric dust are deemed a salient Fe source that fuel primary production in the Southern Ocean (e.g. Cassar et al. 2007).

The complexities in the various bottom up controls of primary production in the Southern Ocean strongly influences the characteristics of the spatial distribution of phytoplankton biomass described above. This study investigates regional differences in the controls of phytoplankton production and export using ^{15}N tracer techniques and tests the light-dependent uptake of oxidised versus reduced N species using Photosynthesis versus Irradiance curves. A discussion of the two methods follows below.

1.6.1 ^{15}N production and export estimates

New and regenerated production is well established as a means of connecting surface N dynamics with biogenic particle flux (Dugdale and Goering 1967, Eppley and Peterson 1979, for review see Cochlan 2008). Phytoplankton harvest nitrogenous nutrients

from a variety of sources and in various chemical forms. According to Dugdale and Goering (1967), the source and oxidation state of the N substrate determines the partitioning of primary production. Nitrate originating from the deep sea (or from the land and / or from atmospheric aerosols – including NH_4^+) is considered 'new' to the euphotic zone, as is N_2 fixation from the atmosphere, while ammonium, urea and amino-acids, originating from microbial and metazoan recycling, are considered 'regenerated'. The proportion of new production (ρNO_3^-) to total N production ($\rho\Sigma N = \rho NO_3^- + \rho NH_4^+ + \rho urea + \rho DFAA$) is described by the f-ratio (Eppley and Peterson 1979) as the proportion of new production relative to total production ($\rho NO_3^- / \rho\Sigma N$). Under stable conditions and over appropriate time scales the f-ratio is analogous to the proportion of production available for export, most often in the form of sinking particles, which does not deplete the system, thus creating a balance of N flux into surface waters with corresponding downward N losses over appropriate time and space scales (Cochlan 2008). Under this scenario, when Redfield ratio C:N stoichiometry is applied, ρNO_3^- gives an indirect estimate of downward carbon flux (Eppley and Peterson 1979, Minas et al. 1986). This concept is, however tempered by the recent discovery of significant surface nitrification rates (Yool et al. 2007) that renders equating ρNO_3^- with carbon (C) export unreliable. However, in regions of upwelling and where ambient NO_3^- concentrations are high (such as in the Southern Ocean) the rate of surface nitrification contributes only a small portion (<~10%) to the ambient surface NO_3^- pool, such that the concepts of the *f*-ratio and its relationship with export production are not excessively compromised. Nevertheless, until we have better estimates of nitrification rates in the Southern Ocean, the use of the f-ratio to infer export production needs to be used with caution.

Since 1977 numerous studies throughout the Southern Ocean have used ^{15}N uptake techniques to calculate f-ratios (for a comprehensive list see Cochlan 2008). An exception is the Atlantic sector around South Georgia and the South Sandwhich Islands which forms the focus region of this study. Several trends to consider from previous bodies of work stand out. First, the permanently open ocean zone characteristically sustains low, regeneration dominated, N uptake rates (except in close proximity to islands), with no noticeable decline in surface NO_3^- concentration, thus equating to low *f*-ratios (~0.2 – 0.3). Second, both the coastal and continental shelf zone and the seasonal ice zone bear resemblance to N uptake

measurements in temperate upwelling systems, but with lower uptake rates. Substantial blooms develop here due to a stable, stratified water column, iron fertilisation and cell seeding from sea ice retreat. These conditions lead to a decrease in surface NO_3^- and with N-nutrition early in the season being dominated by new N, resulting in higher f-ratios (~0.4 – 0.9). Third, in both regions a shift in community structure is generally observed from diatom-dominated to a flagellate-dominated system with a seasonal progression in regenerated production and subsequent increases in surface concentrations of NH_4^+ (Cochlan 2008). For a comparison of previous work on N metabolism in various regions of the Southern Ocean refer to Table 1.1 below.

Table 1.1 Comparison of depth integrated values of ^{15}N uptake ($mmolm^{-2}\ d^{-1}$) by phytoplankton for the following regions of the Southern Ocean. * represents no available data.

Southern Ocean Region	$\int\rho NO^-_3$	$\int\rho NH^+_4$	$\int$purea	$\sum\int\rho N$	*f*-ratio	Reference
Bellinghausen Sea						
Open Pacific (57°S)	2.6	13.65	10.13	26.38	0.09	Waldron et al. 1996
PFZ (64°S)	0.9	8.1	9.61	9.61	0.1	
Indian Sector (summer 1994, ANTARES3)						
Kerguelen Plateau (49°S)	5.7	3.5	2.8	11.9	0.48	Mengesha et al. 1998
Kerguelen Plateau (52°S)	7.7	2	1	10.7	0.72	
Pacific Sector (summer 1997, US-JGOFS)						
PFZ (57–61°S)	2-5±2.3	*	*	*	0.05–0.48	Sambrotto & Mace 2000
Western Bransfield Strait						
Bransfield Strait	13.0±3.1	7.8±2.6	*	*	0.64±0.03	Bode et al. 2000
Bellinghausen Sea	17±2.5	40.9±10.2	*	*	0.31±0.08	
Gerlache Strait	9.0±2.7	24.1±17.0	*	*	0.42±0.08	
Australian Sector (spring 2001, CLIVAR-SR3)						
SAZ/STF (49–51.0_ S)	*	*	*	4.4±0.3	0.53±0.26	Savoye et al. 2004
PFZ/IPFZ (54–57° S)	*	*	*	5.6±0.1	0.56±0.02	
AZ/MIZ (61–65°S)	*	*	*	9.6±2.2	0.61±0.08	
Indian Sector (CROZEX, summer 2004)						
M3 bloom	20.3±5.7	3.6±1.3	6.1±2.0	30.1±7.5	0.67±0.08	Lucas et al. 2007
South of Plateau (HNLC)	1.8±0.8	3.2±0.5	1.1±0.2	6.0±1.5	0.28±0.07	
Atlantic Sector (summer 2008)						
Subtropical Zone(34-41°S)	1.01±0.3	0.69±0.3	6.47±6.7	8.18±6.8	0.24±0.22	Joubert et al. 2010
Subantarctic Zone(42-44°S)	5.11	0.92	4.31	10.34	0.49	
Polar Front Zone(45–50°S)	1.97±0.5	1.16±0.4	2.13±1.8	5.26±2.2	0.41±0.11	
Antarctic Zone(51–57°S)	3.39±1.9	1.27±0.6	2.86±1.6	7.51±3.5	0.45±0.11	
Indian Sector (late summer 1999, MIOS-4)						
STZ (31–40°S)	3.76±4.2	19.83±15.0	22.30±17.8	46.07±33.5	0.07±0.03	Thomalla et al. 2011
SAZ (41–47°S)	2.90±3.4	14.97±16.9	6.86±3.9	24.73±21.6	0.10±0.04	

1.6.2 Photosynthesis versus Irradiance (P - E)

The N uptake response to different light fields is complex since numerous factors affect the relationship between light and the substrate being utilized and the exact mechanism(s) by which light regulates N metabolism is(are) unknown (Cochlan 2008). Three basic models describe the dependence of N uptake by phytoplankton upon irradiance, 1) a rectangular hyperbola similar to that of the Michaelis-Menten equation for N uptake as a function of substrate concentration (MacIsaac & Dugdale 1972), 2) this same model, but modified to include dark uptake (Cochlan et al. 1991), and 3) a 3-parameter, exponential (P vs. E) curve that accounts for photoinhibition (Priscu 1989, Kudela & Cochlan 2000) (Cochlan 2008). In this study, the P - E model is used as it gives a good representation under a wide range of conditions, is easy to fit to real data and is considered useful in predicting primary productivity and carbon fluxes over large areas of the ocean. It also provides information on the photoacclimation status of cells at the time of sampling (Platt & Sathyendranath 1988, Villafane et al. 2004).

The P-E relationship is a building block for the conception of phytoplankton ecology and physiology and has often been used to investigate photosynthesis as a function of light intensity (see Platt & Sathyendranath 1988, Mitchell et al. 1991, Dower and Lucas 1993, Fenton et al. 1994, Dower et al. 1996, Behrenfeld & Falkowski 1997, Bracher et al. 1999, Villafane et al. 2003, Bouman et al. 2005). Parameters that characterize the P-E relationship (see Figure 1.6) are P^B_{max}, a measure of maximum light-saturated photosynthetic capacity (i.e. the light-saturated maximum rate of carbon fixation or production per unit chlorophyll), α^B, the initial light-limited slope of the P-E curve and a measure of the quantum efficiency of photosynthesis, β, the photoinhibition parameter (the negative slope, $E\beta$, of declining photosynthesis at high light intensities), and E_k, the light saturation parameter ($E_k = (P^B_{max} / \alpha^B)$) (Dower and Lucas 1993, Villafane et al. 2003). These parameters are influenced by many factors including, ambient light, the previous history of light exposure, the duration of light exposure, physiological condition of the cells (influenced by light history and nutrient status), species composition, water temperature, CO_2 concentration, environmental and growth conditions, the season in which and the region from where the samples are drawn

(Dower and Lucas 1993, Macedo et al. 2001, Villafane et al. 2003). Other factors such as vertical mixing and ultraviolet radiation may also influence the P-E relationship (Yoder and Bishop 1985, Villafane et al. 2003 respectively).

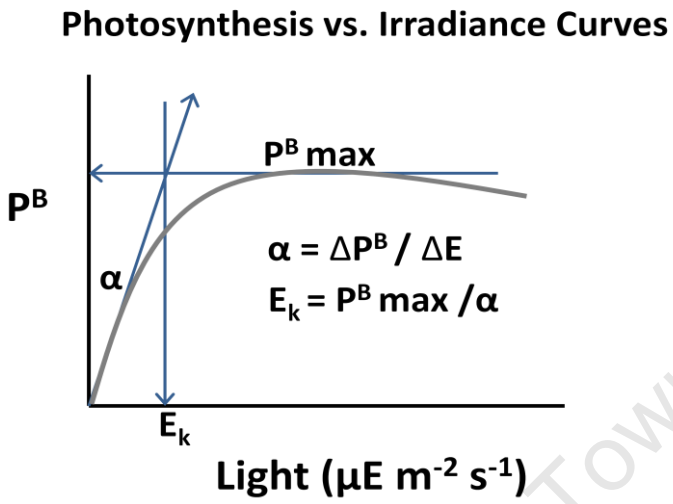

Figure 1.6 Schematic of P vs. E curve. P^{B}_{max}: a measure of maximum light-saturated photosynthetic capacity (i.e. the light-saturated maximum rate of carbon fixation or production per unit chlorophyll), α: the initial light-limited slope of the P-E curve and a measure of the quantum efficiency of photosynthesis, β: the photoinhibition parameter (the negative slope, Eβ, of declining photosynthesis at high light intensities), and E_k: the light saturation parameter ($E_k = (P^{B}_{max} / \alpha^{B})$.

Given that phytoplankton have evolved with the development of the Southern Ocean over the last 15 million years, it is reasonable to expect that phytoplankton growth ought to be conditioned to a low light regime through adaptive physiological responses. When physiological parameters of P. vs. E. curves are examined (Sakshuag et al. 1997), Southern Ocean phytoplankton can show high degrees of photoadaptation to low ambient underwater irradiance (e.g. Dower and Lucas 1993, Dower et al. 1996, Bracher et al. 1999, Strass et al. 2002). In experiments on Antarctic diatoms, increased light utilisation was found in environments characterised by fluctuating light conditions. This is likely to be an adaptation of the microphytoplankton in overcoming such constraints and enabling them to attain a higher than expected productivity (Knox 1994). In a study by Bracher et al., (1999), light saturation (Ek) values were considerably lower for Southern Ocean phytoplankton than are typical for phytoplankton in temperate regions, indicating a degree of photoadaptation to a low light environment. In addition, phytoplankton in polar regions are also known to adapt to their *in situ* irradiances by modifying their maximal light-saturated photosynthetic rates (P^{B}_{max}), and their photosynthetic efficiency (the light-limited rate, α^{B}) whereby low light

communities will have similar or slightly lower values of P^B_{max} and α^B than communities acclimated to higher irradiances (Cochlan 2008).

Excessive irradiance on the other hand inhibits photosynthesis and is known as photoinhibition, whereby damage to the photosynthetic apparatus can cause the (photo)destruction of the photosynthesizing pigments (Powles 1984). More recently however, the term photoinhibition has also been used to define a slow and reversible reduction of the photosynthetic efficiency that depends on the irradiation and leads to a partial loss of capacity to convert radiant energy into dry material and, consequently, into growth (Long et al. 1994, Krause et al. 1995, Laing et al. 1995). Osmond (1994) named the first type 'chronic photoinhibition' and the latter, 'dynamic photoinhibition' (Alves et al. 2002).

Laboratory and field studies have shown that N-limited phytoplankton have greater dark N uptake rates than N-replete phytoplankton. Nevertheless, given the N abundant environment of the Southern Ocean, it is more likely that heterotrophic N uptake versus dark uptake drives this stress response (Cochlan et al. 1991, Cochlan 2008). Not only is the relationship between irradiance and N uptake in the Southern Ocean unclear, it is often fraught with inconsistencies, and most of our previous knowledge is based on comparison of specific N uptake rates measured at multiple depths throughout the euphotic zone utilising either *in situ* or replicated *in situ* irradiance fields (Cochlan 2008). As expected, maximal rates for both NO_3^- and NH_4^+ (and in some studies- urea) are regularly observed at the 100 or 50% isolumes, however maximal specific N uptake rates are also found at the low end of the light spectrum, 1.0- 0.1%% isolume (Cochlan 2008). Very few N uptake versus irradiance experiments have in fact been completed in the Southern Ocean thus enhancing the value of this particular study.

Although the P-E approach can be extended to examine light controls on nitrogen assimilation, this approach has received scant attention (Cochlan 2008). The current debate has focussed heavily on iron and light limitation of photosynthesis (Moore et al. 2007), but we know also that iron and light co-limitation play a significant role in N metabolism, particularly with regard to ρNO_3^-, which is considered more energetically expensive than reduced N assimilation (Lucas et al. 2007, Moore et al. 2007a &b). Conceptually, this becomes important because we suspect that at depth, ρNO_3^- becomes light-limited with respect to reduced N uptake, as often revealed by a declining f-ratio with depth (Lucas et al.

2007). However, the only real way to rigorously test this is by using a P-E approach combined with ^{15}N tracer studies on light-dependent uptake of both oxidised and reduced N species. If such an approach can be translated into quantifying new production at the basin scale using satellite remote sensing, this will be a considerable advance. While variation in P-E parameters may exist due to the above factors, it is still considered a valuable means of describing spatial and temporal patterns in light-dependent phytoplankton production. Furthermore, P-E relationships can be used to develop and verify province-based algorithms central to remote sensing of primary production in the Southern Ocean, as has been done elsewhere (Joint & Groom 2000, Platt et al. 2008). To gain a reliable estimate of global oceanic phytoplankton production, we need to scale local *in situ* measurements to the basin scale. This can be achieved by combining ocean colour remote sensing with *in situ* measurements, P vs. E relationships and regional algorithm development for specific bio-optical provinces (Platt and Sathyendranath 1988, Dower and Lucas 1993, Prince et al. 1995, MacFadyen et al. 1998, Moore and Abbott 2002, Demidov et al. 2007). The establishment of bio-optical provinces throughout the world oceans has progressed since the mid-90s, however, the south Atlantic sector of the Southern Ocean has yet to be described and verified according to its bio-optical properties.

1.7 Goals and Aims of this Study

Both the solubility and the biological pumps help mediate the climate by drawing CO_2 out of the atmosphere and into the surface waters and subsequently the deep sea. While the physicochemical processes operate on relatively shorter timescales (years to decades), biological responses take much longer (centuries to millennia) and are inherently more challenging to discern. The Southern Ocean, a unique and sensitive environment, known to sequester CO_2, is already undergoing marked change through the advent of more positive phases of the SAM, inducing increased upwelling and potentially causing this ocean to become a CO_2 source. While questions of this nature and how biological responses may give rise to or counter these changes is beyond the scope of this study, a significant contribution to 'ground truthing' the biology augments the increasing *in situ* database in a tempestuous and remote part of the world.

During the summer of December 2008 to February 2009 a survey on the *SA Agulhas* crossed six oceanic regions within the south Atlantic sector of the Southern Ocean, providing an opportunity to compare regional differences in the controls on phytoplankton primary production and export. In addition, this study provided a platform to test the light-dependent uptake of both oxidised and reduced N species utilizing ^{15}N tracer studies combined with the P-E method. For the purposes of this study the focus was on the role of irradiance in limiting phytoplankton productivity to help answer the following key questions:

1) What controls the spatial variability in phytoplankton biomass?

2) What do nitrogen assimilation rates reveal about light as a limiting factor?

3) What does the community composition and size based community structure indicate in terms of iron stress and ultimately, CO_2 sequestration?

4) What do P vs. E curves reveal about regional differences in the light dependant uptake of new versus regenerated production?

Answers to the above questions, in a section of the Southern Ocean that is infrequently sampled, provides a more comprehensive view of the factors influencing phytoplankton production and biomass distribution. Such information leads to an improved understanding of the Southern Oceans biological carbon pump, its role in the global ocean carbon cycle and how it is likely to respond to ongoing change. This thesis will address these questions over the course of three chapters. Chapter 2 will introduce the hydrography and nutrient environment across six regions of the Atlantic sector of the Southern Ocean and describe the spatial variability in phytoplankton biomass according to these regions. Chapter 3 will then address the role that light plays on primary production, nitrogen nutrition and phytoplankton assemblages according to these same regions and finally, chapter 4 will close with a thesis summary and concluding remarks.

Chapter 2. Regional distinctions in phytoplankton distribution with respect to hydrography and nutrients in the South Atlantic sector of the Southern Ocean

2.1 Introduction

The Southern Ocean has the greatest inventory of unused macronutrients in the World Ocean (Levitus et al. 1993), but low average phytoplankton standing stocks. Reasons for this include low surface temperatures (Froneman & Perrissinotto 1996a, Atkinson et al. 2001, Boyd 2002), light limitation (Behrenfield 2010, Venables and Moore 2011), deficiency of trace nutrients such as iron and silica (Boyd et al. 2000, Boyd et al. 2002, Arrigo et al. 2008), and grazing by micro- and meso-zooplankton (Froneman & Perrissinotto 1996a, Atkinson et al. 2001).

Regions of high seasonal rates of primary production and phytoplankton biomass do however exist within the Southern Ocean and these are often dominated by diatoms (Lucas & Probyn 1987, Tremblay et al. 2002). These high biomass regions are known for having the greatest rates of biogenic silicate deposition in any of the world oceans. Subsequently, the Southern Ocean is the oceanic province which exports (to 1000 m) the greatest proportion (~3%) of its total production (Honjo et al. 2008), thus making it inordinately important as a biologically mediated sink for atmospheric CO_2 in its more productive regions.

One of the crucial gaps in our understanding of the variability in phytoplankton distribution and production lies in our incomplete understanding of biological responses to physical forcing mechanisms that control the nutrient environment through upwelling and mixing processes, as well as the light environment through buoyancy controls of the mixed layer. Understanding the processes responsible for the variability of the mixed layer depth (MLD) and impacts on primary production is important as they are likely to change in a future characterised by global warming, leading to both positive and negative feedbacks in the global climate system (Sarmiento et al. 1998, Lovenduski et al. 2007).

2.1.1 Hydrographic Fronts and Zones

The south Atlantic sector of the Southern Ocean is one of the most energetic and important hydrographic regions of the world oceans. It is characterised by the close proximity of the Aghulhas retroflection, the Antarctic Circumpolar Current (ACC), the

marginal ice-edge zone (MIZ) and the highly dynamic Subantarctic island area in the western quarter, which is heavily influenced by local bathymetry and subsequent frontal meandering (Lutjeharms 1985, Ansorge et al. 2004, Olbers et al. 2004, Swart et al. 2010).

The ACC extends uninterrupted around Antarctica and is the strongest and longest current system in the world, driven primarily by westerly winds and geostrophic flow. The ACC is largely characterised by a number of circumpolar frontal jets of enhanced flow associated with strong meridional gradients of temperature, salinity and density, which separate zones of uniform water masses (Whitworth 1980, Orsi et al. 1995). South of South Africa the ACC is bounded to the north by the Subtropical Front (STF), and southwards by the Subantarctic Front (SAF), the Antarctic Polar Front (APF), the Southern ACC Front (sACCf), and the Southern Boundary (SBdy), which delineates the southern extent of the ACC (Figure 2.1). Frontal dynamics and variability associated with these fronts are now known to influence phytoplankton biomass as well as provide biogeographic barriers that separate their distribution (e.g. Levy et al. 2001, Klein & Lapeyre 2009, Levy et al. 2009, Sokolov & Rintoul 2007).

Regions between these fronts comprise six distinct oceanic domains. These are the Subtropical zone (STZ) (north of the STF), the northern ACC zone (N-ACC) (from the STF to the APF) comprising the SAZ and the PFZ, the Antarctic zone (AAZ) (from the APF to the Sbdy), the Weddell Gyre region (south of the SBdy to 68°S), and finally the shallow bathymetric regions associated with the Subantarctic islands (SAISB) and the Antarctic Continental shelf zone (ACS) (Treguer and Jaques 1992, Pollard et al. 2002). Each of these zones typically has a characteristic phytoplankton community structure and biomass resulting from variability in the physical forcing mechanisms that drives the nutrient and light environment.

The Subtropical Zone

The STZ is a highly dynamic region characterised by macronutrient limitation and low chlorophyll concentrations. Nutrients are however less limiting in winter when a deepening of the seasonal mixed layer replenishes surface nutrients allowing for a subsequent increase in winter chlorophyll-*a* concentrations. This region is also a major conduit for heat and salt transport from the Indian to the Atlantic Ocean. The Agulhas Retroflection current lies

directly north of the STF and serves as a source of salty warm water brought from the Indian Ocean to the Atlantic Ocean through frequent (about 9 per year) shedding of large Agulhas Rings (Lutjeharms 2006, Swart et al. 2011 *in press*). Recent work reveals the significant yet pervious role that Agulhas Rings have in influencing the position of the STF (Swart et al. 2011 *in press*). The STF forms the northern most boundary of the ACC and marks a dramatic change from warm (>~11.5°C) saline (>~34.9 psu) tropical waters to fresher (34.2 psu), cooler (<~10°C) sub-polar waters to the south. Annual mean chlorophyll-a concentrations range from 0.4 - 0.6 mg m^{-3} in winter, peaking at 1.0 mg m^{-3} in summer (Machu et al. 2005) Highest chlorophyll concentrations tend to be associated with the STF and eddy shedding by the Agulhas Retroflection or meandering frontal activity (Swart et al. 2011). Phytoplankton production is dominated by the microbial web whereby small cells out compete larger ones in low nutrient conditions due to surface area to volume ratios (Falkowski et al. 2008, Froneman & Perissinotto 2008). The implications for this are a very inefficient biological carbon pump in the STZ.

The Northern ACC Zone

The N-ACC extends from the STF to the APF, and thus includes the SAZ between the STF and the SAF and the PFZ between the SAF and the APF (see Figure 2.1). This region is characterised by fresher (~34.1 psu), cooler (~2-5°C), low productivity (0.5–1.0 gC m^{-2} d^{-1} in December [Arrigo et al. 2008]) waters found between fronts, as well as more productive (2 gC $m^{-2}d^{-1}$ [Ariggo et al. 2008]), stable waters at fronts. Enhanced chlorophyll concentrations (>1.0 mg m^{-3} Moore & Abbott 2000) associated with the major fronts have been well documented and attributed to a number of processes that include cross-frontal mixing of macronutrients, an improved light environment through enhanced stratification and increased Fe concentrations from upwelling and the interaction of the fronts with shallow topography (e.g. Lutjeharms et al. 1985, Laubscher et al. 1993, Moore and Abbott 2002). Although traditionally, enhanced chlorophyll concentrations have been associated with mesoscale activities at the frontal features, Sokolov and Rintoul (2007a) more recently revealed that multiple frontal branches delimit regions with similar elevated chlorophyll concentrations and seasonality, rather than the fronts themselves being associated with enhanced productivity, at least where fronts are distant from topography.

Sokolov and Rintoul (2007a) identified the frontal positions using high resolution satellite sampling of sea surface height (SSH) contours. This method allows fronts to be tracked on a larger, more refined spatial scale across large sectors of the Southern Ocean, as well as over weekly periods (Sokolov & Rintoul 2002, 2007a, Swart et al. 2008). This approach enabled a re-investigation of the correlation between surface chlorophyll, fronts and topography. The SAZ is distinguished by deep winter mixed layers, low silicate concentrations, and a phytoplankton assemblage primarily made up of coccolithophores, with few diatoms (Sokolov & Rintoul 2007b). The PFZ, typically shows less seasonal variation in the mixed layer depth compared to the SAZ, has surface waters abundant in macronutrients (nitrate, phosphate, & silicate) year-round, and a phytoplankton community largely comprised of diatoms (Sokolov & Rintoul 2007a).

The Antarctic Zone

The AAZ extends from the APF, characterized by a steep gradient in high biogenic silica content, seasonally prolific large diatom communities and where the northern extent of upwelled circumpolar deep water (CDW) occurs (Moore & Abbott 2002), to the SBdy of the ACC, where deeper mixed layers occur (~100 m) compared to the north (Joubert et al. 2010) and the southern limit of the oxygen minimum is associated with upper circumpolar deep water (UCDW) (Sokolov & Rintoul 2007) (Figure 2.1). The AAZ is most notable because of seasonal sea ice that greatly influences this region. The annual maximum of seasonal sea ice around Antarctica is 50 % greater than the continent itself and covers ~40% of the Southern Ocean at it greatest extent (Lizotte 2001). Highest chlorophyll concentrations are generally associated with the MIZ (Arrigo and van Dijken 2004). A flux of biogenic material from sea ice to the water column and benthos follows ice melt, and some of the sea ice algal species are known to occur in ensuing pelagic phytoplankton blooms. Relative dominance of these species could be important in determining their biogeochemical contribution to the Southern Ocean and their ability to seed blooms in marginal ice zones. The MIZ is a loosely defined term, but for the purposes of this study is described as the region of the pack ice which is significantly affected by ocean swell because of its proximity to the open ocean boundary. This may extend hundreds of kilometres from the ice edge and in some regions right up to the coast. It is an area of enhanced ice drift, deformation and divergence. Large scale annual estimates of primary production have

shown that as sea ice recedes during spring and summer, favourable conditions lead to phytoplankton blooms that persist for weeks and for hundreds of kilometres away from the ice edge. Favourable conditions include the formation of a shallow and stable surface mixed layer driven by fresh water input from ice melt (Smith Jr. & Nelson 1986). The shallow mixed layer creates an optimal light environment for phytoplankton production by favouring increases in specific growth rates that exceed export and losses through grazing, resulting in biomass accumulation (Sverdrup 1953, Mitchell et al. 1991, Comiso et al. 1993). In addition, ice melt is known to provide seed populations of algae (Lizotte 2001) and release stored dissolved Fe (dFe) (de Baar et al. 2005) which fuels primary production (Sedwick and DiTullio 1997, Gao et al. 2003, Grotti et al. 2005, Lannuzel et al. 2008). There are a number of possible sources of this Fe, including aeolian dust originating from Patagonia, ice-sheet contact with the Antarctic continent, or from ice bergs that have run aground over the continental shelf (Klunder et al. 2011). Equally important is the impact of seasonal ice growth and retreat on underwater irradiance for phytoplankton production (Vernet et al. 2008).

The Weddell Gyre

Situated in the Atlantic Sector of the Southern Ocean, the Weddell Gyre is an elongated, mainly wind-driven, cyclonic gyre south of the ACC. Water flows westwards along the southern limb and eastwards along the northern limb of the gyre. Due to its divergent nature, Ekman forcing causes major upward transport of subsurface water in the gyre's centre (Bakker et al. 2008). This circumpolar deep water is enriched with dissolved inorganic carbon (DIC) and nutrients (Hoppema et al. 1997, Bakker et al. 2008). Seasonal ice coverage also strongly influences the cycling of chemical species and biological processes in this region. For example, chlorofluorocarbons (CFCs) and oxygen (O_2) are under-saturated, but CO_2 is over-saturated in ice-covered Weddell Gyre surface waters relative to their atmospheric concentrations (Bakker et al. 2008), indicating that ice caps the water column, thus hindering air-sea gas exchange. Seasonal ice coverage is a significant feature of the Weddell Gyre region. This typical pattern of ice formation and retreat differs longitudinally in the Weddell Gyre, where in the far west perennial ice is found, while towards the east, the vast ice field disappears rapidly in late spring and early summer due to the highly dynamic hydrography of this region (Bakker et al. 2008). Large, pronounced phytoplankton

blooms can occur in the centre of the WG region (Moore & Abbott 2000). Such high biological activity can lead to an effective biological pump resulting in a net CO_2 sink in the gyre centre in summer despite the upwelling of CO_2 rich, CDW (pers. comm. Sandy Thomalla & Pedro Monteiro). However, it is important to note that algal blooms are not intrinsic to sea ice retreat. Variability in bloom formation is more likely as ice recedes because of varying degrees of wind speed (and thus mixed layer depth), differences in Ekman-induced upwelling/downwelling by the winds, and differential accumulation of atmospheric dust on the ice (which affects the amount of iron released to the water column during melting) (Moore & Abbott 2000).

Subantarctic Islands and Shallow Bathymetry Regions

Other areas of high rates of seasonal phytoplankton production (chlorophyll values exceeding 1.0 mg m^{-3}) are in close proximity to the continental and Subantarctic island margins (from here referred to as the SAISB region) (Ward et al. 2005). Here, runoff from the land masses or upwelled macro and micro nutrients (SiO_4, NO_3, PO_4, dFe) fuel phytoplankton productivity that are in stark contrast to the Fe-limited HNLC open ocean zones (Moore & Abbott 2000, Ward et al. 2005). For example, at the Crozet Islands, downstream increases in dFe from both benthic sediments and from island run-off result in elevated nitrate uptake and new production by diatom-dominated phytoplankton blooms, as revealed by high (>0.5) f-ratios (Lucas et al. 2007, Pollard et al. 2009). Moreover, regionally elevated new production rates are thought to stimulate the avifaunal and benthic community food webs, thus promoting a local and seasonal CO_2 "sink", as is evident at the Crozet islands (Bakker et al. 2007). The South Sandwich Islands and South Georgia, located in the NE Scotia Sea, is another example of a biological 'hotspot' where despite their small area relative to the greater Atlantic sector of the Southern Ocean, they provide a rich source of nutrients and seeding of blooms downstream (Ward et al. 2005). Regions such as these create important areas for local but significant POC export and biological CO_2 draw-down in a predominantly HNLC Southern Ocean (Lucas et al. 2007). In these regions of shallow bathymetry, current flow through relative vorticity (Hogg and Blundell 2006, Moore et al. 1999) and/or bottom pressure torque (Sokolov and Rintoul 2007a) is believed to increase the flux of Fe into surface waters (Park et al. 2010, Venables and Moore 2010) which explains the commonly found inverse correlation between depth and chlorophyll in the

Southern Ocean (Comiso et al. 1993). These areas are in stark contrast to the open ocean zones, notorious for being dessert-like, where any combination of limitations including dFe, SiO4 and/or light maintains the HNLC condition.

Antarctic Continental Shelf Zone

The ACS is confined to waters that overlie the continental shelf south of 68°S (Treguer and Jaques 1992, Orsi et al 1995, Arrigo et al. 2008). It is distinguished as a highly productive area in the Southern Ocean where spring/summer chl-*a* concentrations can reach 10 mg m^{-3} (Figuerora 2002, Vaillancourt et al. 2003). These high chl-*a* concentrations are thought to result from dFe and particulate Fe inputs from the ice shelf, melting bay ice, ice bergs (Arrigo et al. 2008, Klunder et al. 2011) and resuspension of continental shelf sediments (Johnson et al. 1999, Grotti et al. 2005). A consequence of the melting ice is a fresher, more stable water column structure allowing for favourable phytoplankton growth conditions (Lizotte et al. 2001). The combination of characteristically high dFe supply (Lannuzel et al. 2008) and improved mean light conditions in the surface mixed layer (Moore and Doney 2006, Arrigo and van Dijken 2004, Sokolov 2008) results in some of the most intense phytoplankton blooms and associated high chl-*a* concentrations of all the southern ocean zones (Moore & Abbott 2000). As an example of the influence of the continental shelf, the semi-enclosed Ross Sea is characterised by strong seasonal blooms of diatoms and *Phaeocystis Antarctica* where maximum surface chl-*a* concentrations have reached 10 – 20 mg m^{-2} during a summer bloom event (Arrigo & Van Dijken 2007).

2.1.2 The Current Study

This study takes advantage of four research cruise transects in summer 2008-2009 that crossed the six distinct biogeochemical provinces described above. The data collected addresses the causes of regionally distinct phytoplankton distribution through changes in hydrography that influences the available macronutrient and light environment. The four transects were as follows: Leg 1) Cape Town to Antarctica, Leg 2) Antarctica to South Georgia, Leg 3) the reciprocal southbound transect from South Georgia to Antarctica and Leg 4) the northbound return leg from Antarctica to Cape Town (see Figure 2.1). Results from this study investigate the main drivers that account for the variability in phytoplankton biomass distribution and the implications for CO_2 flux. In so doing, the response of the

Southern Ocean's biological carbon pump to adjustments in the climate can be better understood and predicted.

2.2 Methods

2.2.1 Study Area and Cruise Track

The South African National Antarctic Expedition (SANAE 48) was carried out on the MV *SA Agulhas* during austral summer (23 December-2 March) of 2008-2009. Four physical oceanography transects were carried out, three of which included biological sampling. The first leg from Cape Town to SANAE (23 December – 04 January, 34°S, 14°E to 70°S, 2°W) was primarily concerned with underway hydrographic sampling of surface waters due to the ship's main role as logistical transport of materials and people to the SANAE base. The second and third legs, however, were dedicated to biological and oceanographic research where station time was available. Leg 2, a northwest track to the South Sandwich and South Georgia Islands (26 January – 02 February, 70°S, 2°W to 52°S, 32°W) and Leg 3, the southeast reciprocal leg from South Georgia Island to SANAE (02 February – 09 February, 52°S, 32°W to 70°S, 2°W) provided the main focus of the biogeochemical observations with both underway and water column sampling using a CTD and in-line messenger triggered 20L General Oceanics sampling bottles. Unfortunately, however, due to winch system failure at the outset of Leg 2, water column sampling was not possible, such that only surface waters (to~5m) were sampled thereafter. The lack of CTD data on legs 2 and 3 prompted additional biological stations on the return leg 4 from SANAE to Cape Town (21 February – 05 March, 70°S, 0° to 37°S, 14°E).

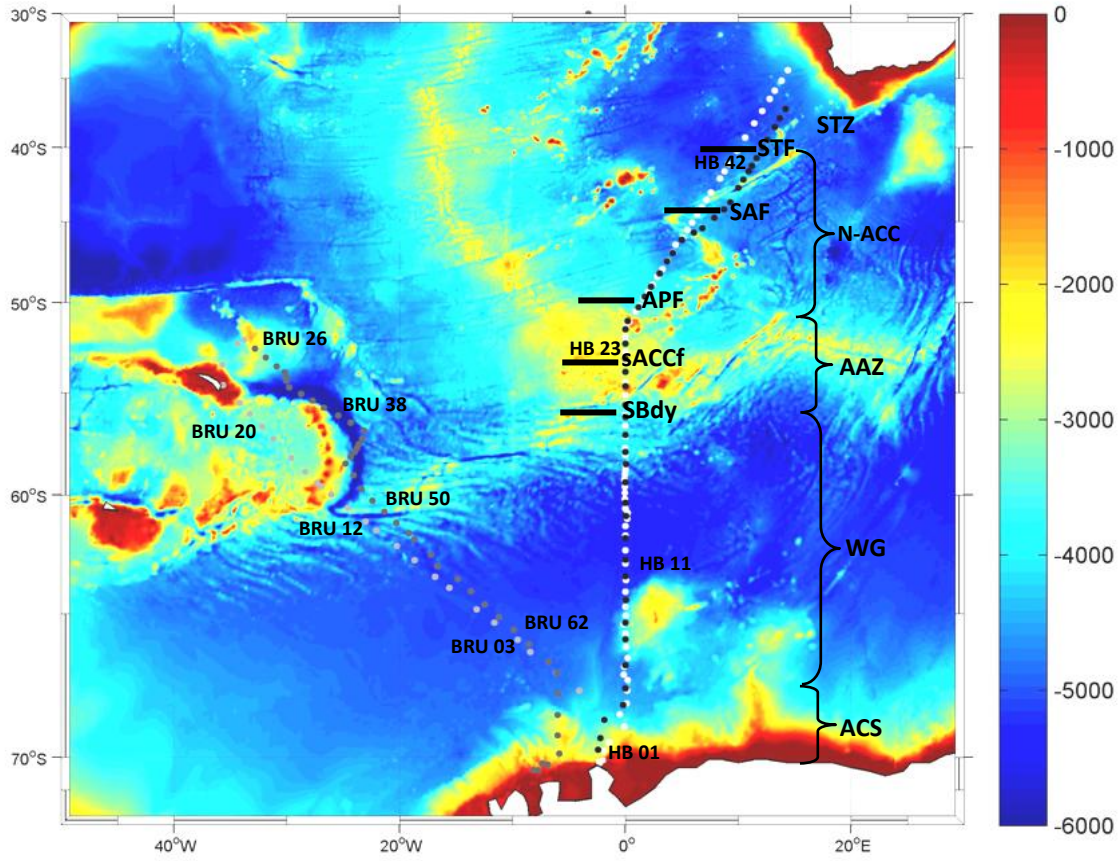

Figure 2.1. Map of cruise track (discrete sampling stations and black labelled productivity stations) overlaid on seafloor bathymetry. The scale bar represents ocean depth in metres. The four legs are represented by progressively darker symbols: Leg 1 from Cape Town to Antarctica in white; Leg 2 from Antarctica to South Georgia Island in light grey; Leg 3 from South Georgia Island to Antarctica in dark grey; Leg 4 from Antarctica to Cape Town in black. Frontal positions, determined for Leg 4, are displayed on the map and brackets delineate zones the study region has been divided into. Fronts from north to south: Subtropical Front (STF), Subantarctic Front (SAF), Antarctic Polar Front (APF), Southern ACC Front (sACCf) and the Southern Boundary of the ACC (SBdy). Zones from north to south: Subtropical Zone (STZ), Northern ACC Zone (N-ACC), Antarctic Zone (AAZ), Weddell Gyre (WG) and Antarctic Continental Shelf Zone (ACS).

2.2.2 Discrete Underway Measurements

On Leg 1 from Cape Town to SANAE, discrete underway samples for nutrients (NO_3, SiO_4, PO_4) and , chlorophyll-*a* were taken from the uncontaminated surface (~5 m) sea water supply in the aft semi-wet lab. Following the winch failure, no CTD's were possible, so an alternative water source for all biological measurements was required. Although the uncontaminated underway lab supply was considered suitable for chemical properties (e.g. nutrients), it was not clear how much stress or damage individual cells would encounter while being pumped from the engine room to the lab. As intact and unstressed cells are

essential for primary production incubation experiments, an alternate water source was sampled directly from the engine room (also at ~5 m). This water source consisted of an inlet pipe from the port side hull of the ship which opened and closed via a valve. As this water source was not subjected to pumping forces or pre-filters, it was considered suitable for incubation experiments. To provide appropriate ancillary biogeochemical variables, this water source was also used for all subsequent nutrient and biological sampling (Legs 2, 3 and 4).

2.2.3 Hydrography

Frontal positions

Temperature profiles to 800 m were obtained at a 20 nautical mile resolution (10 nm across fronts) using Sippican 'Deep Blue' Expendable Bathythermograph's (*XBTs*) on Legs 1 and 4. Data were processed using MATLAB to construct temperature sections and frontal positions were defined according to Orsi et al. (1995) who defined the fronts according to subsurface temperature criteria. Due to the absence of water column temperature data for Legs 2 and 3, fronts were identified using Sea Surface Height (SSH) data from satellite altimetry. The SSH information was derived from the 'Maps of Absolute Dynamic Topography' (MADT) produced by AVISO. This method uses the entire historical weekly dataset to identify the position of the maximum SSH gradient and the associated MADT value/contour where this maximum is found (Swart et al. 2008). Using the frequency distribution of all historical data, an optimised MADT contour is selected to best describe the position of the front and this contour is used to identify frontal positions on weekly maps (Swart et al. 2008). Sea surface temperature (SST) and salinity were recorded underway on the pCO_2 instrument every minute and the data presented have been averaged over 5 minute intervals.

Mixed layer depth

Mixed layer depth (MLD) was calculated from the vertical temperature structure of the water column. MLDs for Legs 1 and 4 were defined as the depth where ΔT°C was >0.2°C relative to the temperature at 10 m, as outlined by De Boyer-Montegut et al. (2004).

However, where stratification becomes dominated by salinity in the MIZ, this reduces the integrity of this proxy as a measure of MLD, so caution must be exercised.

Sea Ice Concentration

Daily sea ice concentrations were downloaded from the AE_SI25.2 dataset (Cavalieri et al. 2004) at the National Snow and Ice Data Centre (NSIDC) Data Pool website: http://nsidc.org/data/data_pool/index.html. These data come from the Advanced Microwave Scanning Radiometer - Earth Observing System (AMSR-E) instrument on the NASA Earth Observing System Aqua satellite. The data are a level-3 gridded product, mapped to a polar stereographic grid at a spatial resolution of 25 km. Images were constructed using the M_MAP mapping package in MATLAB.

2.2.4 Nutrients

Nitrate (NO_3^-), Silicate ($Si(OH)_4$), Phosphate (PO_4^{3-}), ammonium (NH_4^+) and urea measurements were made according to the manual spectrophotometric method described in Grasshoff et al. (1983) and Parsons et al. (1984), scaled to a 5 ml sample volume. On leg 1, only NO_3, $Si(OH)_4$ and PO_4^{3-} concentrations were determined as no productivity measurements were performed. Nitrate concentrations were determined colourimetrically after reduction to NO_2 on a cadmium column and corrected for ambient NO_2 (Nydahl 1976). On Leg 3 of the cruise the light bulb of the spectrophotometer blew and 17 nutrient samples (BRU60 to BRU77) had to be frozen until a replacement bulb was delivered in time for Leg 4.

2.2.5 Phytoplankton Biomass

Chlorophyll-*a*

Throughout this dissertation chlorophyll-*a* (chl-*a*) concentrations are used as a proxy for phytoplankton biomass. The limitations in using chl-*a* are well known, most markedly the fickle C:Chl-*a* cellular ratios of phytoplankton (De Baar et al. 2005, Seeyave et al. 2007, Mills et al. 2010). But despite this variability, chl-*a* prevails as the most practical measurement of phytoplankton biomass and distribution. Chl-*a* samples were collected by filtering 250 ml of seawater through 47 mm glass fibre filters (Whatman GF/F). The initial aim was to measure total chl-*a* fluorometrically on board the ship using a Turner Designs fluorometer, calibrated with fresh chlorophyll standard (Sigma, UK) and set up to measure chl-*a* in the presence of

chl-*b* following Welschmeyer (1994). However, as the fluorometer was malfunctioning, chl-*a* filters were stored at -29^{o}C for later analysis ashore at the Marine and Coastal Management facilities. The samples were homogenized in 10 ml of 90% acetone, centrifuged and measured on a Turner Designs Flourometer calibrated with fresh chl-*a* standards (Sigma, UK) following the Welschmeyer (1994) protocol. Size-fractionated chl-*a* analyses were carried out for 9 of the 11 primary production surface samples. Total chl-*a* was filtered directly onto a Whatman GF/F filter. The <20 µm fraction was pre-screened through a 20 µm mesh screen and then filtered onto a GF/F filter. The < 1 µm fraction was filtered through a 25 mm Nucleopore membrane filter and then onto a GF/F filter. These sizes classes were used to delineate the micro- (>20 µm), nano-(1-20 µm) and picoplankton (<1 µm) size fractions. Where corresponding High Performance Liquid Chromatography (HPLC, see chapter 3) and chl-*a* data were available (Legs 2, 3, and 4), chl-*a* concentrations were compared as a means of quality control. At four stations on Legs 2 and 3, noticeable differences were observed between chl-*a* concentrations derived from fluorescence and HPLC (BR1, BR26, BR60 and BR64). As the HPLC derived values were more consistent with the relative spatial trends seen in the chl-*a* distribution, HPLC values have replaced the fluorescence values for those four stations. HPLC derived chl-a concentrations are however frequently lower than those determined fluorometrically (e.g. Arrigo et al. 2008). A regression analysis of both chl-*a* data sets (excluding the four outliers) confirmed that the HPLC derived chl-*a* concentrations were generally ~15% lower than those derived by fluorometry. Accordingly, the substituted chl-*a* data (from HPLC) have been corrected using the regression equation in Figure 2.2.

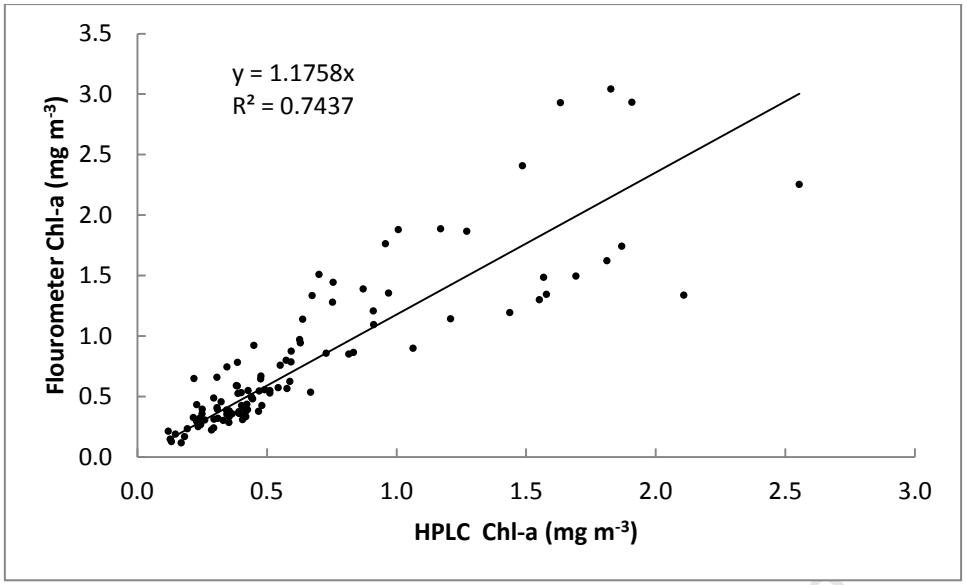

Figure 2.2 Regression analysis of Fluorometer versus HPLC derived chlorophyll-a (n = 108).

Satellite Chlorophyll-*a*

A monthly mean composite of chl-*a* concentration for the months of December 2008, January and February 2009 were created using the GlobColour Project website, http://www.globcolour.info/data_access.html. The Full Product Set (FPS) data set consists of ocean colour merged data products using the merging algorithms recommended at the first GlobColour workshop in Villefranche Sur Mer (France) on the 4-6 December 2006. The FPS includes level 3 merged products as monthly averaged products mapped on a Grid/Projection of 4.63 km equal area bins on an integerised sinusoidal grid. Satellite images from MERIS, MODIS and SeaWiFS products are merged using a Global Simulation Model (GSM) method. Images were constructed using the M_MAP mapping package in MATLAB.

2.3 Results

2.3.1 Hydrography

Water column structure north of the STF was highly stratified on Leg 1. Later in the season stratification is even more pronounced in the subtropical zone (Leg 4) and mixed layer depth shoals. Stratification breaks down south of the SAF (Leg 1) and closer to the APF (Leg 4). Subducting cold water (~1-2°C) reaches the surface south of the Sbdy (~60°S) on Leg

1 and remains submerged below warmer water (~3-4°C) in this area on Leg 4 (Figures 2.3 a & b).

Frontal positions

Temperature sections constructed from XBT profiles together with the five frontal positions (STC, SAF, APF, sACCf, SBdy) are shown for Leg 1 (Figure 2.3a) and Leg 4 (Figure 2.3b) and listed in Table 2.1 (Orsi et al. 1995). Between Legs 1 and 4 all front positions remained the same with exception of a slight southerly shift of the SBdy on Leg 4 (Table 2.1).

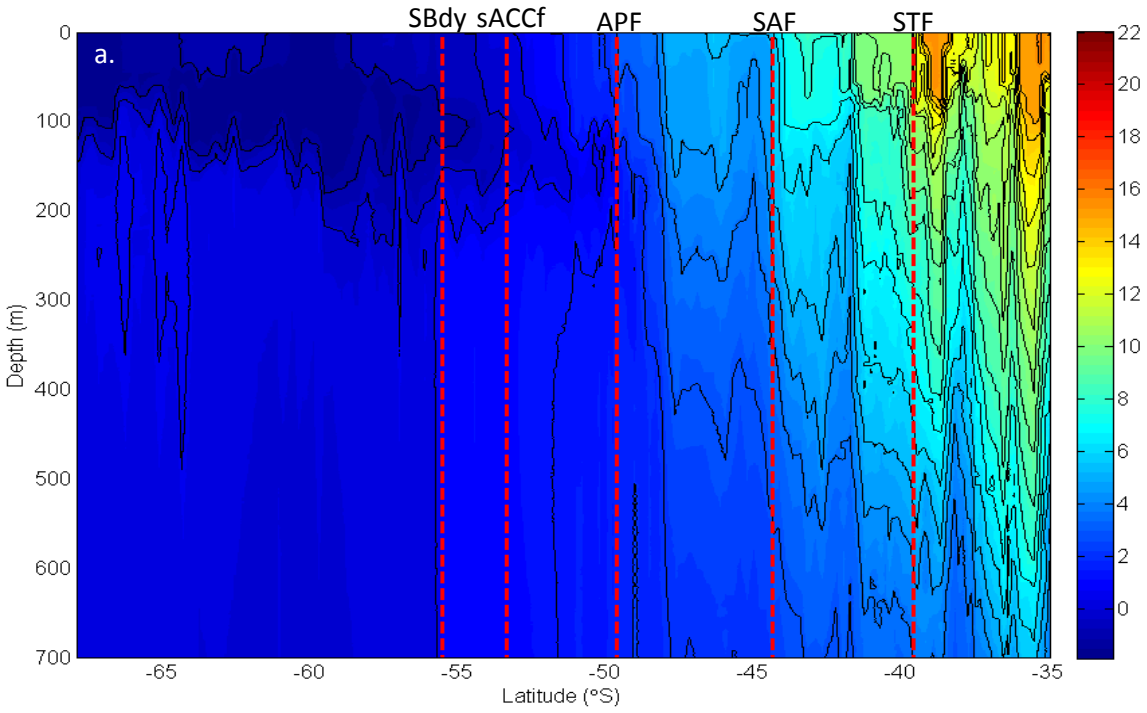

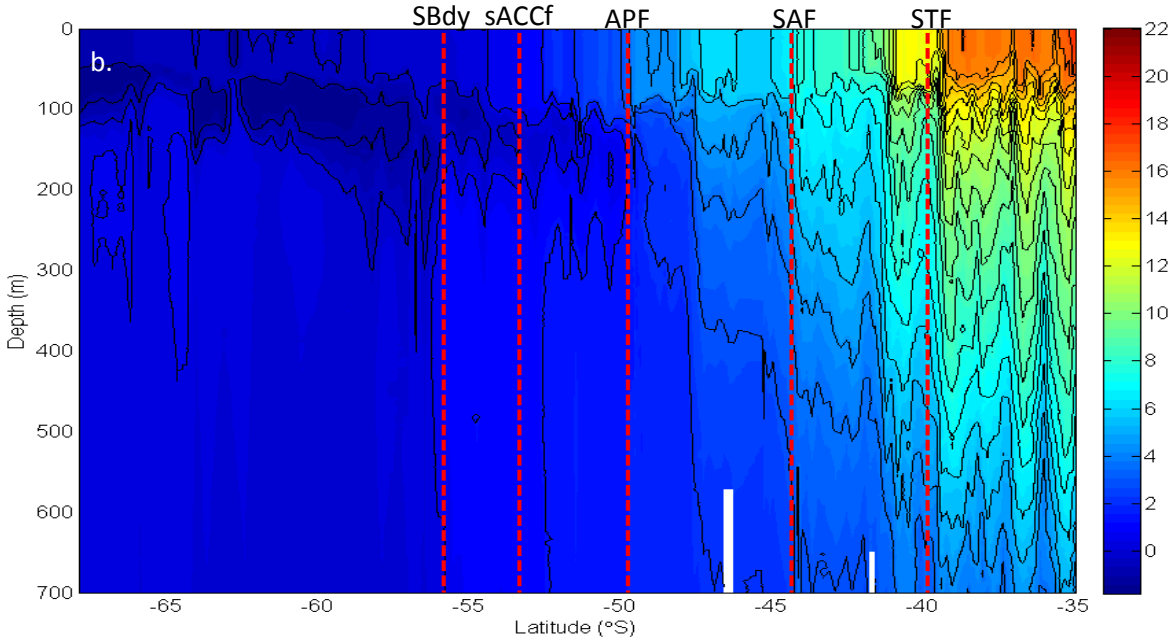

Figure 2.3a & b. Temperature sections for Leg 1 (a) and Leg 4 (b) constructed from XBT data. Fronts are illustrated by red dashed lines. From north to south: Subtropical Front (STF), Subantarctic Front (SAF), Antarctic Polar Front (APF), Southern ACC Front (sACCf) and the Southern Boundary of the ACC (SBdy). The colour bar represents temperature in °C.

The positions of the two fronts on transect Legs 2 and 3 (SBdy, sACCf) are shown in figure 2.4 and listed in table 2.1. After passing south of South Georgia (36°W), the SBdy and sACCf turn north and then back on themselves, returning to their initial latitude (56°S and 57°S, respectively). During Leg 3, the ship's track crossed the SBdy on 3 occasions and for a time travelled along it (Figure 2.3b). This period (55.8-56.7°S) is represented throughout this dissertation by the space between the vertical black dashed lines marking travel along the SBdy.

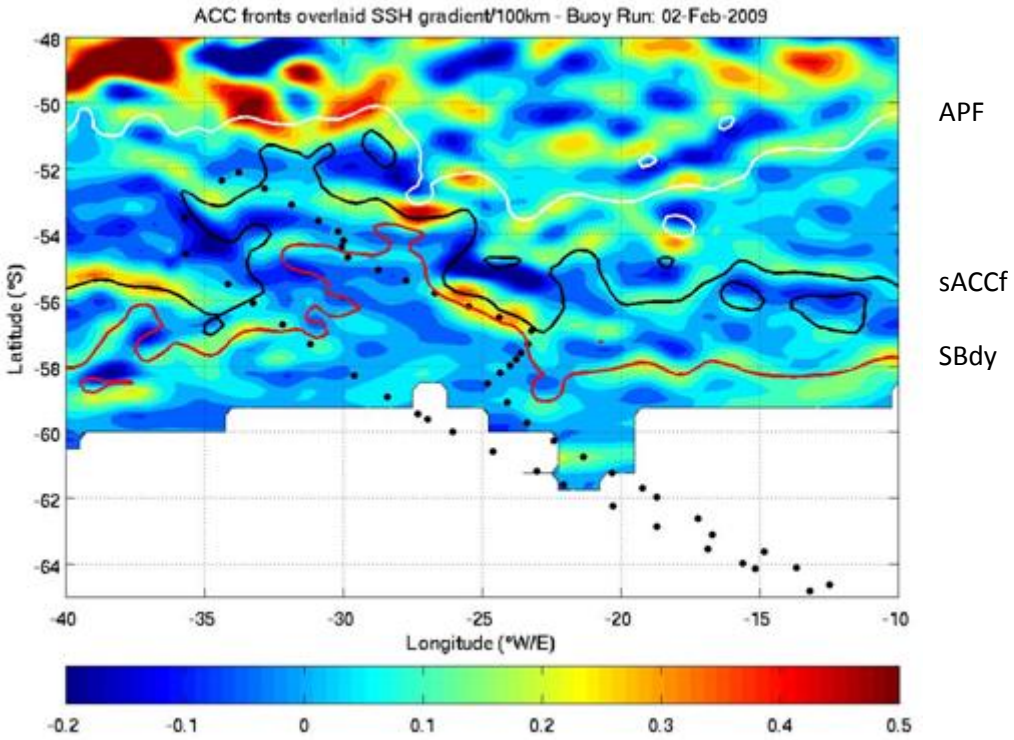

Figure 2.4 Frontal positions for Legs 2 and 3 identified using sea surface height gradients constructed from Maps of Absolute Dynamic Topography (MADT). The white line represents APF, black the sACCf and red the SBdy. The colour bar represents the gradient in metres in sea surface height (SSH) per 100km. The values followed in the MADT for each front are: APF: -0.8058 m, SACCF: -1.0434 m, and the SBdy: -1.1748 m.

The frontal positions derived from both approaches (temperature sections and SSH) shows very good agreement with their classical positions (Orsi et al. 1995) (Table 2.1). Marginal exceptions are on Leg 1 and 4 where the SAF is north of the classical position by ~3°and on Leg 1 and 4 where the sACCf is south of the classical position by ~1° and on Leg 2 where the sACCf is south of the classical position by ~4° (Table 2.1).

Table 2.1 Classical and cruise related frontal positions according to subsurface temperature criteria of Orsi et al. (1995) together with satellite altimetry based estimates of frontal positions according to SSH contours, between 1992-2009, reproduced from Swart et al. (2008). STF is the Subtropical Front, SAF the Subantarctic Front, APF the Antarctic Polar Front, sACCf the southern ACC front, SBdy the southern boundary of the ACC front and θ is potential temperature.

Front	Temperature Criteria	Classical Position (° S)	Leg 1 (° S)	Leg 2 (°S)	Leg 3 (° S)	Leg 4 (° S)
STF	10°C < θ100m < 12°C	39.6	39.9	n/a	n/a	39.9
SAF	θ > 4-5°C at 400m, farther north	47.6	44.4	n/a	n/a	44.4
APF	θ < 2°C along θmin at z <200m, farther south	49.6	49.7	n/a	n/a	49.8
sACCf	θ < 0°C along θmin at z <150m, farther south	52.4	53.4	56	52.6	53.4
SBdy	Southern limit of vertical Maximum of θ > 1.5°C, (~200m)	56.1	55.6	57	54.3, & along edge until 57.3	55.9

Sea Surface Temperature and Salinity

Surface plots of SST and salinity for Legs 1 and 4 are depicted in figure 2.5a,b. SST in the STZ is >20°C and decreases across the ACC to <0°C in the AAZ. A simultaneous decline in salinity occurs from north (~35.5 psu) to south (<34 psu). There is noticeable variability in SST south of the SBdy, while salinities from the APF to the SBdy are continually low. The position of the STF and the SAF coincide with striking gradients in SST and surface salinity. Salinities between the SBdy and APF are again consistently fresher than values to the south of the SBdy, apart from waters against the ice shelf. In Both Leg 1 and 4 there was an exceptionally low decrease in salinity (~33.5 and 34psu, respectively) at ~61°S in the WG region (see feature delineated on Figure 2.5 a, b).

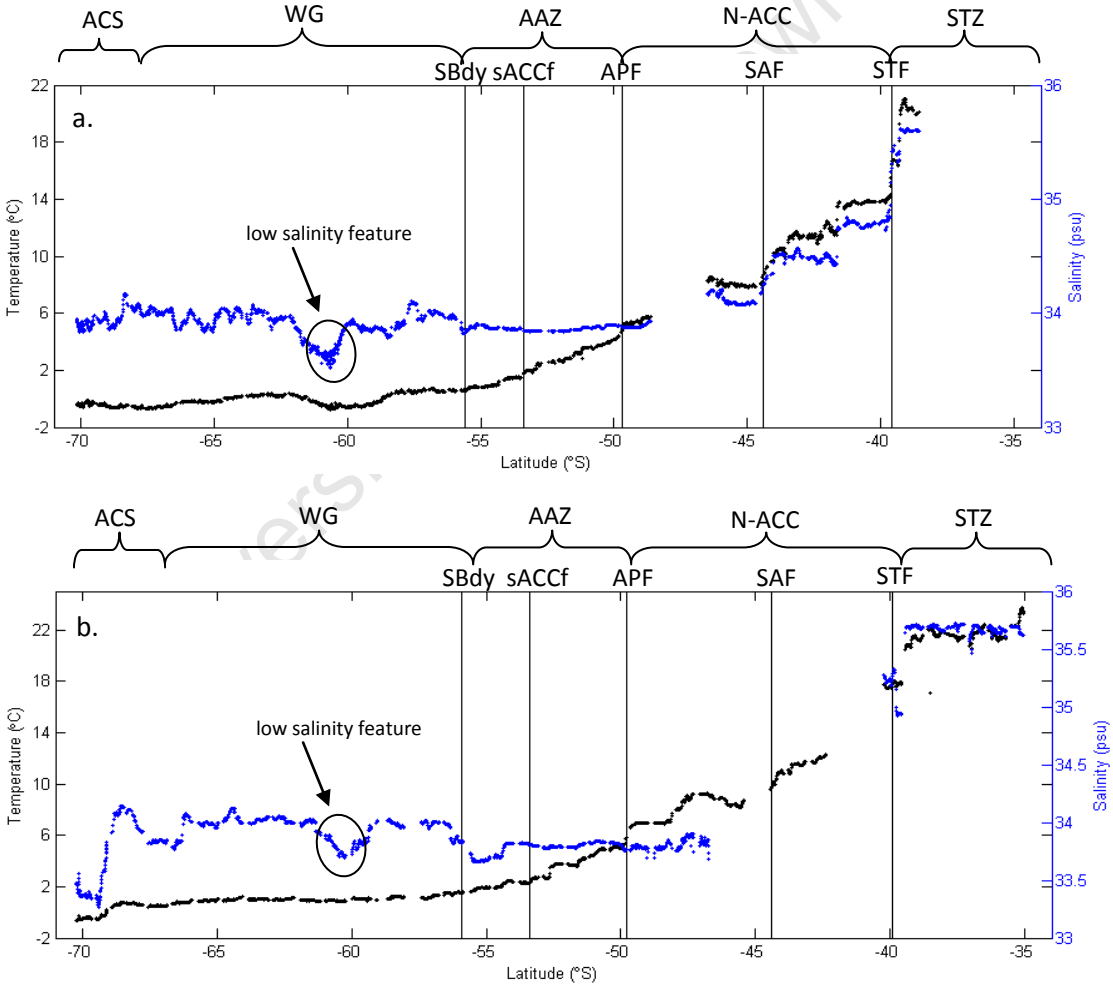

Figure 2.5a & b. Leg 1 and 4 sea surface temperature (black) and salinity (blue). Vertical lines indicate the position of the STF, SAF, APF, sACCf, & SBdy. Brackets on top of the figure indicate the regions: STZ, N-ACC, AAZ, WG, & ACS. The position of the low salinity feature within the WG is indicated.

Along Leg 2, SST rises from <0°C at the southern extent of the transect to ~6°C in the north (Figure 2.6a). Decreased salinities were detected south of 68°S, at ~60.5°S (also

associated with a rise in SST), ~54.5°S and north of the SBdy in the ACC. Along Leg 3 (Figure 2.6b), decreased salinity is evident near the ice shelf (~70°S). There is also a decrease in SST between 58 and 59°S that is coincident with a shallow bathymetric feature in the WG region. Again on both Legs 2 and 3 a very low salinity feature (< 33.5 psu) occurred at ~61°S in the WG region (see feature delineated on Figures 2.6a,b). It appears to be a common characteristic of all 4 legs.

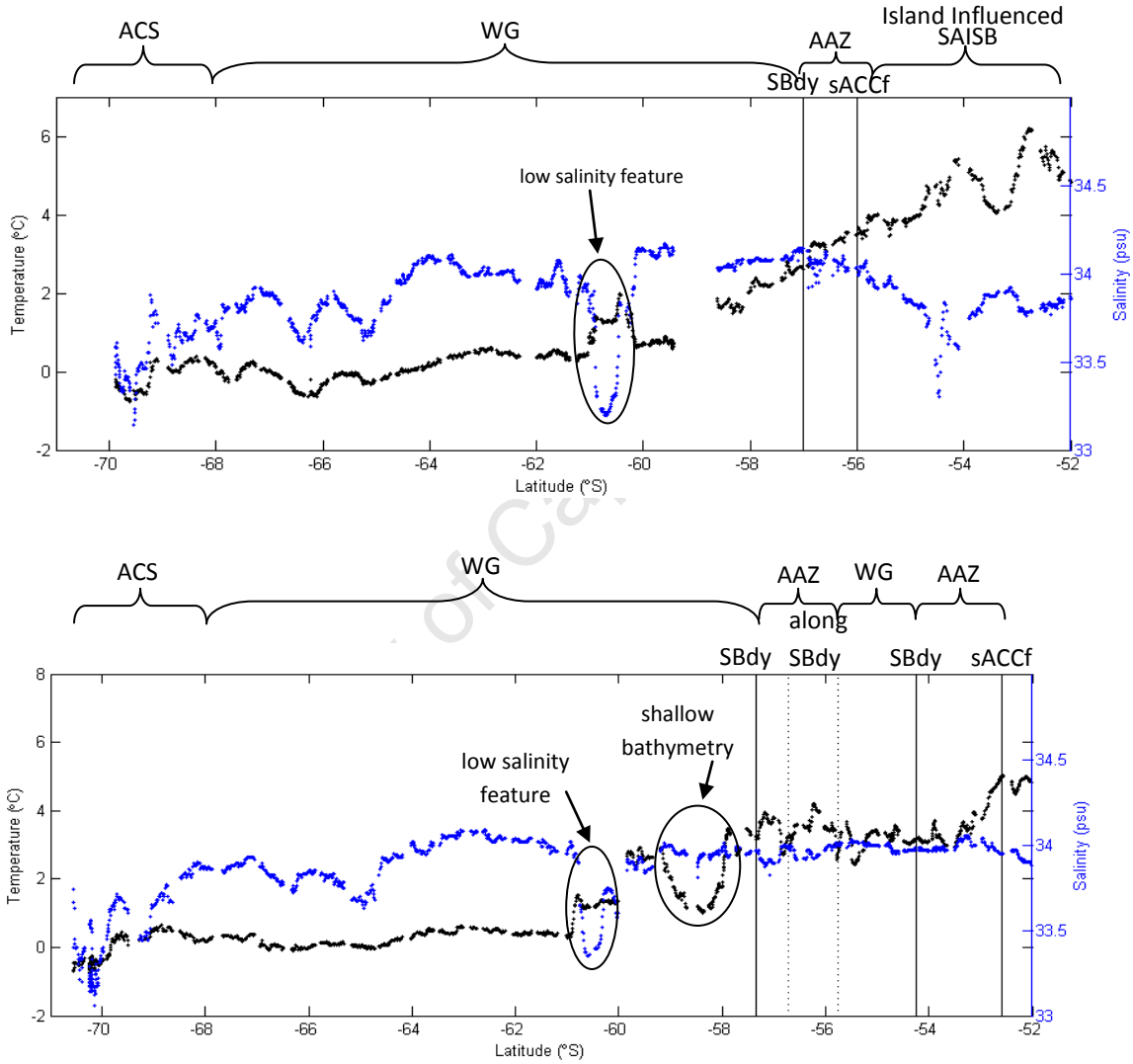

Figure 2.6a & b. Legs 2 and 3 surface temperature (black) and salinity (blue). Vertical lines indicate the position of the STF, SAF, APF, sACCf, & SBdy. Sampling along the SBdy is indicated by the region in between the vertical dashed lines. Brackets on top of the figure indicate the regions: STZ, N-ACC, AAZ, WG, & ACS. The position of the low salinity feature within the WG is indicated.

Seasonal Sea Ice Extent and Retreat

Daily sea ice coverage around Antarctica is depicted in figures 2.7 a-h for the 1st of November, the 15th and 22nd of December 2008; the 1st, 15th and 22nd of January and the 1st

and 15th of February 2009. In the beginning of December, intact sea ice surrounds the continent (Figure 2.7a), by the 15th of December the sea ice begins to break up and leads in the sea ice begin to appear (Figure 2.7b). Sea ice in the eastern Weddell Gyre melts faster than in the west, where the Weddell Sea remains ice-covered throughout the summer (Figures 2.7b-h).

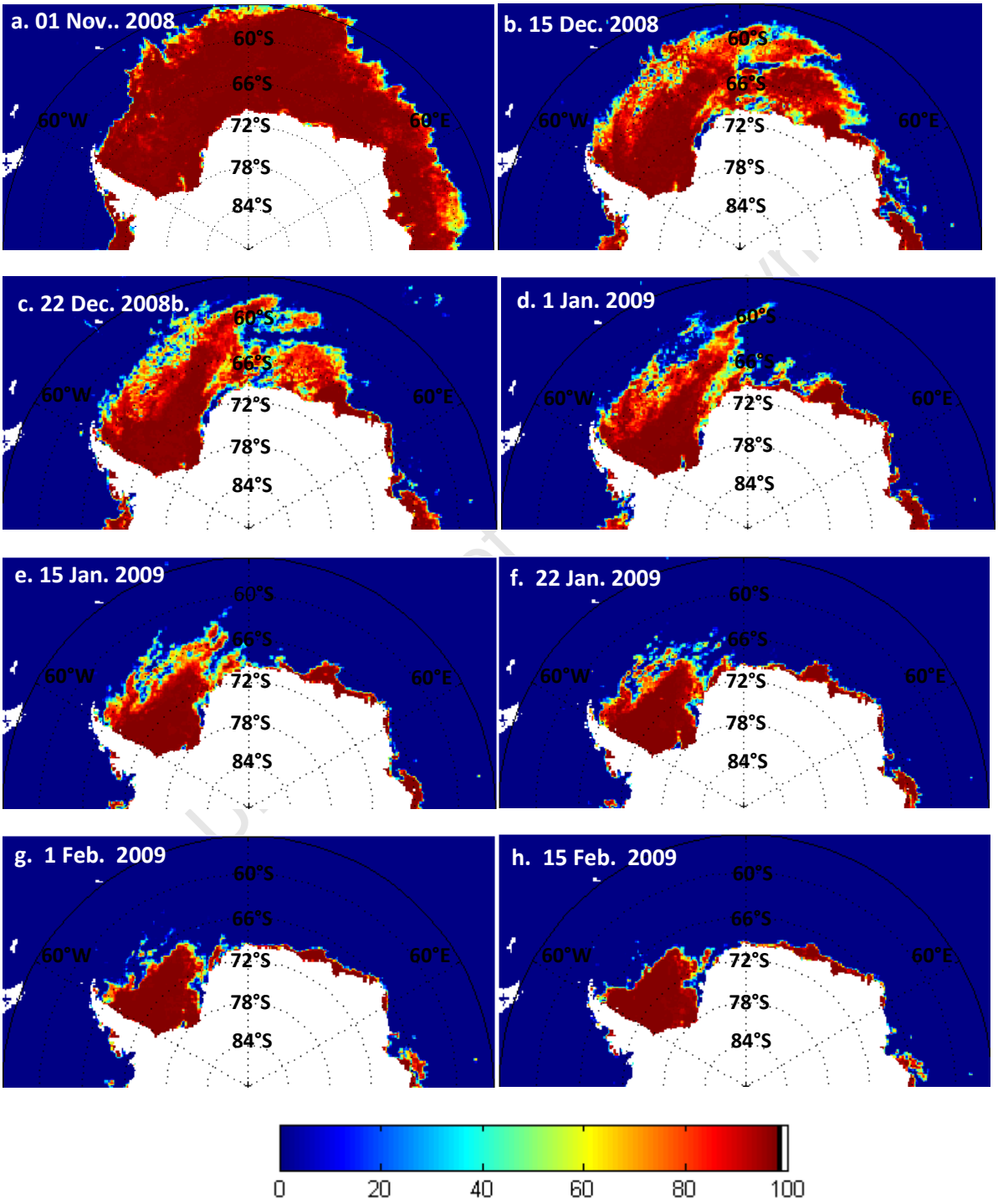

Figures 2.7 a-h. Daily Sea ice concentration (% represented by the colour bar) images for 8 selected days during austral summer of 2008-09.

During Leg 1 the ship travelled through the plume of ice just south of 60°S along the prime meridian on the 31st of December 2008 (Figure 2.7d) reaching the shelf on the 4th of January 2009. The ship departed the ice shelf on the 26th of January 2009 for the start of Leg 2, here the least amount of ice was encountered while in close proximity to the continent. The ship returned to Antarctica on 9th February 2009 where late summer conditions persisted and very little ice was present.

2.3.2 Nutrients

Cape Town to Antarctica (Leg 1)

All nutrients were low throughout the Subtropical Zone (Figure 2.8a). At the STF, nitrate starts to increase to a range of 10-18 µmol l^{-1}. In the N-ACC region (where the SAF the APF are crossed) nitrate concentrations increase to 22 µmol l^{-1} and reach peak concentrations (20-35 µmol l^{-1}) throughout the AAZ, WG and ACS zones. Silicate concentrations start to increase from the APF and peak (35 µmol l^{-1}) after crossing the sACCf in the AAZ there high concentrations are maintained throughout the WG and ACS. There is one notable decline in silicate and nitrate concentrations at ~61°S, in the WG region coincident with the low salinity feature referred to above and marked on figure 2.8a. Phosphate concentrations were between 0-2 µmol l^{-1} for the entire length of this transect. Maximum concentrations of 2 µmol l^{-1} occurred from the APF southwards. A notable decline in the WG region coincided with a decline in nitrate and silicate at ~61°S.

Antarctica to Cape Town (Leg 4)

Nutrient concentrations follow a very similar pattern to Leg 1, where peak concentrations occur south of the APF, in the AAZ, WG and ACS regions (Figure 2.8b). Notable peaks in silicate occur at the sACCf (23 µmol l^{-1}) and in the ACS zone (35 µmol l^{-1}). Ammonium and urea concentrations are highly variable with one notable peak in ammonium at the STF (2 µmol l^{-1}).

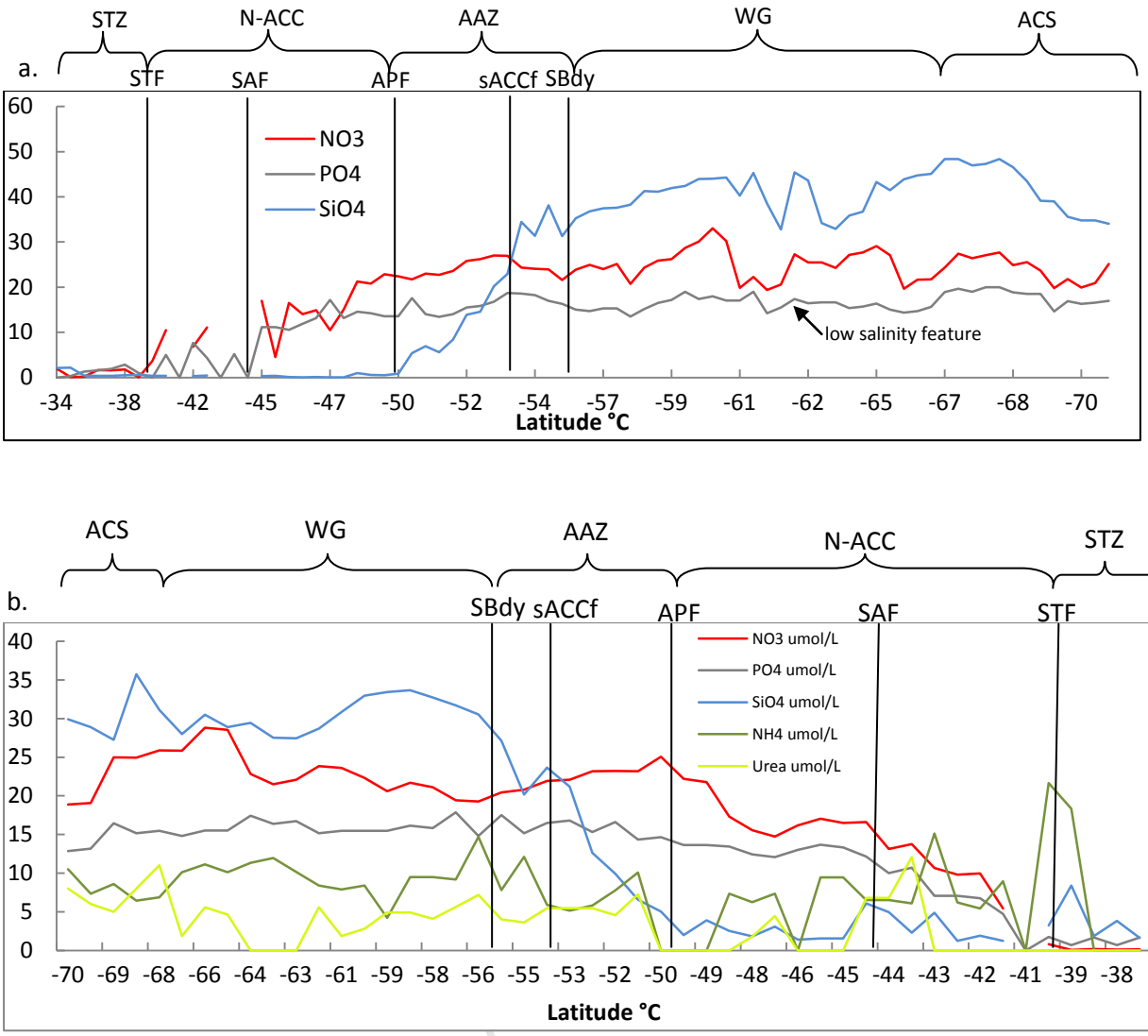

Figure 2.8a & b. Nutrient concentrations Leg 1(a) and Leg 4 (b). PO_4^{3-}, NH_4^+, and urea concentrations have been scaled by a factor of 10 to display $Si(OH)_4$ and NO_3^- on the same axis. Vertical lines indicate the position of the STF, SAF, APF, sACCf, and SBdy. Brackets on top of the figure indicate the regions: STZ, N-ACC, AAZ, WG, & ACS. The position of the low salinity feature within the WG has also been indicated (a).

Antarctica to South Georgia (Leg 2) and South Georgia to Antarctica (Leg 3)

Nitrate and silicate are highest in concentration (ranging from 20 - 27 µmol l^{-1} and 20 - 56 µmol l^{-1} respectively) throughout the ACS and WG regions and decline significantly when passing through the South Sandwich and South Georgia Island region (13 µmol l^{-1} and 2 µmol l^{-1} respectively) (Figure 2.9). Another notable decline occurred in nitrate and silicate when travelling along the SBdy. On both legs sharp declines in silicate occurred at ~61°S which coincides with the low salinity feature referred to above (Figure 2.9). A prominent peak also occurred over the region of shallow bathymetry in the WG on Leg 3. Ammonium and urea are highly variable throughout both transects (Figure 2.9), however a prominent peak in NH_4+ occurred at 61°S.

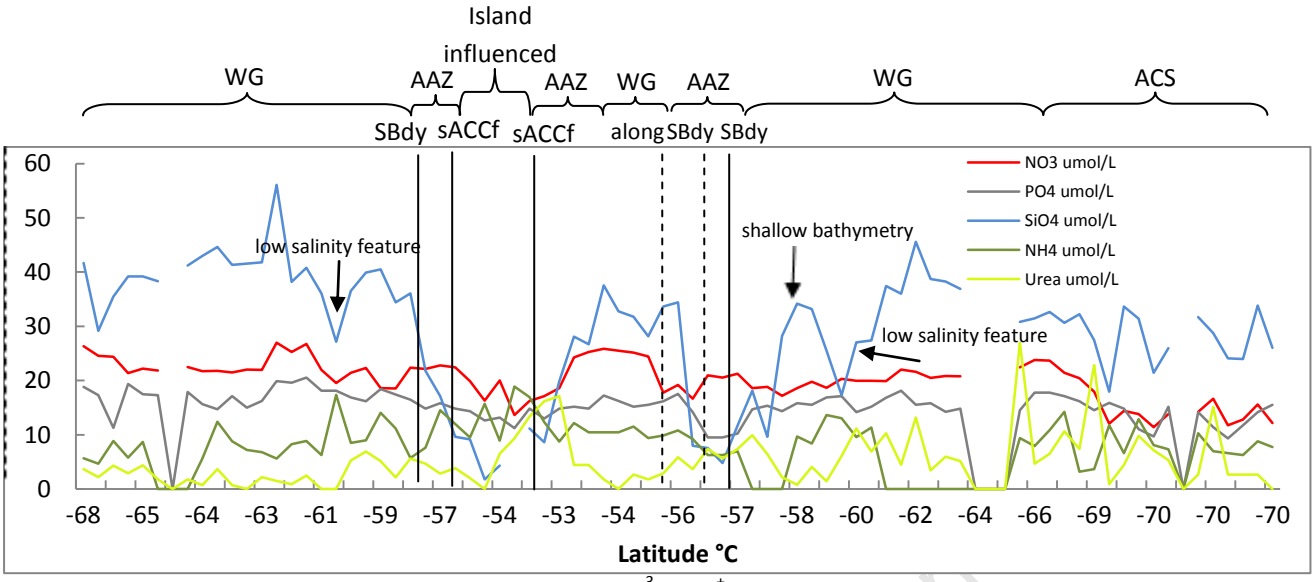

Figure 2.9 Nutrient concentrations along Legs 2 and 3. PO_4^{3-}, NH_4^+, and urea concentrations have been scaled by a factor of 10 to display $Si(OH)_4$ and NO_3^- on the same axis. Vertical lines indicate the position of the STF, SAF, APF, sACCf, and SBdy. Sampling along the SBdy is indicated by the region in between the vertical dashed lines. Brackets on top of the figure indicate the regions: STZ, N-ACC, AAZ, WG, SAISB (Island Influenced) and ACS. The position of the low salinity and shallow bathymetry features within the WG has also been indicated.

2.3.3 Chlorophyll-*a* and Mixed Layer Depths

Cape Town to Antarctica (Leg 1)

Chl-*a* ranged between 0-3.3 mg m^{-3} along Leg 1 (Figure 2.10a). Chl-*a* concentrations north of the SAF were generally low (< 1 mg m^{-3}), except for the first station at 34.36°S where a concentration of 1.2 mg m^{-3} occurred. Elevated chl-*a* concentrations coincided with the SAF at 44°S and continued to increase southwards reaching a peak of 1.35 mg m^{-3} (46°S) and 1.75 mg m^{-3} (48°S) in the N-ACC zone. A sharp decline followed this, where values remained under 1 until reaching 58.1°S (WG region), where highest chl-*a* concentrations of 2.24 mg m^{-3} at 58.1°S and 2.58 mg m^{-3} at 65°S were encountered. In the ACS region a peak of 3.27 mg m^{-3} occurred at 69°S.

Mixed layer depths (MLDs) were variable along this transect, ranging from 17 m close to the SAF to >80 m north of the STF (Figure 2.10a). An alternating pattern from very shallow (<20 m) to deep (>80 m) MLDs was prominent north of the STF. MLD shallowed to ~20 m to the north and the south of the SAF. In the AAZ, MLDs extended to >60 m south of the APF. South of the sACCf MLDs were ~50 m. An uncharacteristic deepening of the MLD (~80 to 90 m) occurred in close proximity to the sea ice in the ACS region (68-69°S).

Antarctica to Cape Town (Leg 4)

Chl-*a* concentrations were generally low along the length of this transect (mean 0.49 mg m^{-3}) (Figure 2.10b). The greatest values were encountered at 68°S in the ACS region (1.5 mg m^{-3}), 60°S in the WG region (0.96 mg m^{-3}), 52.3°S in the AAZ (0.66 mg m^{-3}) and at the STF, ~40°S (0.62 mg m^{-3}).

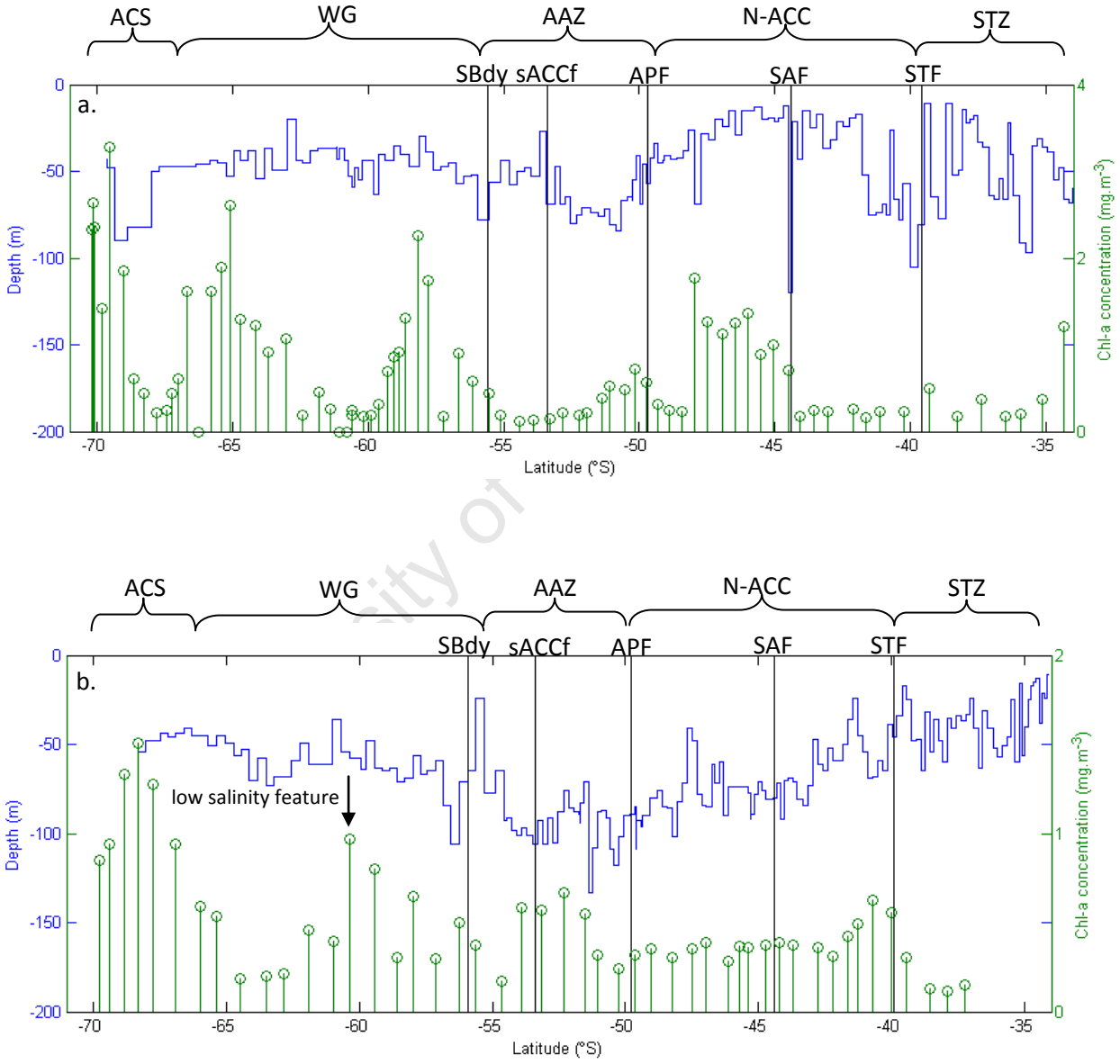

Figure 2.10a & b. MLD (blue) and chl-*a* concentration (green) along Leg 1 (a) and Leg 4 (b). Vertical lines indicate the position of the SBdy, sACCf, APF, SAF and STF. Brackets on top of the figure indicate the regions: STZ, N-ACC, AAZ, WG, and ACS. The position of the low salinity feature within the WG has also been indicated.

MLDs along this transect were generally deeper than those experienced on leg 1 (Figure 2.10b). In the AAZ, MLDs were generally ~100 m while in the PFZ MLDs were ~80 m. There were two regions, however, in the middle of these zones where the MLD had shoaled to ~50 m (55.6 and 47.5°S). North of the STF, MLDs were again highly variable with depths alternating between 60 m and 20 m in close proximity to one another.

Antarctica to South Georgia (Leg 2) and South Georgia to Antarctica (Leg 3)

On Leg 2 chl-*a* concentrations were generally < 1 mg m^{-3} with peaks in chl-*a* occurring in the WG region at ~68°S and at ~61°S where the low salinity feature is delineated (2.25 mg m^{-3} and 1.7 mg m^{-3} respectively) (Figure 2.11a). Another two notable peaks (2.94 and 1.80 mg m^{-3}) occurred in the island influenced area (52.3°S and 52.1°S respectively).

Along Leg 3, chl-*a* concentration again peaked in the WG region at latitude ~61°S (low salinity feature) and ~59°S (2.4 and 1.5 mg m^{-3} respectively), and in the ACS zone at 68.5°S (3.0 mg m^{-3}) (Figure 2.11b). A decline in chl-*a* concentration (0.6 mg m^{-3}) occurred along the SBdy, in the AAZ region.

Satellite Chlorophyll

Satelite chl-*a* concentraitons for summer (December 2008 to February 2009) allow us to see the transects in a larger spatial and temporal context. Greatest concentrations of Chl-*a* (> 3 mg m^{-3}) are found in the continental shelf region of Antarctica (the ACS region), sampled on three of the four legs of the cruise and in close proximity to South Georgia (> 2.5 mg m^{-3}) (the SAISB region), sampled on Legs 2 and 3 (Figure 2.12). The greatest chloropohyll concentrations associated with the island were found to the North West of the island just outside of our sampling area (Figure 2.12). Ensuing storm conditions unfortunatly neccessitated Eastward adjustments in our cruise track to turn away from the storm and the region of highest chl-*a*. Another prominent peak in chlorophyll concentration (1 to 2.5 mg m^{-3}) occurs along the South Sandwich Island chain (~55 to 60°S, ~25°W) just to the west of our cruise track (Leg 3). Also noteable are the areas in the 1-2mg m^{-3} concentrations in the WG region (65°S, 17°W) which was crossed on Legs 2 and 3 (figure 2.12). Lowest chl-*a* concentrations (< 0.2 mg m^{-3}) occur to the east of the Weddell Gyre (~62 - 70°S, 25°E)

outside of our cruise sampling and north of the APF until the STF, in the N-ACC region along Legs 1 and 4 where concentrations ranged from 0.1 to 0.3 mg m^{-3}.

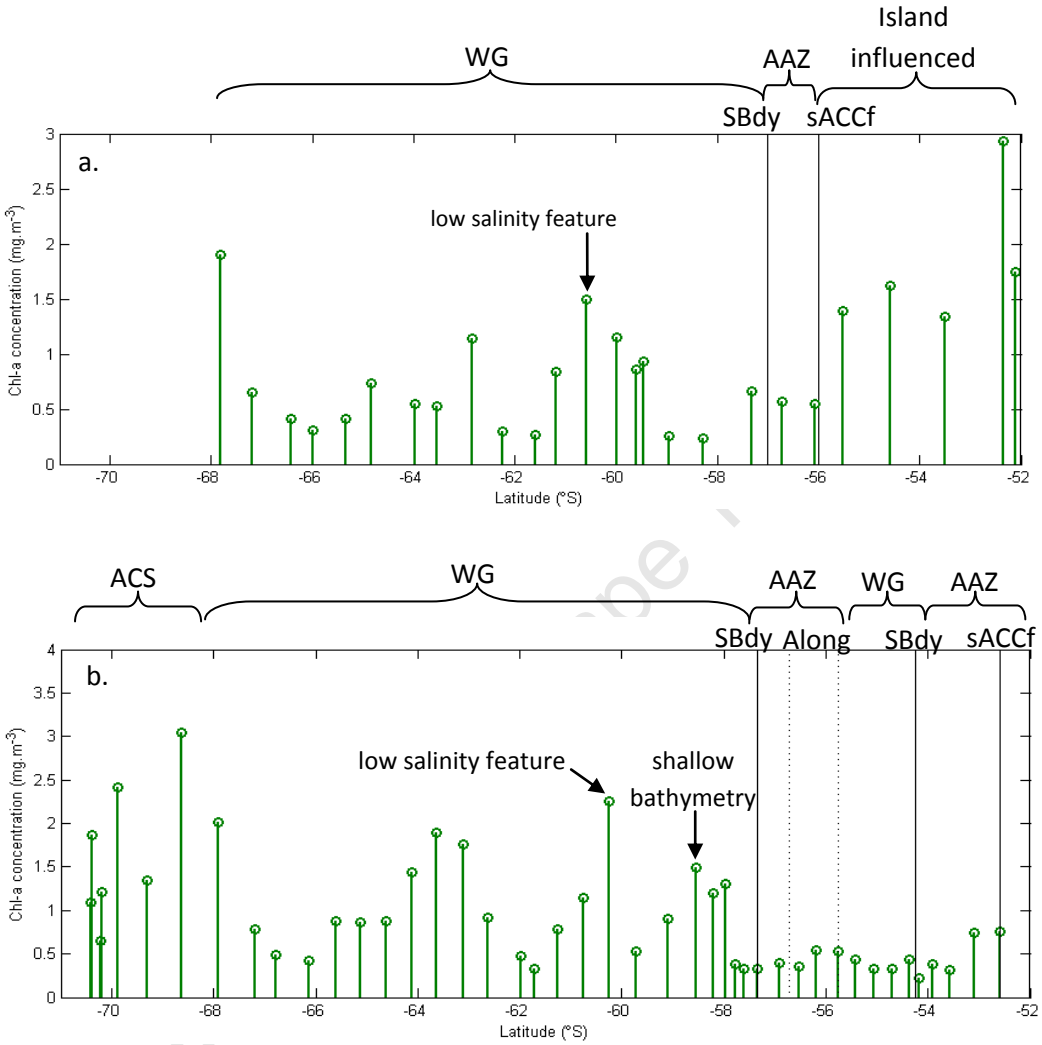

Figures 2.11 a & b. Chlorophyll-a concentrations along Leg 2 (a) and Leg 3 (b). Vertical lines indicate the position of the SBdy and the sACCf. Sampling along the SBdy is indicated by the region in between the vertical dashed lines. Brackets on top of the figure indicate the regions: AAZ, WG, the SAISB (Island Influenced) and ACS. The position of the low salinity and shallow bathymetry feature within the WG has also been indicated.

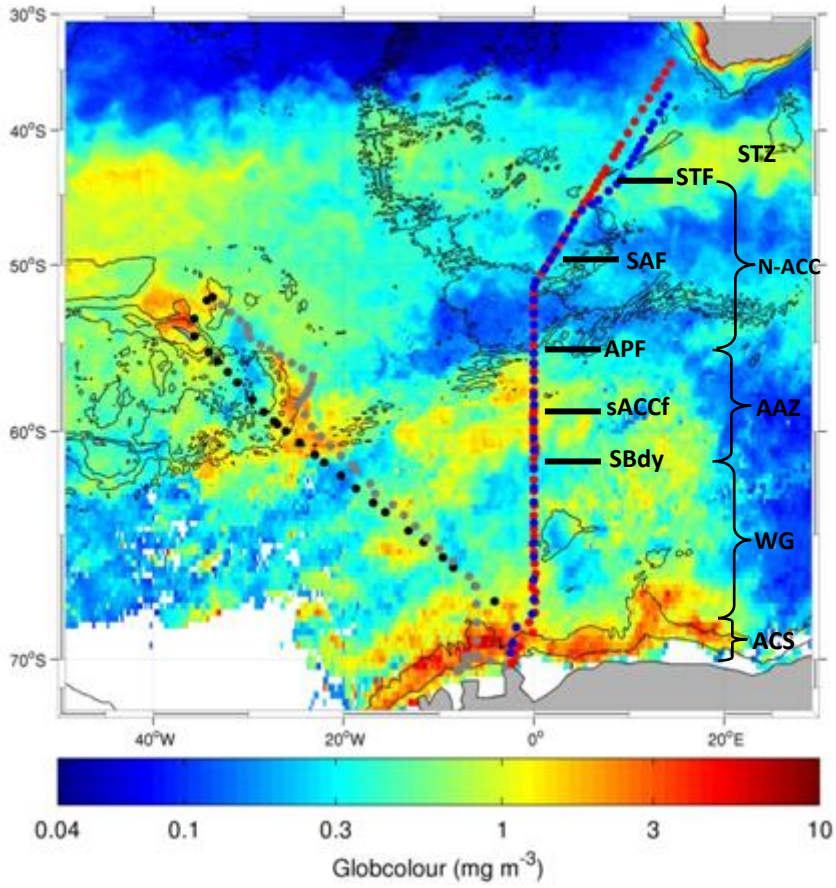

Figure 2.12 Monthly mean chlorophyll-a concentration (mg m^{-3}) for the entire South Atlantic sector of the Southern Ocean with overlaid cruise track (Leg 1 red dots, Leg 2 black, Leg 3 grey, leg 4 blue). A three month composite satellite image from the beginning of December 2008 through the end of February 2009, white areas delimit where no data was available. Data for this image was extracted from the website GlobColour http://www.globcolour.info/data_access.html

2.4 Discussion

In the following discussion the spatial distribution of chlorophyll in the South Atlantic sector of the Southern Ocean is investigated in relation to the physical factors that regulate the nutrient and light environment through evolving contributions of temperature and salinity to changes in stratification and the MLD. According to the literature, this region of the Atlantic Sector of the Southern ocean can be divided into 6 regions with distinct chlorophyll signatures and physical control mechanisms, these are 1) the STZ, 2) the N-ACC, 3) the AAZ, 4) the WG, 5) the SAISB region and 6) the ACS region. The four legs of this cruise crossed each of these regions whose results will be discussed in turn.

The Subtropical Zone

The Agulhas Retroflection Current dominates this highly dynamic area, known for its warmer (>18°C), saltier (>35.5 psu) waters north of the STF (Figure 2.5 a, b). The surface temperature and salinity plots provide an accurate picture of this subtropical environment (Figures 2.3a & b., 2.5a & b), in which SST maxima at ~36°S and ~39°S (Figure 2.3a) illustrate the remnants of a warm core Agulhas Ring. The MLDs on the southbound transect from Cape Town to Antarctica (Leg 1) in December 2008 varied from 20 m to 80 m (Figure 2.10a) in close proximity to one another, thus also indicating the turbulent and dynamic nature of this zone, i.e. dynamic front positions, meanders, and eddy shedding (Swart et al. 2011 *in press*). On the northbound transect, from Antarctica to Cape Town (Leg 4) in February 2009, three months later, surface waters were more stratified and MLDs were shallower (mean = 36 m on Leg 4 compared to 46 m on leg 1) and less variable (~20 m to ~50 m). Later in the season, these more stratified and stable waters (Figure 2.3b) limit the nutrient environment by reducing upwelling and the replenishment of deeper nutrient rich waters to the surface zone. This scenario was evident when comparing mean surface NO_3^- concentrations which were much higher on Leg 1 (1.03 ±0.87 µmol l^{-1}) than on Leg 4 (0.13 ±0.05 µmol l^{-1}) (Table 2.2). The large difference in mean chl-*a* concentrations from early in the season (Leg 1 = 0.43 mg m^{-3}) compared to later in the season (Leg 4 = 0.17 mg m^{-3}) highlights the impact of nutrient limitation on the phytoplankton community with seasonal progression.

In this region, all nutrient concentrations were low (NO_3^- <2 µmol l^{-1}, Si <4 µmol l^{-1}, PO_4^{3-} <2 µmol l^{-1}) with the exception of NH_4^+ (~2 µmol l^{-1}) on Leg 4. Low NO_3^-, Si and PO_4^{3-} concentrations suggest reduced vertical mixing that leads to a nutrient impoverished euphotic zone, while high NH_4^+ concentrations suggest high zooplankton grazing and excretion rates, where phytoplanktonic uptake of NH_4^+ does not exceed NH_4^+excretion rates (Figure 2.8a & b) (Bopp et al. 2005, Lucas et al. 2007, Thomalla et al. 2011). Low chlorophyll-*a* concentrations (generally <0.5 mg m^{3-}) (Figures 2.10a, b) throughout most of this zone support the case for low primary production (Froneman et al. 2001, Joubert et al. 2011, Thomalla et al. 2011a) and / or high grazing rates that suppress biomass accumulation (Smetacek 2004).

NO_3^- limitation in this region establishes a phytoplankton community comprising small-celled organisms that thrive primarily on 'regenerated' vs. 'new' nitrogen, resulting in typically low *f*-ratio's (Lucas et al. 2007). Such a community results in an inefficient biological pump where little or no C is exported from surface waters (Cullen 1991, Salter et al. 2007, Pollard et al. 2009).

Table 2.2 Table of means and standard deviation of Chl-a (mg m^{-3}), MLD (m), and all nutrients (µmol L^{-1}) by zone for each leg of the SANAE 48/49 cruise.

Zone	Leg	Chl-*a*	MLD	NO_3^-	$SiOH_4$	PO_4	NH_4^+	Urea
STZ	1	0.43 ±0.36	46±23	1.03±0.87	0.93±0.83	0.13±0.09	n/a	n/a
	4	0.17 ±0.09	36±16	0.13±0.05	3.91±3.14	0.14±0.06	n/a	n/a
N-ACCZ	1	0.64 ±0.51	38±23	14.05±6.04	0.35±0.27	1.11±0.39	n/a	n/a
	4	0.39 ±0.09	71±18	13.84±5.55	2.72±1.50	1.03±0.40	0.89±0.46	0.32±0.42
AAZ	1	0.31 ±0.19	62±14	24.25±1.88	19.42±12.03	1.63±0.18	n/a	n/a
	4	0.43 ±0.18	91±18	22.50±1.50	15.79 ±8.32	1.59±0.11	0.78±0.25	0.51±0.12
	2	0.59 ±0.06	n/a	22.47±0.32	16.16 ±6.13	1.52±0.06	1.14±0.35	0.38±0.09
	3	0.44 ±0.16	n/a	21.61±3.40	22.39±11.87	1.42±0.27	0.96±0.20	0.58±0.51
WG	1	0.79 ±0.70	46±10	25.26±3.34	41.48 ±4.64	1.66±0.18	n/a	n/a
	4	0.55 ±0.32	59±13	23.16±2.96	30.51 ±2.13	1.59±0.09	0.96±0.24	0.40±0.30
	2	0.63 ±0.37	n/a	22.39±2.33	37.68 ±4.23	1.73±0.20	0.86±0.33	0.30±0.20
	3	1.12 ±0.71	n/a	20.45±1.70	30.56 ±8.33	1.59±0.13	1.01±0.31	0.74±0.57
SAISB	2	1.17 ±0.59	n/a	17.19±2.44	7.00 ±3.83	1.32±0.13	1.37±0.41	0.79±0.63
	3	n/a	n/a	n/a	n/a	n/a	n/a	n/a
ACS	1	1.86 ±0.99	68±26	22.70±2.40	38.42 ±4.57	1.72±0.14	n/a	n/a
	4	1.16 ±0.31	n/a	21.97±3.46	30.46 ±3.69	1.44±0.17	0.82±0.18	0.68±0.15
	3	1.70 ±0.93	n/a	13.88±2.04	27.18 ±4.94	1.31±0.23	0.81±0.25	0.63±0.67

The Northern ACC Zone

The steep gradient in SST and surface salinity as the STF was crossed (39.9°S) indicates the expected change from a subtropical to a subpolar ocean (Figure 2.5a). Surface temperature and salinity continued to decrease throughout this zone (Figure 2.5a & b), but even so, temperature still dominated over salinity in the control of density (Pollard et al. 2002). North of the APF, temperature decreases with depth (Figure 2.3a & b), and although subsurface salinity data were not available, this zone is defined by a subsurface salinity minimum. This is due to fresh (and cooler) inputs of AAIW and Subantarctic surface water from the PFZ further south, driven by wind and Ekman transport (Pollard et al. 2002).

South of the STF, NO_3^- and PO_4^{3-} concentrations increased to ~15 µmol l^{-1} and ~17 µmol l^{-1} respectively, while silicate concentrations remain low (<1 µmol l^{-1}) (Figure 2.8a). A similar nutrient environment has been found in previous studies (Read et al. 2000, Boyd 2002, Pollard et al. 2002, Joubert et al. 2010), where it is understood that nutrients are brought to the surface from depth by isopycnic transport (advection and mixing along upward sloping isopycnals) and diapycnic mixing (near-vertical mixing across density surfaces) (Pollard et al. 2002). Nutrient concentrations in the surface layer (i.e. above the winter mixed layer) can be entrained from below by winter mixing events and potentially too by northward Ekman advection (Pollard et al. 2002).

In summer, phytoplankton production in the euphotic zone diminishes nutrient concentrations, concurrently with an increase in chl-*a* concentrations, at least before zooplankton grazing pressure crops the biomass. The summer season is also associated with warmer surface waters, hence greater stratification and MLD shoaling. Later in the season as surface waters cool and wind-strength once more increases, MLD's deepen again, resulting in lower chl-*a* concentrations. This typical seasonal progression was observed during this study.

Incredibly calm and stable seas were encountered during the crossing of this region on Leg 1 (Cape Town to Antarctica) (44.5°S to 48°S; 27-28 December 2008). These calm conditions are likely what led to the particularly shallow MLDs (~20 m) and an improved light environment that allowed for the peak in chl-*a* biomass (max 1.75 mg m^{-3}) (Figure 2.10a). Mean MLDs (37.9 ±23.09 m) were shallower at the beginning of summer (Leg 1,

Figure 2.10a; 26-28 December 2008) compared to the beginning of autumn (70.9 ±17.9 m) when deeper mixing events occurred (Leg 4, Figure 2.10b; 26-28 February 2009), as epitomised by a storm on 26 February 2009 at ~48°S. This deepened the MLD to ~70 m such that dilution and an unfavourable light environment resulted in a low chl-*a* biomass of <1.0 mg m^{-3}, (Figure 2.10b). In general, low biomass occurred throughout this zone during autumn, attributed to light and nutrient (including Fe) co-limitation when mixed layers deepen and winter Fe stores are depleted following the phytoplankton growth season (Coale et al. 2004, Pollard et al. 2009).

Even so, when MLDs were shallow (~20 m) along much of the early summer transect from Cape Town to Antarctica (Leg 1), chl-*a* concentrations were predominantly low (mean = 0.43 mg m^{-3} ±0.36), indicating additional limiting factors such as nutrient (Si and / or Fe) limitation, as well as losses due to grazing (Read et al. 2000, Boyd 2002, Pollard 2002, Trull et al. 2002).

The Antarctic Zone

All four transects passed through the AAZ which comprises the area from the APF to the SBdy. Characteristic differences in water mass properties between the AAZ and waters south of the Sbdy are driven by differential upwelling in the respective zones. In this region UCDW upwells and is notably fresher and cooler than LCDW which upwells in the WG region and is warmer and saltier (Orsi et al., 1995). South of the APF, colder (~0°C) fresher water from sea ice melt overlays slightly warmer water (2°C), showing that salinity controls density in this region. Seasonal changes in MLD are smaller in the AAZ than those found in the SAZ (change in MLD for AAZ = ~28 m vs. change in MLD for SAZ = ~45 m, see Table 2.2). Surface waters in this region are known to be rich in nitrate, phosphate and silicic acid year-round, with nitrate at its maximum. South of the APF, nitrate and phosphate concentrations gradually increased (from ~20 to 25 µmol l^{-1} and from ~10 to 15 µmol l^{-1}, respectively), while silicate concentrations rose sharply from ~1 to ~30 µmol l^{-1}. In such an environment, diatoms typically dominate the phytoplankton community as long as Fe and sufficient light are present (Pollard et al. 2002, 2009, Sokolov & Rintoul 2007).

This pool of unused nutrients is the largest in any of the world's oceans (Levitus et al. 1993, Boyd et al. 2000, Boyd et al. 2002, Arrigo et al 2008), and the reasons for this have

attracted considerable attention since the 1930's. As winter reserves of the macronutrient environment have been set through physical processes, any change in concentrations over the course of the growing season is due to biological activity. Even so, there is little seasonal variability in macronutrient concentrations. Chl-*a* concentrations in this zone were very low throughout this summer study (generally <0.5 mg m^{-3}) (Figures 2.10a & b, 2.11a 7 b), indicating very little biological activity. A deepening MLD in this region, particularly on Leg 4, suggests light limitations to phytoplankton growth (Figure 2.10a, b). This zone embodies the HNLC condition, where Fe and light co-limitation (Moore et al. 2007a, b) results in a shift from a diatom-dominated community (where Fe is available) to one dominated by small cells (or scarce heavily silicified diatoms, Poulton et al. 2007) characterised by low rates of primary production (Seeyave et al. 2007) and regenerated rather than new production (Lucas et al. 2007). Furthermore, extensive microzooplankton grazing controls biomass accumulation within a classic 'microbial loop' (Froneman et al. 1996a, Fielding et al. 2007), resulting in little carbon export (Salter et al. 2007, Pollard et al. 2009). Exceptions to this scenario are however, found where Fe inputs from shallow bathymetry or from recently receding ice–melt lead to a diatom-dominated community and carbon export as the HNLC condition is released, as occurs around Subantarctic islands (Pollard et al. 2009).

The Weddell Gyre

Near the centre of the WG, LCDW continually upwells enriching the surface water with macronutrients (Bakker et al. 2008). Evidence of this is seen in subsurface water temperatures which increase just south of 65°S and relatively high concentrations of macronutrients where mean Si (41.48 ±4.6 µmol l^{-1}), NO_3^- (25.26 ±3.3 µmol l^{-1}) and PO_4^{3-} (1.7 ±0.18 µmol l^{-1}) attained their maximal geographically distributed values (Figure 2.8a & b and 2.9 and Table 2.2). Even so, seasonal depletion of nutrients to support phytoplankton growth was apparent from early summer to early autumn (Table 2.2), although concentrations remained variable. Between 61°S and 65°S, a decrease in Si and NO_3^- coincided with recent sea-ice retreat (see Figures 2.7c & d 22 December to 1 January), a salinity minimum, and related peaks in chl-*a* biomass (2.24 mg m^{-3} at 58.1°S; 2.58 mg m^{-3} at 65°S). Arrigo et al. (2008) concluded that sea-ice recession has a lasting impact on the biological community for up to 14 days, further facilitated by high mean dFe concentrations of ~0.5 nM attributed to LCDW upwelling under the ice in winter as well as increases in Fe

concentration due to accumulation of Fe deposited over the ice (Klunder et al. 2011). Observations of locally elevated chl-*a* made during this study were well within the 14 day period, and quite plausibly were in response to Fe enrichment and an enhanced light environment due to freshwater stratification, as has been found in many MIZ studies (Lizotte 2001, Garibotti et al 2005a, Vernet et al. 2008).

During the transects from Antarctica to South Georgia (Leg 2) and South Georgia to Antarctica (Leg 3), elevated chl-*a* biomass (2.0 and 2.1 mg m^{-3} respectively) and a concurrent decline in Si concentrations (from 41 to 29 µmol l^{-1} and 39 to 28 µmol l^{-1}) at ~68°S was most likely due to recent sea ice retreat, where positive buoyancy forcing, increased stratification and potential dFe addition, led to an increase in diatom production and a peak in chlorophyll. However, at another region of elevated chl-*a* biomass (~64°S) (2.11b) sea-ice may not have played a role since more than 14 days had elapsed since sea ice melt (Figure 2.7g), pointing speculatively instead to the upwelling of Fe-enriched LCDW as the driver in phytoplankton production, a situation known to occur in the centre of the Weddell Gyre (Hoppema et al. 1997, Bakker et al. 2008, Klunder et al. 2011). The close proximity of the Maud Rise and current flow of CDW over this local topographic feature could have provided an additional source of dFe (Bakker et al. 2008).

On all four transects crossing the WG there was a persistent low salinity feature (33.1 – 33.5 psu, Figures 2.5a, b & 2.6a, b) at ~61°S, perhaps originating from melt-water flowing eastwards from the Antarctic Peninsula as part of the northern branch of the Weddell Gyre circulation. From this study, such fresher and most likely Fe-enriched water (de Baar et al. 1995) probably lead to the enhanced phytoplankton biomass (~ 1.0 – 2.4 mg m^{-3}) observed on three of the four transects (Legs 2,3 and 4, Figures 2.10b and 2.11 a, b).

The Subantarctic Island and Shallow Bathymetry Region

Coastal and shelf waters (<500 m deep) of the continent and oceanic islands make up a significant proportion of primary production in the Southern Ocean, where although only ~2.5% of the Southern Ocean by area is represented, ~9% of total primary production occurs here (Moore & Abbott 2000, Ward et al. 2005). Areas of shallow bathymetry are known to benefit from run off or from shelf sediment additions of dFe into the euphotic zone (Korb et al. 2005, Planquette et al. 2007, Blain et al. 2007, Pollard et al. 2009).

Stations north of the sACCf on Leg 2 (from Antarctica to South Georgia) and south of the SBdy at ~58°S (west of the South Sandwich Trench, north of the South Scotia Ridge, in close proximity to Saunders and Montagu Islands) are within this classification (Figure 2.1). The shallow bathymetry areas south of 68°S are classified separately due to observed differences in the mechanism of dFe delivery there and are discussed under the Antarctic Continental Shelf section described below.

The spring bloom historically associated with South Georgia (Ward et al. 2008) and evident in the satellite composite image from this cruise (Figure 2.12) is generally found extending north and to the east of the island, entrained in the ACC flow before it retroflects in a southerly direction. The APF lies to the north of the island and the sACCf to the south. The island and surrounding bathymetry cause a divergence of the eastward flowing ACC whereby the Scotia Ridge deflects waters to the northwest before returning to an eastward flow as they approach the APF. The sACCf passes from the southwest and is steered along the edge of the northern shelf before it resumes its eastward flow. Current flow patterns and frontal positions at the time of sampling on this cruise resemble very similar characteristics to those described in Korb et al. (2004) (Figure 2.4). It is therefore expected that downstream inputs of dFe into the euphotic zone will only enhance waters to the north of the sACCf in similar fashion to that reported for the Kerguelen and Crozet island regions (Blain et al. 2007, Pollard et al. 2009 respectively) and for this area by Korb et al. (2004 and 2005) and Whitehouse et al. (2008).

It is not surprising therefore that chl-*a* biomass at all stations north of the sACCf was >1 mg m^{-3}, with the greatest concentration (2.94 mg m^{-3}) being recorded at ~52°S (Figure 2.11a). Although these values are lower than those measured by Korb et al. (2004), where mean *in situ* values were 4.3 mg m^{-3} ±2.0 to the south east of South Georgia, they still represent bloom conditions likely fuelled by dFe inputs from this shallow bathymetric region. Biomass concentrations were only moderately high because of the spatial and temporal aspect of the cruise track in relation to the bloom over time. Figure 2.12 details the extent of the seasonal bloom and shows our stations just south of the most concentrated bloom to the north west of South Georgia. At the time of sampling, we were forced to turn south due to storm conditions and subsequently missed sampling the area of greatest biomass concentration. As expected in highly productive waters, nutrient

drawdown ocurred down-stream of South Georgia. Macronutrient concentrations all declined, with Si dropping to concentrations of 1.76 µM at 54.6°S and 0.69 µM at 52.3°S (Figure 2.9), indicative of intense diatom production that would likely soon become Si-limited unless replenished by deep mixing or upwelling. Since the bloom did indeed persist over the time of our sampling (Figure 2.12), such a replenishment mechanism seems plausible (Whitehouse et al. 2008). Coincident with nutrient drawdown was an increase in NH_4^+ concentrations (Figure 2.9). This signifies heterotrophic excretion of regenerated N that exceeds autotrophic uptake (Banse 1995), indicating increased grazer biomass and resultant strong grazing control that could account for only moderately high chl-*a* biomass values.

Along Leg 3 (from South Georgia to Antarctica), the area of greatest chl-*a* biomass (1.5 mg m^{-3}, Figure 2.11b) was in close proximity to the East Scotia Ridge where the South Sandwich Islands are located. Here, shallow bathymetry (<1000 m) likely plays an important role by contributing dFe to a system primed for production, as at the Crozet Islands (Pollard et al. 2009). Local upwelling is signified by a spike in the Si (Figure 2.9) concentration and a simultaneous drop in SST (Figure 2.6b). Natural Fe fertilization in shallow plateau areas of Subantarctic islands plays an essential role in boosting phytoplankton abundance and ultimately enhances the likelihood of biologically mediated CO_2 drawdown (Pollard et al. 2009)

The Antarctic Continental Shelf Region

This zone, by far, exhibits the greatest biomass relative to all other zones in this study (see Table 2.2 for comparison of mean biomass from each zone). Legs 1, 3 and 4 show the highest chl-*a* concentrations, where maximal values reach 3.3 mg m^{-3} at 69°S, 3.0 mg m^{-3} at 69°S, and 1.5 mg m^{-3} at 68°S, respectively (Figures 2.10a, 2.11b, & 2.10b). All macronutrients were relatively high throughout the region, thus not considered limiting. Here the seasonal melting of ice cover provides a two-fold benefit to enhance phytoplankton growth (as in the MIZ). First, melting ice sets up a fresh, buoyant layer that prevents vertical mixing and increases mean irradiances in a shallow surface mixed layer (Sokolov 2008). Second, recent ice melt provides a significant source of Fe (Sokolov 2008). Figures 2.5a & b and 2.6a & b clearly show the dramatic decline in salinity in the ACS region

due to seasonal ice-melt. Previously, it was believed that another significant source of dFe in this zone was the Antarctic continental shelf and slope, similar to the Crozet, Kerguelen, or South Georgia Island's scenario (Planquette et al. 2007, Blain et al. 2008, Korb et al. 2005). However, in a recent study along the prime meridian, it was observed that Antarctica is unique, because unlike all other continents in the world, dissolved Fe around the continent decreases as you approach its extent (Klunder et al. 2011). It is understood that at continental shelves Fe originates from below by upwelling and upward mixing of deeper waters rich in dFe. Klunder et al. (2011) have found that because the ice sheet over the Antarctic continent extends beyond the grounding line and subsequently covers the water column over the shelf and slope, biological production is essentially capped. This drastically reduces biogeochemical cycling over and within the shelf and slope and equates to a minimal lateral supply of Fe from this area to adjacent open waters. This finding therefore supports the theory that this highly productive region is largely fuelled by seasonal ice melt and Fe release into surface waters. Even still, the chl-*a* concentrations are much higher in the ACS compared to any other region in this study including the MIZ where shelf Fe inputs are absent and Fe additions occur through the same mechanisms (i.e. seasonal receding ice). So what sets the ACS apart? Until additional investigations like Klunder et al. (2011) can advance the argument for little to no influence from the continental shelf, it is evident that a combination of environmental conditions and multiple mechanisms for Fe injections set this region apart from the rest. Spring and summer ice retreat (Figure 2.7 a-h), glacial and ice berg melt, more stratified thus stable water column structure due to less frequent strong wind events (evident in shoaling MLD, ~50m on average Figure 2.10a, b), subsequent enhanced light conditions, reduced cloud cover that increases the photosynthetically active radiation close to the coast, and the shallow continental shelf as a source of dFe (no data, but sustained high macro nutrient concentrations suggests upwelling, thus would include micro nutrients when in coastal areas Figures 2.8a, b & 2.9) all help to sustain high phytoplankton production and great concentrations of biomass (Moore & Abbott 2000, Sokolov 2008).

2.5 Conclusions

The south Atlantic sector of the Southern Ocean has vast areas of open ocean where the macronutrient environment remains replete, but chl-*a* concentrations are low. In such a

physically dynamic area of the world's oceans, phytoplankton biomass is highly variable in time and space. Deciphering reasons for patterns of high versus low biomass is complicated and confounded by its remoteness and relatively infrequent sampling. Even so, it is a relatively productive body of water compared to other sectors of the circumpolar Southern Ocean and is becoming better understood through the advent of combined remote sensing, multi-scale modelling and remotely controlled, multi-depth sampling strategies. What is evident from this chapter is that shallow bathymetric features, close proximity to land masses, or in the case of the marginal ice zone (which includes the ACS, WG, and a portion of the AAZ), recent melting of sea ice in its various forms all coincide with significant increases in phytoplankton biomass. Although speculative, this suggests the introduction of Fe to catalyze phytoplankton growth in combination with a more stratified water column and an improved light regime, as well as longer light exposure due to increased day length in summer. In regions of low biomass (STZ and AAZ for example) NO_3^- limitation and light limitation (respectively) prevent phytoplankton production. While frontal positions historically have been coincident with the spatial distribution of increased chl-*a* biomass, this study shows a more current scenario of fronts serving as boundaries to distinct zones with similar characteristics and elevated or depleted biomass, depending on the region as in the case when crossing the STF from the STZ to the N-ACC in terms of temperature salinity and biomass or when crossing the APF from the N-ACC to the AAZ in terms of the steep increases in the macro nutrient environment, particularly Si, for example.

Chapter 3. The Role of Light on Primary Production, Nitrogen Metabolism and Phytoplankton Community Structure in the South Atlantic Sector of the Southern Ocean

3.1 Introduction

The previous chapters have highlighted the complex role of the physical and chemical environment in controlling phytoplankton biomass distribution in the Southern Ocean. Discerning how marine phytoplankton production is controlled is essential in understanding the global carbon cycle, since algal carbon fixation plays a critical role linking ocean-atmosphere carbon fluxes (Van Oijen et al. 2004). In addition, knowledge of the key physiological responses of plankton is needed if we are to understand the carbon-climate system and its response to environmental and climate change. In order to achieve this, one needs to assess not only variability in primary productivity, but also to routinely provide information on phytoplankton functional types and physiology, as these can dramatically affect carbon export to depth.

3.1.1 Community Structure

Phytoplankton taxonomic composition and size structure is integral to upper ocean biogeochemistry, export production, and food web architecture and efficiency (Poulton et al. 2006 & 2007, Boyd and Trull 2007). Spatial and temporal variability of the factors that influence the composition and progress of a phytoplankton community (nutrient and light availability, turbulence and predation) lend to greater variance in phytoplankton diversity and growth rates (Poulton et al. 2006). Algal groups may be classified according to cell size (e. g. Sieburth 1979) and defined as small picoplankton (0.2 – 2 µm in diameter; e.g. prochlorophytes, *Synechococcus spp*., and small eukaryotes), medium-sized nanoplankton (2 – 20 µm; e.g. prymnesiophytes, pelagophytes, small diatoms and dinoflagellates), and large microplankton (>20 - 200 µm; e.g. diatoms and dinoflagellates). At present, oligotrophic open ocean ecosystems are dominated by small photosynthetic cyanobacteria and heterotrophic bacteria that make-up the microbial loop where organic carbon is recycled within the lower trophic groups (hetrotrophic bacteria, nanoflagellates, ciliates, and heterotrophic dinoflagellates) such that there is little availability for higher trophic groups or for export (Poulton et al. 2006). It is well known that the majority of primary production

and phytoplankton biomass in the HNLC Southern Ocean falls in the pico and nano size fractions that make up the microbial loop (Smetacek et al. 2004) where small cells are better able to scavenge limiting Fe at low ambient concentrations.

Increases in biomass over the stable background level (~0.2mg chl-*a* m^{-3}) of this pervasive recycling community is caused by blooms of larger phytoplankton in Fe replete systems that include the diatom species *Corethron, Thalassiothrix* and *Fragilariopsis,* as well as *Phaeocystis antarctica* colonies, whose development is regionally and seasonally tempered (Smetacek et al. 1990, 2004, Waters et al. 2000, DiTullio et al. 2003). These blooms form the basis of food–webs that support large numbers of higher biomass species and ends in considerable export of organic matter to the deep ocean (Blain et al. 2007, Pollard et al. 2009). Grazing pressure by microzooplankton on the smaller sized phytoplankton community is high since both predator and prey have similar growth rates, whereas the faster growing larger phytoplankton are able to temporarily escape their slower-growing grazers, allowing them to form blooms. Under a bloom-forming life cycle, phytoplankton population size has an annual fluctuation of over three orders of magnitude, while in all other species, annual population abundance is restricted to within two or fewer orders of magnitude. Alternatively, large, Fe-limited and slow-growing but highly silicified diatoms use silification "armouring" as a defence mechanism to avoid grazing pressure (Smetacek et al. 2004). In these conditions, the vertical flux of organic matter and opal into the ocean interior is greatly enhanced through the rapid sinking of large ballasted diatoms and faecal pellets (Falkowski et al. 1998, Tremblay et al. 2000) and carbon is efficiently passed to higher trophic levels with minimal respiratory CO_2 losses.

An improved understanding of how phytoplankton community size structure will likely respond to climate change will advance our knowledge of the biological carbon pump and the ability of the Southern Ocean to remain a long-term sink for atmospheric carbon-dioxide (Kohfeld et al. 2005). For example, changes in climate may facilitate a shift in the species composition in a manner that can alter the elemental composition of particulate matter, cell size and the trajectory of primary production through the food web, influencing the proportion of biomass exported to the deep sea (Finkel et al. 2010). We thus need to expand our investigations of how phytoplankton community structure, size characteristics and biogeography are influenced and how future climate change may alter the biological

pump and the ocean's role in mediating atmospheric carbon dioxide over time (Boyd &Trull 2007, Arrigo et al. 2010).

3.1.2 Primary Production

Discerning how marine phytoplankton production is controlled is essential because oceanic algal carbon fixation critically governs ocean-atmosphere CO_2 fluxes (Van Oijen et al. 2004). Research spanning the past two decades has distinguished iron availability as a major factor governing phytoplankton production in the Southern Ocean. Following the original iron hypothesis of Martin (1990), several i*n situ* iron-addition experiments such as SOIREE (Boyd et al. 2000), EISENEX (Gervais et al. 2002), SOFEX (Coale et al. 2004) and EIFEX (Hoffmann et al. 2006) have provided convincing proof of Fe-limited phytoplankton growth in most regions of the Southern Ocean. Further studies of naturally iron-fertilized systems such as CROZEX (Pollard et al. 2007, 2009) and KEOPS (Blain et al. 2007) provide unequivocal evidence that Fe introduced into the euphotic zone not only stimulates phytoplankton growth, but leads to CO_2 draw-down and enhanced carbon export to the ocean floor.

Iron additions operate via two distinct but related mechanisms. When iron concentrations are low or unavailable, the functioning of the photosynthetic apparatus (PhotoSystem II and PhotoSystem I) and many metabolic processes (e.g. nitrate assimilation and intracellular reduction to NH_4^+) are adversely affected (Geider & La Roche 1994, Van Oijen et al. 2004, Lucas et al. 2007, Cochlan 2008). Disparities in iron stocks between oceanic regions may explain differences in productivity during austral spring (de Baar et al. 1995, VanOijen et al. 2004, Cochlan 2008). Additionally, there are signs of further seasonal development in the environmental control of phytoplankton. Irradiance is the primary trigger for phytoplankton growth in early spring (Venables et al. 2007), where the magnitude of the spring bloom is determined by winter Fe accumulation. Next, *in situ* measurements in addition to modelling indicate that production becomes co-limited by iron and light in early summer (Lancelot et al. 2000, VanOijen et al. 2004), and in late summer declines substantially as Fe concentrations become exhausted (de Baar et al. 1995, Boyd et al. 2000, VanOijen et al. 2004, Cochlan 2008). Co-limitation of iron and silicic acid may also limit and regulate production, particularly north of the APF where Si concentrations are low

(Franck et al. 2000, Hutchins et al. 2001, Nelson et al. 2001, VanOijen et al. 2004, Cochlan, 2008).

Deep mixing and its relationship to Sverdrup's critical depth hypothesis (where water column photosynthesis and respiration balance, Sverdrup 1953), emphasises the role of light in controlling phytoplankton growth in the often deeply mixed (>50-120 m) surface waters of the Southern Ocean. Yet light alone cannot account for low productivity, as revealed by elegant light-iron incubation studies performed in the Southern Ocean by Moore et al. (2007a, b). These experiments not only provide good evidence for iron-light co-limitation, but also show that in an Fe-limited environment, the Si:N uptake ratio of phytoplankton shifts from ~1:1 (normal) to 2:1 or even 3:1 as diatoms became more heavily silicified.

The inter-play between light, Fe-availability and nitrogen metabolism is complex. The rate of photosynthesis is clearly light dependent, as revealed by photosynthesis vs. irradiance curves. The photosynthesis-irradiance response (P-E) curve gives an advantageous and objective means of discerning between (and parameterizing) light-limited and light-saturated photosynthesis (MacIntyre et al. 2002). The P-E curve is the foundation for models of phytoplankton productivity; where the shape and magnitude indicates the underlying biophysical, biochemical and metabolic processes that govern photosynthesis (Platt et al. 1977, Fasham et al. 1990, Falkowski 1992, Falkowski & Raven 1997, MacIntyre et al. 2002). Variability in the P-E curve and variability in the ratio of carbon to chl-*a* (C:chl-*a*) serve as a means to determine photoacclimation. Photoacclimation, as defined by Falkowski & La Roche (1991), describes phenotypic adjustments that manifest in response to variations in the ambient light experienced (MacIntyre et al. 2002). Different from photoadaptation, where changes in the genotype occur either from mutations or from changes in the alleles within a gene pool, acclimation does not signify a change in the genetic structure of a population. Photoacclimation generally evolves as an ordered reduction of photosynthetic pigment content in response to increased irradiance (MacIntyre et al. 2002).

When photosynthetic organisms are contained in an enclosed volume there is a net exchange of CO_2 and O_2 between the organism and the medium. This exchange is light

dependent. In darkness there is a net consumption of O_2 and evolution of CO_2 due to respiratory processes. As organisms are exposed to light, O_2 is ultimately evolved and CO_2 is consumed as a result of photosynthesis (Falkowski & Raven 2007). The rate of photosynthesis is controlled by the efficiency of light utilization to drive the ensemble of photosynthetic reactions from water splitting to carbon fixation (Falkowski & Raven 2007).

Photosynthesis itself requires Fe in the protein form, ferredoxin (Fd). In the thylakoid membrane of an algal cell, chlorophyll is organized along with proteins and other organic molecules into photosystems. A photosystem is made up of a light-gathering "antenna complex" that has an array of a few hundred chl-*a*, chlorophyll *b* and carotenoid molecules (Campbell & Reece 2002). When the "antenna" absorbs a photon of light, a specific chl-*a* molecule located next to the reaction centre and an electron acceptor within the photosystem, loses an electron in an oxidation-reduction reaction. The "capture" of high energy electrons and subsequent chl-*a* florescence is the first part of the light-driven chemical reaction, photosynthesis. Each photosystem within a chloroplast is essentially a light-harvesting unit that contain and use Fe. The thylakoid membrane has two types of photosystems that work together to generate ATP and NADPH and are called Photosystem I (PSI) and Photosystem II (PSII). In the second phase of the light-harvesting process where the redox reaction occurs and stores high energy electrons in NADPH for later use in the Calvin cycle, PSI passes photoexcited electrons via a second electron transport chain, which transmits them to ferredoxin (Fd). The enzyme $NADP^+$ reductase then transfers the electrons from Fd to $NADP^+$. In this manner, iron is essential to the production of NADPH, which serves as reducing power in the Calvin cycle where CO_2 is fixed and converted to carbohydrate as the three-carbon sugar called glyceraldehyde-3-phosphate (Campbell & Reece 2002). Thus, the apparatus of the thylakoid membrane converts light energy to the chemical energy stored as NADPH and ATP. Oxygen is a by-product and the Calvin cycle uses the light reaction products to synthesize sugar from CO_2 (Campbell & Reece 2002).

3.1.3 Nitrogen Metabolism

Nitrogen uptake is also light and iron-dependent. Fe requirements for NO_3^- metabolism and its intracellular reduction to NO_2^- and NH_4^+ by nitrate (requires one atom of Fe) and nitrite reductase (requires five atoms of Fe) respectively, and either ferredoxin or

flavodoxin (a non-ferrous e- donor) are substantial (Sunda and Huntsman 1997, Cochlan 2008). It has been shown in theory and in laboratory cultures of diatoms that Fe utilization efficiencies and cellular metabolic Fe demands are greater in phytoplankton growing on NO_3^- versus those growing on NH_4^+ (60% more Fe for NO_3^- based growth) (Cochlan 2008). In light of observations in HNLC regions of the Southern Ocean, where NH_4^+ is preferentially utilized over NO_3^-, it is assumed to be a more energetically efficient strategy for harvesting N in response to Fe-limitation (Cochlan 2008). Phytoplankton's ability to glean nutrients at low ambient concentrations is size dependent (Lucas et al. 2007). Nitrate uptake kinetics are also governed by Fe availability (De Baar et al. 2005). When ambient Fe concentrations become limiting, smaller cells will most likely dominate new production assuming that neither NO_3^- nor light becomes limiting due to their higher surface area to volume ratio (De Baar et al. 2005, Lucas et al. 2007). Meanwhile, Si concentrations will determine whether diatoms or other taxa dominate. However, there is a point at which the benefits of a smaller cell size to facilitate Fe assimilation are eclipsed by increased mortality due to micro-zooplankton grazing (Smetacek et al. 2004, Lucas et al. 2007).

Alternatively, NH_4^+ regeneration regulated by micro-zooplankton grazing may largely underpin nano- and pico-plankton N nutrition that may rely on regenerated rather than new Fe inputs (Lucas et al. 2007). This has implications for *f*-ratios, such that high *f*-ratios are conceivably correlated with large cells and 'new' Fe additions, while low *f*-ratios, associated with smaller cells, presumably rely on 'regenerated' Fe (Lucas et al. 2007). Additionally, there is evidence for NH_4^+ inhibition of NO_3^- uptake where at high NH_4^+ concentrations (for example >~0.6 µmol l^{-1}) inhibition can be extreme, while at low concentrations (for example <~0.25 µmol l^{-1}) inhibition is often relieved (Lucas et al. 2007). Of course this is compounded by depth and light considerations as well as preferential selection of N substrates by phytoplankton, which will all play a part in the resultant community succession (Lucas et al. 2007).

Lastly, when light and iron controls on nitrate uptake are considered together, some sense of often declining *f*-ratios with depth becomes clear. In their CROZEX study, Lucas et al. (2007) showed that in a diatom bloom in surface waters, nitrate uptake exceeded regenerated N (ammonium, urea) uptake, leading to high (~0.6) *f*-ratios. But deeper in the water column, *f*-ratios declined to ~0.2, as nitrate uptake became more light-limited than

reduced N uptake. Furthermore, the size-structure of the community was also important, with small cells better able to scavenge Fe at low concentrations exhibiting higher *f*-ratios than larger cells, which consequently exhibited lower *f*-ratios. Further evidence for Fe limited nitrate uptake and growth can be garnered when specific nitrate uptake rates ($V_{NO3}d^{-1}$) are employed. When N uptake rates are expressed in terms of PON and/or chl-*a* specific values, information on turnover times, and the potential for light, macronutrient or Fe limited growth is revealed, whereby high values indicate faster growth rates in light and nutrient-replete environments (Lucas et al. 2007). Alternatively, $V_{NO3}d^{-1}$ in Fe limited HNLC areas are reduced by ~10 fold when compared to prolific oceanic systems (Dugdale & Wilkerson 1991, Lucas et al. 2007).

Light, iron and nitrogen therefore play a crucial role in controlling not only productivity, but also size-based new production, with consequent implications for carbon export. Convincing evidence for this requires a better understanding of the relationship between light intensity and new and regenerated production, particularly with respect to iron availability. One of the best ways to tackle this problem is through the use of P vs. E curves, based on the dual-labeling (^{13}C, ^{15}N) approach which gives rates of both new and regenerated production rather than the more widely used ^{14}C approach that only gives total production.

In this chapter, phytoplankton community structure, nitrogen metabolism and the potential for region based physical and biogeochemical controls of these processes are investigated. Sampling and experiments included diagnostic phytoplankton pigment analysis using HPLC to determine community structure, and measurements of duel labelled (^{13}C and ^{15}N) new production (nitrate), regenerated production (ammonium, urea) and total production (carbon fixation) versus irradiance (P vs. E). Additionally, the *f*-ratio is calculated and used as a proxy for the proportion of production that is exported to the deep sea. These measurements were conducted at 11 biological production stations on the SANAE 48 cruise from Cape Town to Antarctica and South Georgia during the austral summer of 2008/9 in the south Atlantic sector of the Southern Ocean.

3.2 Methods

3.2.1 Diagnostic Pigment Analysis

HPLC

For High Performance Liquid Chromatography (HPLC) analyses, 500 - 2000 ml water samples were filtered under positive pressure through 25 mm Whatman GF/F filters and stored in liquid nitrogen. The aim was to filter a maximum volume of 2000 ml for each sample, but in productive waters this was not always possible and where not, the filtration was terminated after 2 hours and the filtered volume recorded. On a few occasions when the 25 mm filtration rig was unavailable, ~ 4000 ml was filtered through 47 mm GF/F filters.

In each case, phaeopigments were measured utilizing the method described by Barlow et al. (1997) and more recently updated in Barlow et al. (2010) and summarized here. Pigments were extracted in 90% acetone, aided by ultrasonication, clarified by centrifugation and analysed using a 5-mm Hypersil HyPURITY C8 column, a Varian ProStar ternary high-pressure pump, a Thermo Electron AS3000 autosampler, a Thermo Electron UV6000 diode array absorbance detector and ChromQuest chromatography software. Pigments were detected at 440 and 665 nm and identified by retention time and by on-line diode array spectra. Chlorophyll *a* standard and trans-b apo-80 carotenal internal standard (Fluka) were obtained from Sigma-Aldrich Ltd. and other pigment standards were purchased from the DHI Institute for Water and Environment, Denmark. The method separates divinyl and monovinyl chlorophyll *a*, zeaxanthin and lutein, and achieves partial separation of divinyl and monovinyl chlorophyll *b*. Limits of detection were of the order of 0.001 mg m^3.

Diagnostic pigment indices were derived to determine the composition of phytoplankton communities and were defined as the sum of seven chosen biomarker pigments given in Table 3.1. Total chlorophyll *a* concentration (TChl*a*) was estimated as the sum of monovinyl chlorophyll *a*, chlorophyllide *a* and chlorophyll *a* allomers and epimers. A linear regression between DP and TChl*a* showed a strong linear relationship (r^2 = 0.83, n = 112) signifying that DP is also a valid estimate of phytoplankton biomass (Barlow et al. 2010) (Figure 3.1). Four major phytoplankton groups were delineated, namely diatoms, peridinin-containing dinoflagellates, small flagellates and prokaryotes. The indices representing these groups were labelled DiatDP, DinoDP, FlagDP and ProkDP and the proportion of each group

contributing to the biomass was defined as given in Table 3.1. The justification for the derivation of these indices using the appropriate biomarker pigments has been discussed extensively by Barlow et al. (2007, 2008). Divinyl chlorophylls *a* and *b*, the biomarkers for the prokaryote *Prochlorococccus sp*., were not detected and therefore chlorophyll *b* was considered to indicate chlorophytes (Jeffrey and Vesk 1997) and allocated to the small flagellate fraction (Barlow et al. 2010).

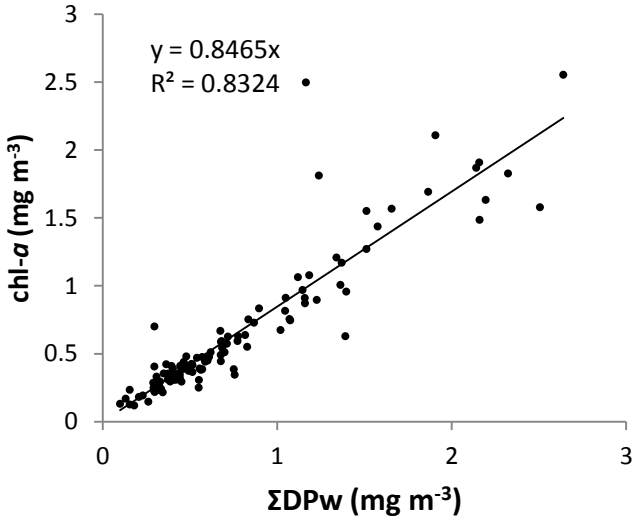

Figure 3.1 Regression of chl-*a* and ΣDPw. (n =112)

Finally, as described by Barlow et al. (2010), photo-pigment indices were derived to determine the changing contribution of chlorophylls and carotenoids to the total pigment pool. The chlorophylls were proportioned into TChl*a* and the sum of chlorophyll *b* plus chlorophyll *c*'s (Chl*bc*). The carotenoids were distinguished as photosynthetic carotenoids and photoprotective carotenoids. The photosynthetic carotenoids (PSC) included 190-butanoyloxyfucoxanthin, fucoxanthin, 190-hexanoyloxyfucoxanthin and peridinin, while the photoprotective carotenoids (PPC) were composed of alloxanthin, bb-+be-carotene, diadinoxanthin, diatoxanthin, lutein, violaxanthin and zeaxanthin. Photo-pigment indices were defined as given in Table 3.1 and labelled as TChl*a*TP, Chl*bc*TP, PSCTP and PPCTP.

Diagnostic Pigments as a determinant of phytoplankton community structure

HPLC pigment analysis enables the detection of a range of pigments (generally up to 15). Total Chlorophyll-*a*, the first group of pigments, is comprised of chlorophyll-*a*, divinyl

chlorophyll-*a* and chlorophyllide *a*, whose sum is noted [Chl *a*]. Other pigments, referred to as accessory pigments, can also be identified via HPLC. Several are indicative of specific phytoplanktonic groups and can be used as biomarkers. To consolidate the information contained within the full range of pigments, and in accordance with previous studies (Gieskes et al. 1988, Claustre 1994, Vidussi et al. 2001, Barlow et al. 2007 & 2008), an index of pigments is developed to quantify taxonomic composition by using a minimal set of representative pigments (Uitz et al. 2006). Seven major pigments were subsequently chosen as being indicative of distinct phytoplankton groups (Uitz et al. 2006). Their taxonomic significance is summarized in Table 3.1 (see Vidussi et al. 2001, Table 1, and other supporting references therein). The seven pigments are Fucoxanthin, Peridinin, 19'-hexanoyloxy fucoxanthin, 19'-butanoyloxy fucoxanthin, Alloxanthin, chlorophyll *b* + divinyl chlorophyll *b*, and Zeaxanthin. It is important to note that in comparison to the flourimetric method, which underestimates chlorophyll *a*, but overestimates phaeopigments when chlorophyll *b* is present, the HPLC method precisely separates chlorophyll *a* from phaeopigments (Gibbs 1979, Mantoura et al. 1997, Uitz et al. 2006).

To infer phytoplankton size classes, Claustre (1994) established a method to quantify the relative proportion of diatoms plus dinoflagellates (conjointly called 'microplankton') within an algal stock, based on the presence of fucoxanthin and/or peridinin. Their proportion is expressed by the ratio of concentrations:

([Fuco] + [Perid])/DP,

Where DP is the sum of all 'diagnostic pigments' concentrations:

DP = [Fuco] + [Perid] + [Hex-fuco] + [But-fuco] + [Allo] + [TChlb] + [Zea]

In 2001, Vidussi et al. expanded on this method by assigning three independent groupings of specific pigments (among the seven significant ones), with the aim of identifying three size classes and quantifying their relative proportion (Uitz et al. 2006). These classes are the microplankton (quantified by the ratio introduced above, Claustre 1994), the nanoplankton (2-20 µm), and the picoplankton (<2 µm); these two new classes are described by the (mutually independent) ratios:

Nanoplankton = *([Hex-fuco] + [But-fuco] + [Allo])/DP*,

and

Picoplankton = *([TChlb] + [Zea])/DP*

As previously mentioned (Vidussi et al. 2001 & Uitz et al. 2006), the pigment grouping presented here does not assume rigid classification of true phytoplankton community size classes. Of course, some taxonomic pigments could be present in each phytoplankton group. For example, small amounts of fucoxanthin, the main carotenoid of diatoms, may also be found in some prymnesiophytes and pelagophytes. Some phytoplankton groups may be present across a broad size-spectrum, such as diatoms, which generally belong to microplankton (20-200+ µm), but which can often also be found in the nanoplankton (2-20µm). However, any ambiguities and concerns about the strict definition of size classes aside, these terms (and their abbreviations pico-, nano-, and micro-) will be employed here (see also Uitz et al. 2006).

These combined size-classes and pigment groupings make up a phytoplanktonic assemblage in terms of diagnostic pigments, DP (Uitz et al. 2006). To obtain a best estimate of the seven ratios $\{Chl\textit{a}\}z_{eu}/\{P\}z_{eu}$ (chl-*a* content and the seven pigment contents), Uitz et al. (2006) used a multiple regression approach coupled with the three distinct groupings introduced by Vudussi et al. (2001). The regression was found to be highly significant (r^2 = 0.76, n= 2419, $p < 0.001$; see Table 3.1), where the slopes are utilized to calculate the weighted sum of all the diagnostic pigments concentrations, ΣDP_w, expressed as:

$$\Sigma DP_w = 1.41[Fuco] + 1.41[Perid] + 1.27[Hex\text{-}fuco] + 0.35[But\text{-}fuco] + 0.60[Allo] + 1.01[TChlb] + 0.86[Zea] \quad (1)$$

Unlike DP, ΣDP_w equals the chl-*a* concentration, which can be derived from the concentration of the seven other pigments. The fractions of the chl-*a* concentration correlated with each of the three phytoplanktonic classes (f_{micro}, f_{nano}, and f_{pico}) are thus derived according to (Uitz et al. 2006)

$$f_{micro} = (1.41[Fuco] + 1.41[Perid])/ \Sigma DP_w \quad (2a)$$

$$f_{nano} = (1.27[Hex\text{-}fuco] + 0.35[But\text{-}fuco] + 0.60[Allo])/ \Sigma DP_w \quad (2b)$$

$$f_{pico} = (1.01[TChlb] + 0.86[Zea])/ \Sigma DP_w \quad (2c)$$

When summed, the three distinct groups equal 1, which indicates they are not mathematically independent. The categorical chl-*a* concentration associated with each of the three classes is derived according to:

$$micro\text{-}[Chla] = f_{micro}\, x\, [Chla] \quad (3a)$$

$$nano\text{-}[Chla] = f_{nano}\, x\, [Chla] \quad (3b)$$

$$pico\text{-}[Chla] = f_{pico}\, x\, [Chla] \quad (3c)$$

A recent HPLC intercomparison exercise of pigment determination on natural samples, involving four laboratories, showed that [Chla] can be determined to within an uncertainty of approximately 8% (Claustre et al. 2004); the accuracy for accessory pigments is generally less (Uitz et al. 2006). It was shown, however, that pigment ratios (as in equations (2)) are determined with a better accuracy than individual accessory pigment concentrations by virtue of normalization, which cancels some analytical uncertainties (Uitz et al. 2006). Subsequently, the use of equations (2) and (3) is considered the most accurate approach to date when combining different data sources.

Table 3.1 Diagnostic pigments used in the present study as biomarkers and their taxonomic significance (Vidussi et al. 2001). The associated mean size class, and the corresponding $\{Chla\}Z_{eu}$ to $\{P\}Z_{eu}$ ratios ± SD, with their significance level are also given.

Diagnostic Pigments	Abbreviations	Taxonomic Significance	Phytoplankton Size Class	{Chla}Zeu: {P}Zeu	Significance Level
Fucoxanthin	Fuco	diatoms	microplankton	1.41 ± 0.02	$p < 0.001$
Peridinin	Perid	dinoflagellates	microplankton	1.41 ± 0.10	$p < 0.001$
19'-hexanoyloxy fucoxanthin	Hex-fuco	prymnesiophytes = chromophytes nanoflagellates	nanoplankton	1.27 ± 0.02	$p < 0.001$
19'-butanoyloxy fucoxanthin	But-fuco	chyrsophytes = chromophytes nanoflagellates	nanoplankton	0.35 ± 0.15	$p = 0.02$
Alloxanthin	Allo	cryptophytes	nanoplankton	0.60 ± 0.16	$p < 0.001$
chlorophyll b + divinyl chlorophyll b	TChlb	prasinophytes = green flagellates prochlorophytes	picoplankton	1.01 ± 0.10	$p < 0.001$
Zeaxanthin	Zea	cyanobacteria prochlorophytes	picoplankton	0.86 ± 0.09	$p < 0.001$

3.2.2 Dual labelled primary production

The transects from Antarctica to South Georgia and back to Antarctica (Legs 2 and 3) were intended to be the main focus for the biogeochemical observations with both underway and water column productivity sampling. However, due to a permanent failure of the CTD winch, no CTD casts or water column productivity measurements were possible. This limitation inspired the inclusion of size fractionated productivity measurements from surface waters in addition to the experimental P vs. E productivity measurements. Due to these unexpected circumstances (plus no 2 µm membrane filters), the size fractions utilized were microphytoplankton (>20 µm), nanophytoplankton (>1 and < 20 µm) and picophytoplankton (< 1 µm).

Production measurements were made at eleven stations on Legs 2, 3 and 4 (Antarctica to South Georgia, South Georgia to Antarctica, and Antarctica to Cape Town respectively) (see Table 3.2 and Figure 3.4). Photosynthesis versus irradiance (P vs. E) measurements of dual labelled (^{13}C + ^{15}N) nitrate, carbon and ammonium uptake after a 4 hr incubation period were made at each station. P vs. E biomass and productivity data will be presented and discussed.

P vs. E incubations

In this study, the P-E approach was used to examine photoacclimation and to establish PE parameters (α, P^b_{max}, E_k & β; see Table 3.3 for list of P-E parameters) in surface water samples after the incorporation and subsequent uptake of ^{13}C by phytoplankton, as well as by light controls on nitrogen assimilation using ^{15}N stable isotopes.

Water samples for dual-labelled (^{15}N, ^{13}C) P vs. E incubations were collected from the surface (~5 m) engine room supply clean intake. One litre water samples were collected in two sets of 15 x 1L polycarbonate bottles and 2 x 1L dark bottles. One set of 16 bottles (15 light and one dark bottle) was inoculated with ^{15}N (1 µmol $K^{15}NO_3$ / 100 µl) and ^{13}C (4.2507 g sodium bicarbonate / 100 ml Milli-Q water) spikes to achieve ^{15}N-NO_3 and ^{13}C enrichments of ~10 and 5% respectively. The second set of 16 bottles was spiked with 0.1 µmol $^{15}NH_4Cl$ / 100 µl at ~10% of ambient NH_4 concentration. The two sets of bottles were incubated in two identical linear box incubators with an artificial light source at one end and Lee 'misty blue' filters specifically placed to remove red light and to recreate water-column light attenuation

(see Figure 3.1 for example). Two 2000-W tungsten-halogen lamps were used as the light sources: photon flux (I) ranged from 0 to 390 µE m^{-2} s^{-1} and irradiance levels in the photosynthetron were measured using a Biospherical Instruments probe (QSP200).

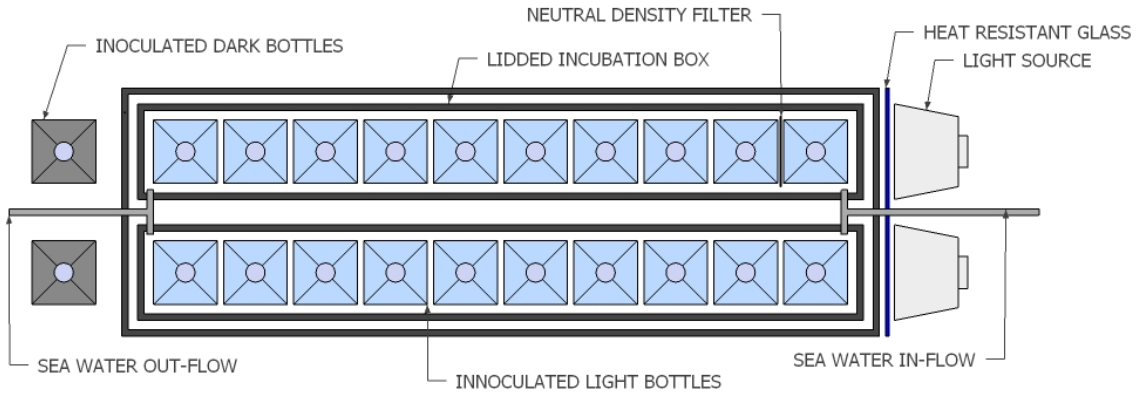

Figure 3.2 Simplified plan view of P vs. E incubation box design created in Google Sketch Up.

The bottles were placed alongside one another in the incubation boxes to create a diminishing light gradient away from the light source (~400 to 0 µE m^{-2} s^{-1}) (Figure 3.2). The incubators had a circulating water bath between the bottles and the light source to absorb the majority of the heat generated from the lamps, and surface sea water was also continuously circulated through the incubator boxes to maintain near ambient temperatures in all sample bottles. Samples were incubated for 4 hours, after which the samples were filtered onto 25 mm ashed GF/F filters, dried in an oven at 50˚C and stored in tin foil wrapped petri dishes for future analysis on a mass spectrometer back at the University of Cape Town.

Table 3.2 PE-curve parameters used in the text.

P (≡ P^B)	Production or (production per unit chl-*a*)	mgC (mgChl*a*$^{-1}$) h^{-1}
P^B_{max}	Chl-*a* specific maximum light-saturated photosynthetic rate	mgC mgChl*a*$^{-1}$ h^{-1}
α	Maximum light utilisation coefficient	mgC mgChl*a*$^{-1}$ h^{-1}(µE m^{-2} s^{-1})$^{-1}$)
β	Slope of photoinhibition	mgC mgChl*a*$^{-1}$ h^{-1}
E_k	Irradiance at saturation (light adaptation index)	µE m^{-2} s^{-1}

Mass spectrometry

The samples were prepared for mass spectrometry by punching 17-40 mm discs out of the filters depending on the amount of material present and whether a 25 or 47 mm filter had been used, and pelleted into Toluene rinsed and dried tin capsules (5 mm X 12 mm Santis Ananlytical tin capsules for solids). The isotopic composition of all samples was determined on a Flash EA 1112 series elemental analyzer (Thermo Finnigan, Milan, Italy). Combustion gases were passed to a Delta PlusXPIRMS (isotope ratio mass spectrometer; Thermo electron, Bremen, Germany), via a Conflo III gas control unit (Thermo Finnigan, Bremen, Germany). The in-house standard used was DL Valine purchased from Sigma. The in-house standard was calibrated against IAEA (International Atomic Energy Agency) standards. Nitrogen is expressed in terms of its value relative to atmospheric nitrogen, while carbon is expressed in terms of its value relative to Pee-Dee Belemnite.

Analytical Principle

Samples first pass through the Flash EA 1112 series elemental analyzer where reduction of particulate organic nitrogen to N_2 gas and subsequent elemental analysis is achieved via the Dumas combustion method (Preston & Owens 1983, Slawyk et al. 1988). Samples are placed into a carousel autosampler that sequentially drops pelletted samples into a combustion furnace (850°C for CuO) where flash combustion takes place after injection of O_2 (~23-175ml min^{-1} for an average of 8 seconds). Here, the major elements in the sample (C, H, N) are oxidised to CO_2, H_2O, N_2O and N_2 gases respectively. These gases are carried by a helium gas carrier flow (flow rate 100 ml min^{-1}) into the reduction furnace (650 °C), where N_2O is reduced to N_2 in the presence of a copper catalyst and excess O_2 is removed by copper oxidation. The remaining gases pass through a water trap (anhydrous magnesium perchlorate). If C is not being analysed, CO_2 is also removed by a trap ("Pelisorb", Santis Ananlytical). However, in this case very little CO_2 was generated so the 'trap' was not necessary and CO_2 was allowed to pass out of the system. The gases then pass through a gas chromatograph (GC) column (at 40 °C), which temporally separates the gases. Nitrogen gases elute before CO_2 so that two separate peaks occur on the chromatogram with a smaller CO_2 peak indicating correct system function. The N_2 gas is then introduced into a triple collector mass spectrometer where it is ionised by an electron impact ionisation source (accelerating voltage 3400 V). The resulting ions pass through a

flight tube then a fixed magnet separates the ions on the basis of their mass to charge ratio (m/z). Ions of mass 28 ($^{14}N^{14}N$), 29 ($^{14}N^{15}N$) and 30 ($^{15}N^{15}N$) are detected by the triple collector, composed of Faraday cups, which become charged when hit by ions. The ion flux is converted to a proportional electrical current corresponding to masses 28, 29 and 30. A reference gas of known isotopic composition is measured once before each sample and used to correct for any instrument drift. A constant vacuum is maintained by a Turbomolecular pump which clears the instrument of waste gases. Delta values (δ, the excess of ^{15}N in the sample relative to the reference gas) are then calculated (by the software) from the expression:

$$\delta = ((R_{sam} - R_{ref})/ R_{ref}) * 1000 \quad (4)$$

where δ is in ‰ and R_{sam} and R_{ref} are the sample and reference ratios of minor (mass 29) to major beams (mass 28). At low enrichments (<5%), the contribution of mass 30 is insignificant and is therefore excluded in the calculation of δ, which is then corrected for the enrichment of the reference gas relative to air. Isotopic abundance (At%) is calculated from Equation 4, which can also be expressed as:

$$\delta = (At\%_{sam} - At\%_{nat})/ (At\%_{nat}) * 1000$$

$$At\%_{sam} = \delta * At\%_{nat} / 1000 - At\%_{nat}$$

where $At\%_{nat}$ is the natural isotopic abundance of ^{15}N (0.3663%).

Nitrogen Uptake Calculations

Nitrogen uptake (ρ, µmol N L^{-1} h^{-1}) was calculated from the equation of Dugdale & Wilkerson (1986):

$$\rho N = r * PON/ (R * t) \quad (5)$$

where PON is particulate organic nitrogen (µmol N L^{-1})

t is incubation length (h)

r is At% excess of the particulate fraction (=$At\%_{sam}$ - $At\%_{nat}$)

R is At% enrichment of the aqueous medium:

$$R = (S * At\%_{nat}/ 100 + s * p)/ (S + s) * 100 - At\%_{nat} \quad (6)$$

where S is substrate concentration (µmol N L^{-1})

s is the ^{15}N concentration after spike addition (µmol N L^{-1}) and

p is the ^{15}N spike purity.

Correction for isotopic dilution

For ρNH_4, ammonium regeneration, R, is likely to change considerably during the course of the incubation due to microzooplankton excretion. To take this into account, R was calculated at the start (R_0) and at the end (R_t) of each incubation. The amount of $^{15}NH_4$ present at T_0 and T_t can be expressed in two ways:

$$^{15}NH_4 = V * S_x * R_x + At\%_{nat} * C \quad (7a)$$

or

$$^{15}NH_4 = r_x (V * S_x + C) \quad (7b)$$

where V is sample volume (L)

S_x is substrate concentration at t_x (µM)

C is the amount of NH_4 added as "carrier" (µmol) and

r_x is the measured enrichment at t_x (At%).

These can be combined to calculate R_0 and R_t:

$$R_x = (r_x (V * S_x + C) - r_{nat} * C)/ (V * S_x)$$

R_0 values were calculated from the initial spike addition following equation 6. Using these values, the average R over the time course of the incubation was then calculated based on the assumption that R decreases exponentially over time, following the equation of Glibert et al. (1982):

$$R_G = R_0/ (ln (R_0/ R_t)) * (1 - (R_t/ R_0)) \quad (8)$$

This corrected value of aqueous enrichment (R_G) was then substituted for R in the calculation of uptake (Equation 5).

Carbon fixation

Similarly to nitrogen uptake, carbon fixation was calculated from the equation

$$\rho C = (r * POC) / (R * t) \quad (9)$$

where POC is particulate organic carbon (µmol C l^{-1}) and S (from Equation 6) is assumed to be 2100 µmol C l^{-1}.

All PON/POC and r values were blank corrected to remove any signal expressed by the filters themselves.

3.2.3 Photosynthetically Available Radiation (PAR)

The ship's PAR system malfunctioned regularly and was deemed untrustworthy, so in addition to daily weather observations recorded from the ship by the South African Weather Service, weekly (8 day composite) averaged PAR values were obtained from NASA's SeaWiFS satellite data archive to give an accurate indication of the photosynthetic available irradiance at the sea surface.

3.3 Results

3.3.1 Sampling Stations

Legs 2 (Antarctica to South Georgia) and 3 (South Georgia to Antarctica) traversed through three zones (WG, SAISB and AAZ) and crossed the SBdy and the sACCf (Figure 3.2). For a period of time Leg 3's transect ran along the SBdy. Leg 2 had 2 stations in the WG (BR3 & BR12), one station in the AAZ (BR20) and one in the SAISB (downstream of South Georgia, BR26). Leg 3 had one station in the AAZ (along the SBdy, BR38) and two in the WG (BR50 & BR62). Leg 4 (Antarctica to Cape Town) had one station in the ACS (HB1), one station in the WG (HB11), one station in the AAZ (HB23) and one in the N-ACC (HB42).

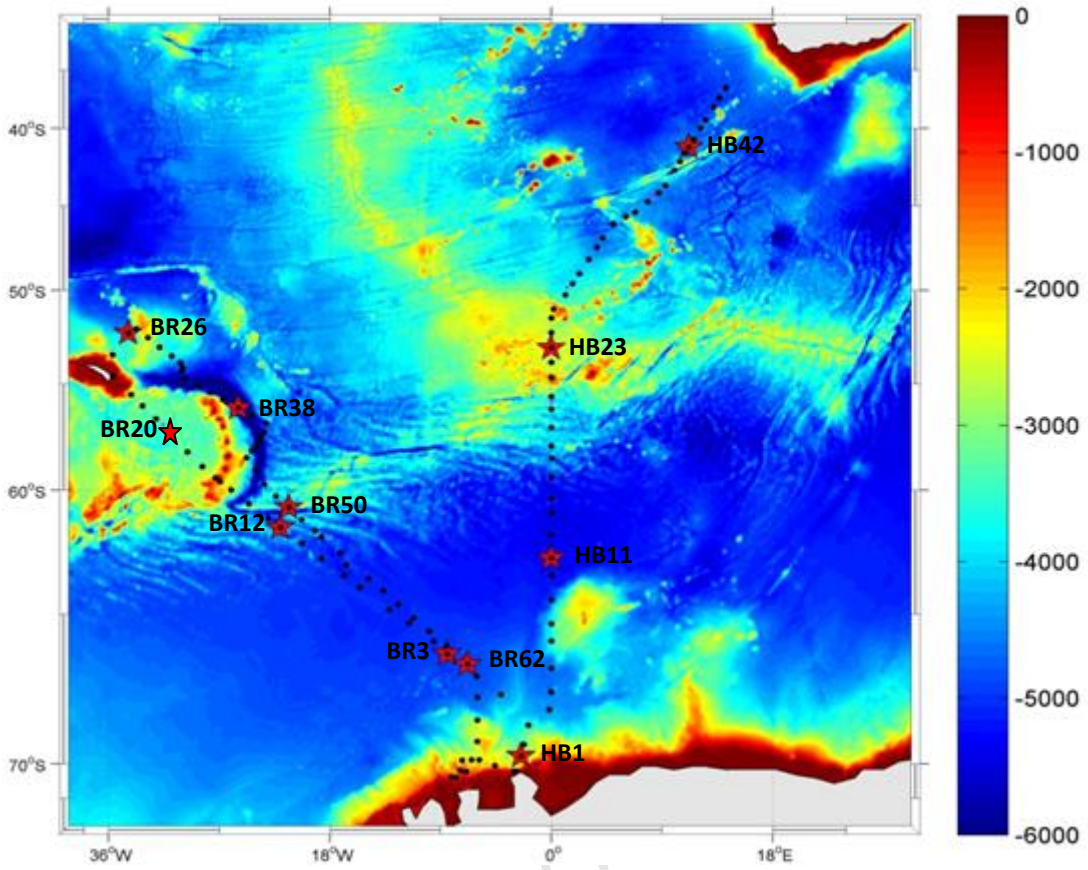

Figure 3.3 Map of the cruise track for Legs 2, 3 and 4 with the 11 productivity stations (represented by red stars) layered on top of seafloor bathymetry.

Table 3.3 Dates, start time and position of the 11 productivity stations

Station	Date	Time (GMT)	Lat	Lon
BR3	2009/01/27	06:43	-66.43	-8.45
BR12	2009/01/29	07:10	-61.59	-22.04
BR20	2009/01/31	07:07	-57.32	-31.19
BR26	2009/02/01	05:07	-52.35	-34.38
BR38	2009/02/03	06:14	-56.18	-25.46
BR50	2009/02/05	06:08	-60.75	-21.35
BR62	2009/02/07	07:00	-66.79	-6.83
HB01	2009/02/21	15:11	-69.76	-2.443
HB11	2009/02/23	05:39	-62.84	0.010
HB23	2009/02/25	05:38	-53.16	0.002
HB42	2009/02/28	05:02	-41.27	11.184

3.3.2 HPLC

Antartica to South Georgia (Leg 2)

Mean chlorophyll-*a* concentration was 0.96 mg m^{-3}. On Leg 2 chlorophyll-*a* concentration peaked in the WG region at 68°S and at 61°S (2.25 mg m^{-3} and 1.7 mg m^{-3}) (Figure 2.11a, Chapter 2). Another notable peak (2.25 to 3.09 mg m^{-3}) occurred in the island influenced area at ~52°S.

The accessory pigment Fucoxanthin (diatoms) makes up the greatest proportion of total chlorophyll-*a* followed by 19'-Hexanoyloxyfucoxanthin (prymnesiophytes) and Peridinin (dinoflagellates) (Figure 3.4). Diatoms peak in abundance between 62 and 59°S and again between 56 and 52°S. Prymnesiophytes show a slight increase at 63°S and again at 60°S. Dinoflagellates surpass prymnesiophytes, but not diatoms at 55°S.

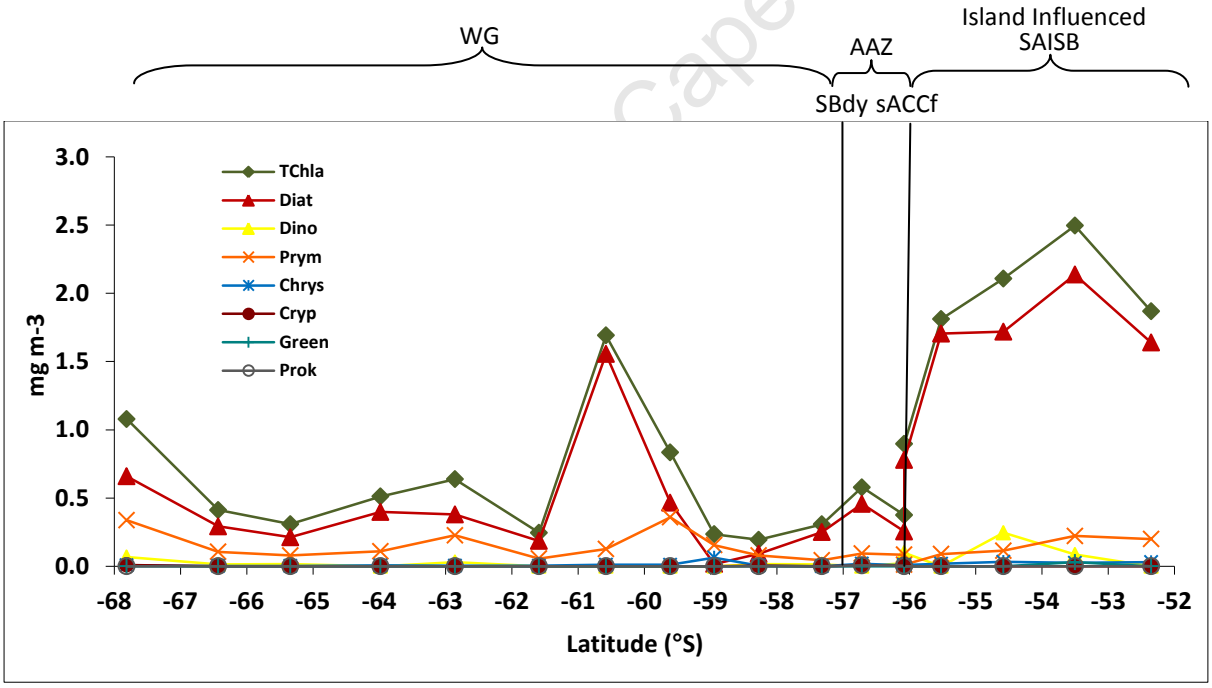

Figure 3.4 Community structure along Leg 2 (Antarctica to South Georgia) displayed as group contribution to total chl-*a*.

South Georgia to Antarctica (Leg 3)

Along Leg 3, chl-*a* again peaked in the WG region (2.4 and 1.5 mg m^{-3}), and in the ACS zone (3.0 mg m^{-3}) (Figure 2.11b, Chapter 2). Unexpectedly, a decline in concentration to 0.6 mg m^{-3} occurred along the SBdy, in the AAZ region.

Again the accessory pigment Fucoxanthin (diatoms) dominated, making up the greatest proportion of TChl*a* followed by 19'-Hexanoyloxyfucoxanthin (prymnesiophytes) (Figure 3.5). The greatest abundance of diatoms occurred between 62 and 60°S followed by a smaller peak at 59°S.

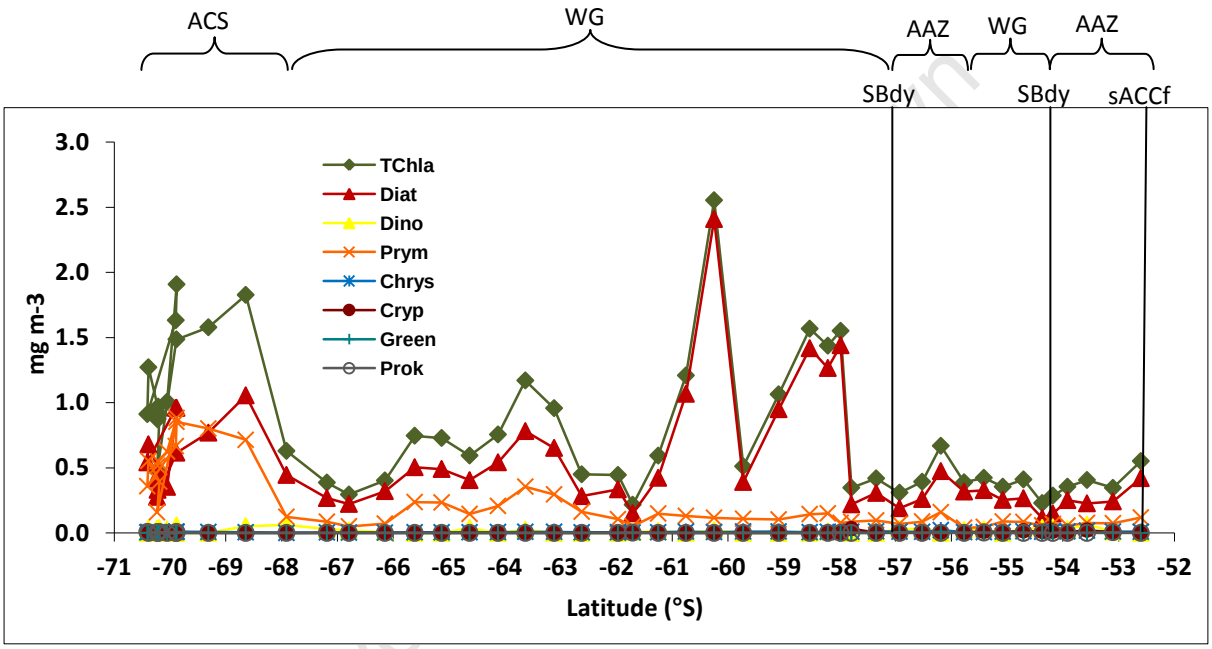

Figure 3.5 Community structure along Leg 3 (South Georgia to Antarctica) shown as group contribution to total chl-*a*.

Antarctica to Cape Town (Leg 4)

Chl-*a* concentrations were generally low along the length of this transect (mean 0.49 mg m^{-3}) (Figure 2.10b, Chapter 2). The greatest values were encountered at 68°S in the ACS region (1.5 mg m^{-3}), at 60°S in the WG region (0.96 mg m^{-3}), at 52°S in the AAZ (0.66 mg m^{-3}) and at the STF, ~40°S (0.62 mg m^{-3}).

The accessory pigment Fucoxanthin (diatoms) made up the greatest proportion of Tchl-*a*, followed closely by 19'-Hexanoyloxyfucoxanthin (prymnesiophytes), with Peridinin (dinoflagellates) and total chl-*b* (smaller green algae -flagellates) making up the next greatest proportion (Figure 3.6). Prymnesiophytes peaked when diatoms were low in

abundance at 71°S, 69°S, and 59°S, and from 47°S to 39°S they remained in greater proportion to diatoms, with notable peaks at 45°S and 40°S. Green algae (flagellates) peaked at 49°S, but still remained lower in proportion to the other dominant groups. North of the STF prokaryotes replaced prymnesiophytes as the dominant algal group.

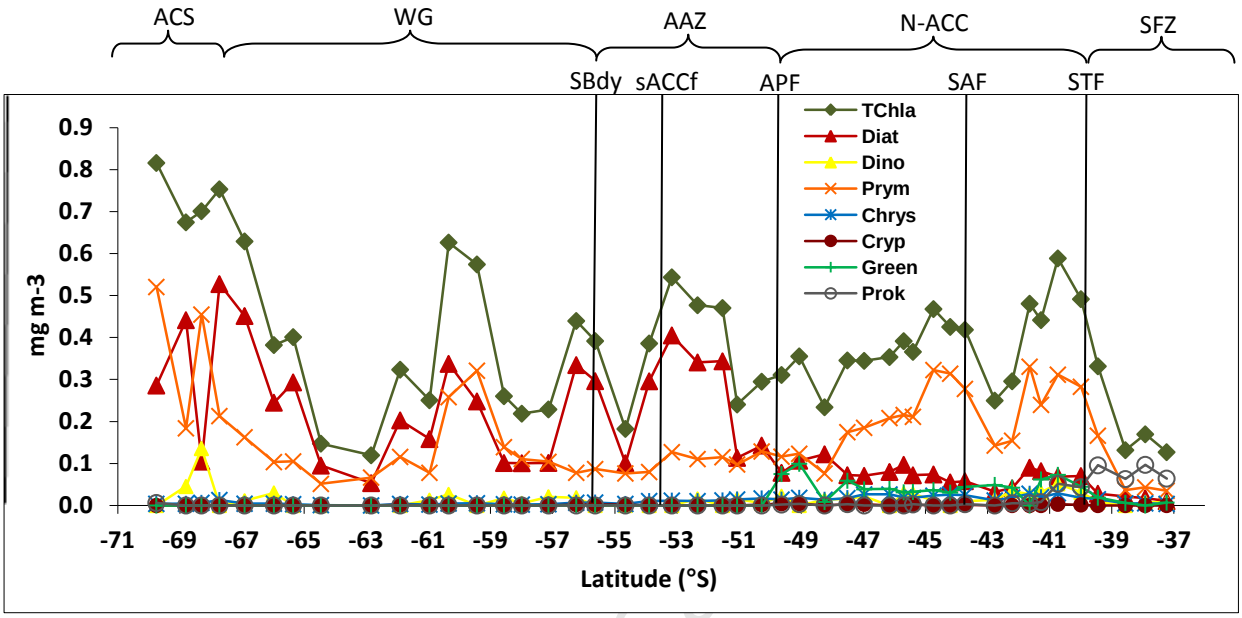

Figure 3.6 Community structure along Leg 4 (Antarctica to Cape Town) displayed as group contribution to total chl-*a*.

3.3.3 Pigment Indices

Total chl-*a* made up the greatest proportion (~35 – 55%) of the total pigment pool at all stations except BR20 (~25%) (Figure 3.7a). Chl *b* + *c* contributed ~20% to the total pigment pool at each station (Figure 3.7a). There was a greater proportion of photosynthetic carotenoids (~31%) than photoprotective caratenoids (~8-10%) which contributed the smallest proportion of total pigments at all productivity stations (Figure 3.7a and b). Photoprotective caratenoids increased from 10 to 40% of the total pigment proportion at the end of Leg 4 (Figure 3.7b).

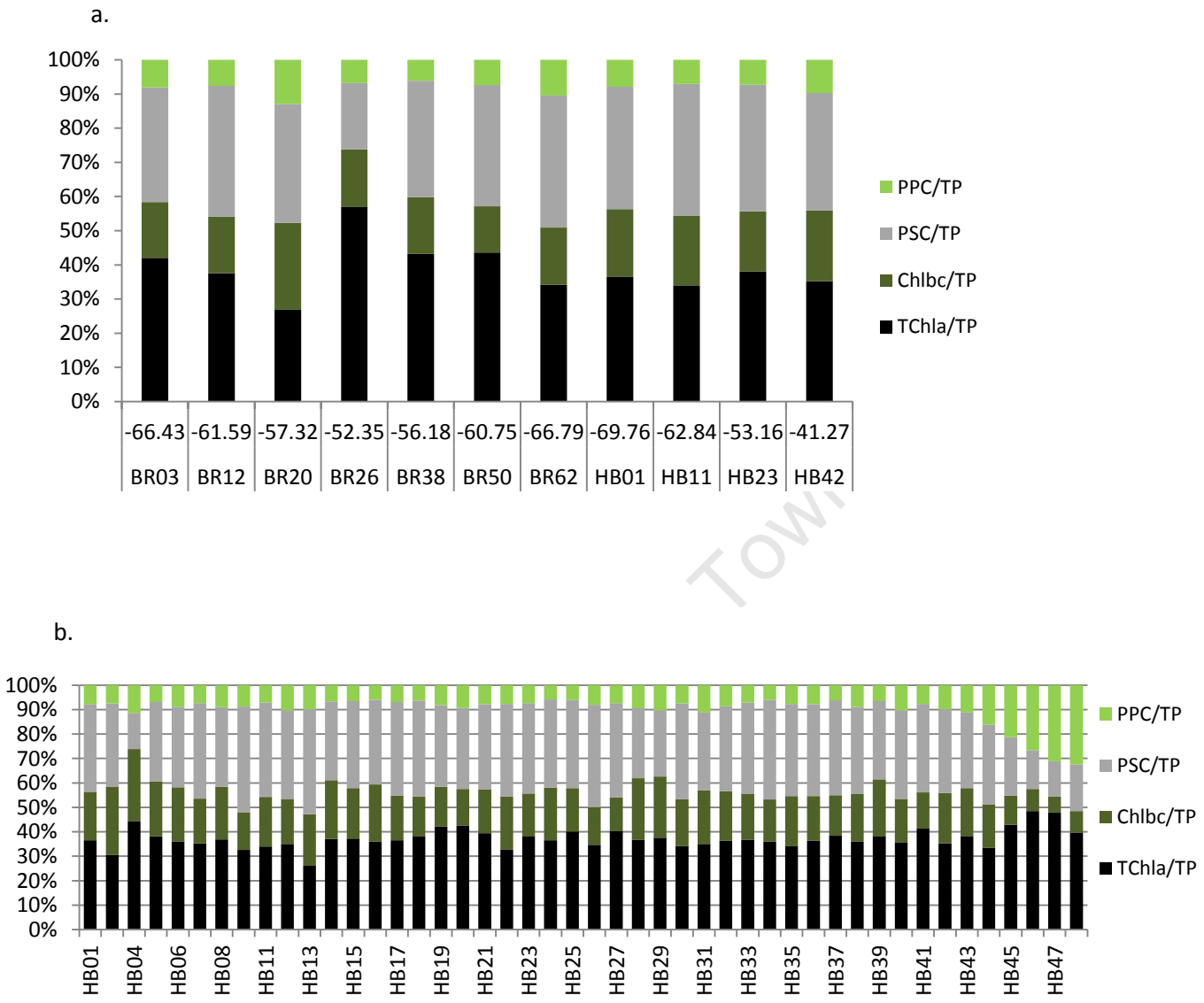

Figure 3.7a & b. a.) Pigment type ratios for each productivity station along Legs 2, 3 and 4. Stations BR3, BR12, BR20, BR26 are Leg 2, BR38, BR50, BR62 Leg 3 and HB1, HB11, HB23, HB42 Leg 4. b.) Pigment type ratios for all HPLC stations along Leg 4, expanded upon here to show that change occurred in PPC along this leg. For both figures Black is Total Chl-*a*:Total Pigment, dark green is Chl*b*+*c*:Total Pigment, grey is Photosynthetic Carotenoid:Total Pigment and light green is PhotoprotectiveCarotenoid:TotalPigment.

3.3.4 Size Class Structure

Microplankton dominated at all productivity stations except HB1, HB11 and HB42 where nanoplankton were in greatest relative abundance (Figure 3.8). Picoplankton made up a small part of the entire community at HB1 and HB42. The greatest contribution of microplankton to TChl-*a* occurred at BR26 (2.3 mg m^{-3}) followed by BR50 (1.2 mg m^{-3}). Nanoplankton contributed the greatest part of TChl-*a* (0.6 mg m^{-3}) at HB1.

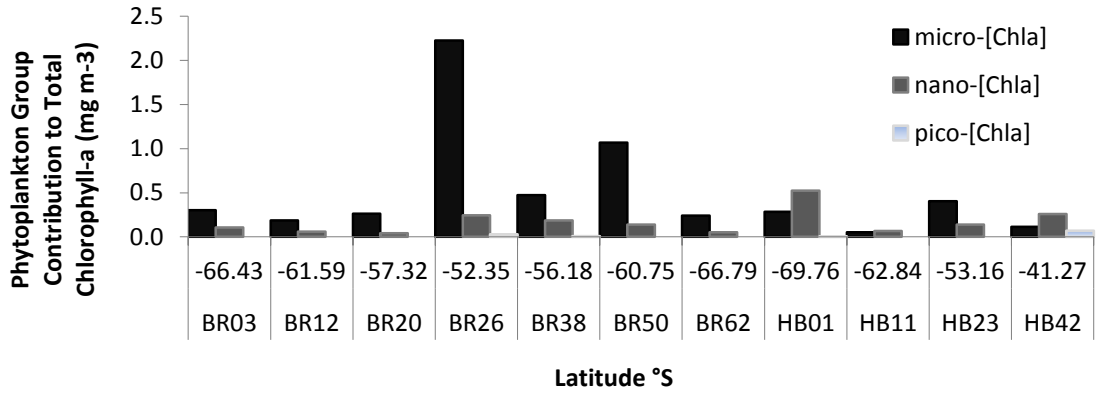

Figure 3.8 Size class structure at each productivity station along Legs 2, 3 and 4. Microplankton (>20 µm), shown in black, nanoplankton (>1 and < 20 µm) in dark grey, and picoplankton (< 1 µm) in light grey.

Table 3.4 Overview of initial parameters of the incubation experiments for the sample locations:N-ACC, AAZ, WG, SAISB and ACS (*no data available).

Station Number	Region	SST	Salinity	Chl-*a* [mgm^{-3}]	Si [µmolL^{-1}]	NO3 [µmolL^{-1}]	PO4 [µmolL^{-1}]	NH4 [µmolL^{-1}]	Urea [µmolL^{-1}]	Dominant Algal Group
BR 03	WG	-0.8	33.7	0.412	35.47	24.35	1.13	0.88	0.43	Diatoms
BR 12	WG	0.2	33.5	0.268	40.80	26.72	2.05	0.88	0.25	Diatoms
BR 20	AAZ	2.6	34.1	0.659	21.76	22.15	1.48	0.76	0.47	Diatoms
BR 26	SAISB	5.4	33.8	2.94	*	13.62	1.12	1.89	0.93	Diatoms
BR 38	AAZ	3.8	33.9	0.535	7.96	16.62	1.42	0.92	0.36	Diatoms
BR 50	WG	1.1	33.6	1.142	27.36	19.93	1.52	1.13	0.69	Diatoms
BR 62	WG	-0.3	33.8	0.487	32.66	23.65	1.77	1.09	0.65	Diatoms
HB 01	ACS	-0.8	33.4	0.851	29.94	18.90	1.29	1.05	0.80	Prymnesiophytes
HB 11	WG	0.7	34	0.213	27.46	22.09	1.67	1.01	0	Prymnesiophytes
HB 23	AAZ	2.4	33.8	0.573	21.20	22.11	1.68	0.51	0.55	Diatoms
HB 42	N-ACC	12	*	0.491	1.24	5.42	0.47	0.89	0	Prymnesiophytes

3.3.5 Primary Production

Primary production varied from 0.15 to 3.26 mg C m^{-3} hr^{-1} (Table 3.5, values calculated from P^B max, carbon fixation). Production was highest along Leg 2 (from Antarctica to South Georgia) at stations BR20 and BR26 in the AAZ (3.26 mg C m^{-3} hr^{-1}) and in the SAISB (2.18 mg C m^{-3} hr^{-1}) zones respectively. Lowest production occurred along Leg 4

(Antarctica to Cape Town) at HB11 (0.15 mg C m^{-3} hr^{-1}) in the WG region, followed by stations HB1 (in the ACS region) and HB23 (in the AAZ) (0.28 mg C m^{-3} hr^{-1} at both). Leg 3 (South Georgia to Antarctica) exhibited relatively low production at all three stations (0.60, 0.50, and 0.25 mg C m^{-3} hr^{-1}).

Table 3.5 Phytoplankton productivity at all productivity stations along Legs 2, 3 and 4.

Region	Stn	chl a (mg m^{-3})	POC (µg l^{-1})	POC:Chl a	PP (mg C m^{-3} hr^{-1})	P^{chl} (mg C mg chl-$a^{-1}hr^{-1}$)
WG	BR3	0.412	195.34	474	0.420	1.02
WG	BR12	0.268	95.89	358	0.309	1.15
AAZ	BR20	0.659	410.03	622	3.260	4.31
SAISB	BR26	2.940	163.22	55	2.180	0.74
AAZ	BR38	0.535	73.00	136	0.600	1.12
WG	BR50	1.142	70.33	62	0.497	0.45
WG	BR62	0.487	55.17	113	0.250	0.51
ACS	HB1	0.851	41.23	270	0.280	0.33
WG	HB11	0.213	29.59	48	0.150	0.70
AAZ	HB23	0.573	26.18	46	0.280	0.49
N-ACC	HB42	0.491	78.73	160	0.580	1.18

3.3.6 POC:Chl-*a* ratios

POC:chl-*a* ratios were calculated from fluorometric chl-*a* (see chapter 2, section 2.2.5) and from POC concentrations determined from the mass spectrometer results (for P^B max of C) and are highly variable (range 46 to 622 µg C µg chl-a^{-1}). There was no consistent pattern where high biomass coincided with greater carbon biomass. Normalized production also showed no clear trend with POC: Chl-*a* ratios.

3.3.7 Photosynthetically Available Radiation

PAR ranged from 24 to 48 E m^{-2} d^{-1} along Leg 2 (Antarctica to South Georgia) with greatest amounts occurring as the ship headed northwards (Figure 3.9a). Along Leg 3 (South Georgia to Antarctica) PAR values were slightly lower, ranging from 16 to 45 E m^{-2} d^{-1}, with the lowest value occurring at ~60°S, 20°W (Figure 3.9b). Leg 4 (Antarctica to Cape Town) had

the greatest range in PAR, which spanned 8 to 52 E m^{-2} d^{-1} along the length of the transect with the increase from south to north (Figures 3.9c & d). A seasonal progression in PAR was apparent when comparing the three legs, Leg 2 (mid-summer) having the highest overall PAR values for the entire region (Figure 3.9a).

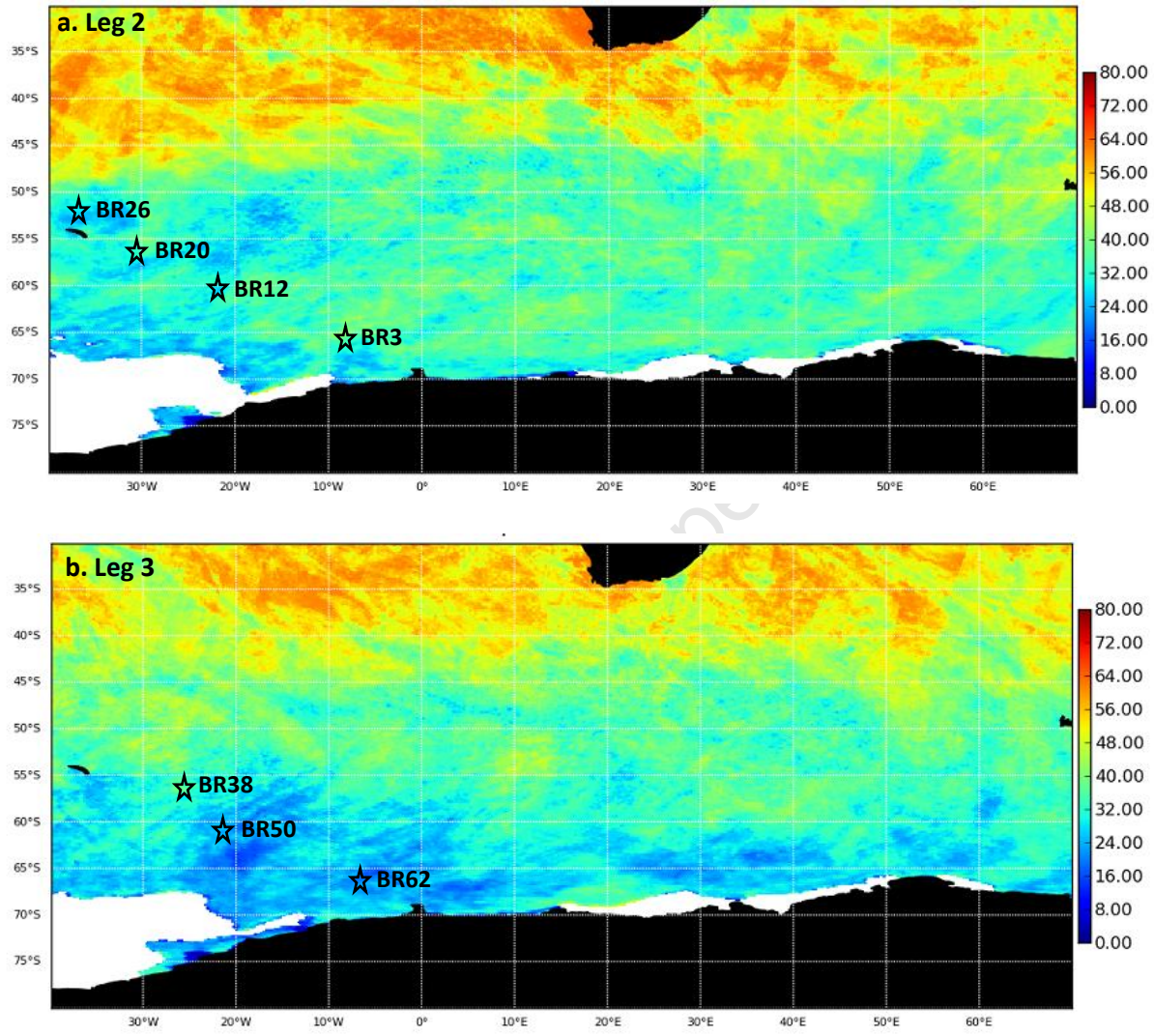

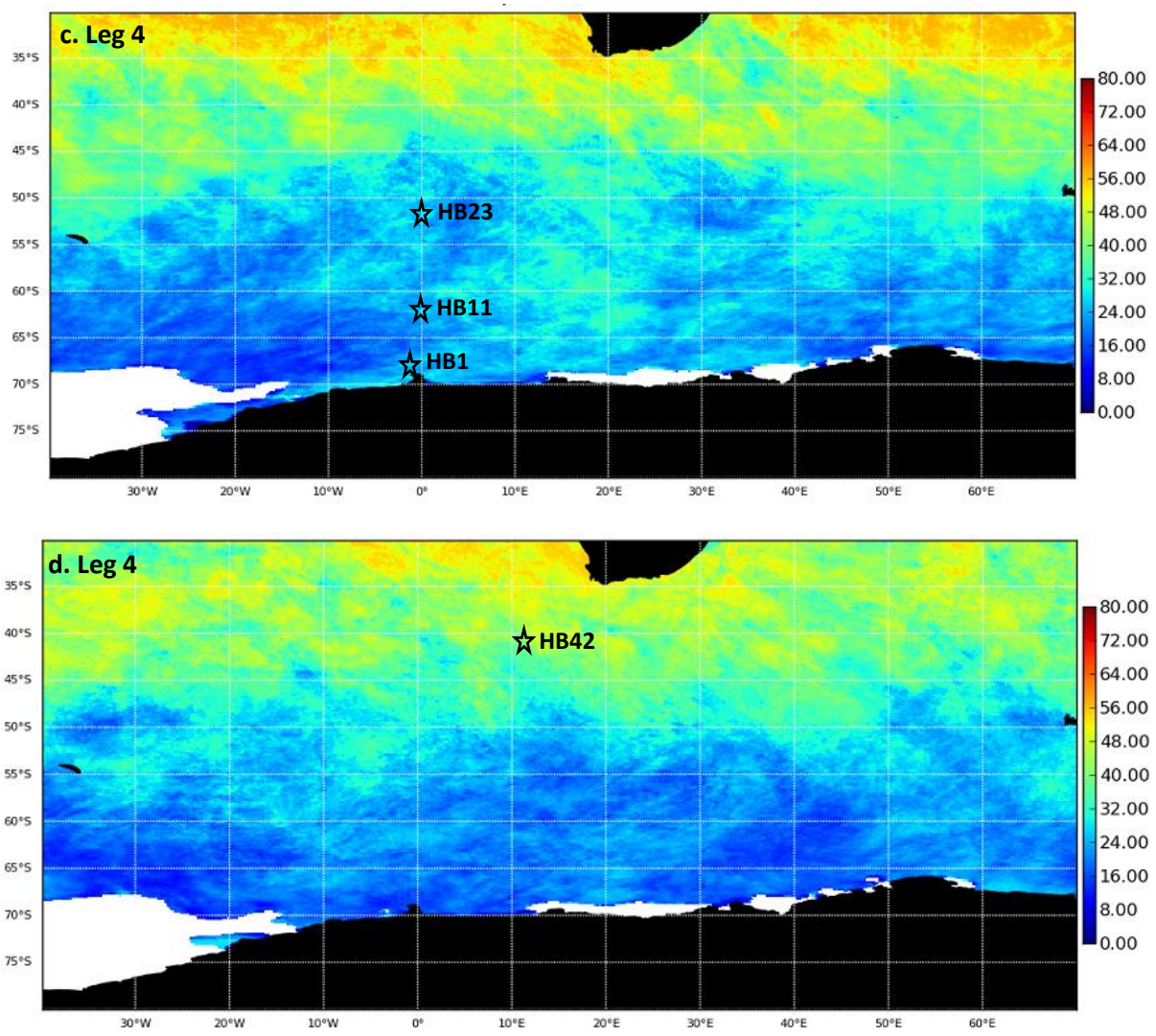

Figure 3.9a-d. Photosynthetically Available Radiation (PAR) 8 day satellite composites given for the periods a.)25 January to 1 February 2009, b.) 2 February to 10 February 2009, c.) 18 February to 26 February 2009, d.) 27 February to 3 March 2009. Black stars indicate position of the productivity stations. Colour bar represents PAR in Einsteins m^{-2} d^{-1}, images were compiled from Sea WiFs Level 2 Geophysical data products, http://www.class.ngdc.noaa.gov/d

3.3.8 P vs. E Curves

P-E parameters for nitrate and ammonium uptake and carbon fixation are represented in the P-E curves (Figures 3.10a, b, c and 3.11a, b, c, respectively and summarised in Table 3.4). General observations from these results were that pNH_4^+ curves always achieve a higher P^B_{max} than pNO_3^- curves. C-fixation curves always achieve a higher P^B_{max} than pNH_4^+ and pNO_3^- curves, except for at BR26 in the Subantarctic and shallow bathymetry region (SAISB) where pNH_4^+ P^B_{max} was highest (Figures 3.10c, 3.11c and Table 3.6). The relationship between P^B_{max} and dominant algal groups for each station indicates

diatoms have higher C-fixation P^B_{max} than the second most dominant group, prymnesiophytes (Figure 3.12).

P^B_{max} was greatest along Leg 2 (Antarctica to South Georgia) and specifically at station BR20 (4.31 mgC mgChl*a* h^{-1}). BR26 also had relatively high photosynthetic rates for all three nutrient substrates (0.741 mgC mgChl*a* h^{-1} [C-fix], 0.765 [NH4], and 0.096 [NO3] mgN mgChl*a* h^{-1}). Both higher values coincided with higher chl-*a* concentrations (0.659 and 2.94 mg m^{-3} respectively). BR3 and BR12 had high P^Bmax values for C-fixation (1.02 and 1.15 mgC mgChl*a* h^{-1} respectively), but low surface chl-*a* concentrations (0.412 and 0.268 mg m^{-3} respectively). Leg 3 (South Georgia to Antarctica) had one high P^B_{max} value at BR38 (1.09 mgC mgChl*a* h^{-1}) and the remaining stations were low, however BR50 did have a fairly high surface chl-*a* concentration of 1.14 mg m^{-3}. Leg 4 (Antarctica to Cape Town) had low P^B_{max} values with the northern most station, HB42 displaying the greatest value (1.19 mgC mgChl*a* h^{-1}).

E_k values ranged from 88 to 340 µE m^{-2} s^{-1} along the three transects. There was not a strong relationship between E_k and PAR for each substrate (pNO_3^- r^2 = 0.016, pNH_4^+ r^2 = 0.344, C-fix r^2 = 0.097), contrary to expectations that E_k would decrease with a decrease in PAR, or alternately an increase in latitude (Figure 3.13). Photoinhibition (β) was neglible for all stations. The light limited region of the P-E curves given as a measure of quantum efficiency of photosynthesis (α) followed a similar pattern for all stations whereby the slopes were all low, decreasing in the order C > NH_4 > NO_3.

Low *f*-ratios (mean 0.18±0.10) indicate preferential uptake of regenerated N species. Furhtermore, while the relationship between total nitrogen uptake and C-fixation was poor (r^2 = 0.032) due to two outliers (BR20 and BR26), four out of eleven stations fall very close to the expected Redfield ratio slope (~6:1) and an additional four out of eleven stations fall just below the Redfield slope as further evidence of N recycling based communities (Figure 3.14).

Table 3.6 Production station data showing depth (surface for all stations ~5m) with corresponding replicated percent light levels, chlorophyll-*a* (mgm^{-3}), and P. E. Parameters, P^{B}_{max} (mgCmgChl*a*$^{-1}$h^{-1}), α ((mgCmgChl*a*$^{-1}$h^{-1})(µEm-²s-^{1})$^{-1}$), E_k (µEm-²s-^{1}), β ((mgCmgChl*a*$^{-1}$h^{-1})(µEm-²s-^{1})$^{-1}$), PAR (µEm-²s-^{1}) as well as the P-E curve fit coefficients and level of significance. For nitrate and ammonium uptake, the units are in mg N rather than mg C.

Station		Z (%light)	Chl-*a*	P^{B} max	α	E_k	PAR	β	r	p
Leg 2	**Antarctica to South Georgia**									
BR3	NO_3^-	84	0.412	0.011	$5.94x10^{-5}$	190	370	0.000061	0.67	0.012
	NH_4^+	84	0.412	0.026	$1.57x10^{-4}$	164	370	0.000046	0.55	0.035
	C	84	0.412	1.021	$5.06x10^{-3}$	201	370	0.0045	0.74	0.002
BR12	NO_3^-	84	0.268	0.0315	$2.10x10^{-4}$	150	417	0.000031	0.82	0.000
	NH_4^+	84	0.268	0.086	$3.09x10^{-4}$	279	417	0.00023	0.70	0.005
	C	84	0.268	1.153	$6.36x10^{-3}$	182	417	0.0023	0.88	0.000
BR20	NO_3^-	34	0.659	0.031	$2.49x10^{-4}$	126	347	n/a	0.87	0.000
	NH_4^+	n/a	0.659	n/a	n/a	n/a	347	n/a	n/a	n/a
	C	56	0.659	4.313	$4.27x10^{-2}$	101	347	n/a	0.86	0.000
BR26	NO_3^-	84	2.94	0.096	$4.50x10^{-4}$	154	324	0.00061	0.85	0.000
	NH_4^+	22	2.94	0.765	$2.47x10^{-3}$	309	324	0.0019	0.60	0.018
	C	34	2.94	0.741	$8.13x10^{-2}$	136	324	0.0575	0.82	0.000
Leg 3	**South Georgia to Antarctica**									
BR38	NO_3^-	56	0.535	0.009	$4.32x10^{-5}$	199	486	n/a	0.98	0.000
	NH_4^+	56	0.535	0.089	$3.89x10^{-4}$	228	486	n/a	0.83	0.000
	C	56	0.535	1.086	$6.37x10^{-3}$	170	486	0.000031	0.87	0.000
BR50	NO_3^-	22	1.142	0.002	$2.16x10^{-5}$	88	301	n/a	0.80	0.000
	NH_4^+	34	1.142	0.081	$5.48x10^{-4}$	149	301	n/a	0.65	0.008
	C	22	1.142	0.455	$2.83x10^{-3}$	161	301	0.00075	0.58	0.025
BRU62	NO_3^-	34	0.487	0.020	$1.54x10^{-4}$	133	255	n/a	0.84	0.000
	NH_4^+	22	0.487	0.154	$1.32x10^{-3}$	116	255	n/a	0.60	0.040
	C	34	0.487	0.532	$3.64x10^{-3}$	146	255	n/a	0.83	0.000
Leg 4	**Antarctica to Cape Town**									
HB1	NO_3^-	16	0.851	0.012	$1.26x10^{-4}$	92	278	n/a	0.85	0.000
	NH_4^+	56	0.851	0.048	$1.92x10^{-4}$	249	278	n/a	0.85	0.000
	C	22	0.851	0.269	$2.58x10^{-3}$	104	278	n/a	0.82	0.001
HB11	NO_3^-	56	0.213	0.011	$4.04x10^{-5}$	275	301	n/a	0.87	0.000
	NH_4^+	100	0.213	0.129	$6.80x10^{-4}$	189	301	n/a	0.84	0.000

	C	22	0.213	0.699	$5.69x10^{-3}$	123	301	0.00125	0.74	0.002
HB23	NO_3^-	56	0.573	0.016	$9.93x10^{-5}$	158	347	n/a	0.87	0.000
	NH_4^+	84	0.573	0.053	$5.60x10^{-4}$	94	347	n/a	0.88	0.000
	C	56	0.573	0.528	$1.92x10^{-3}$	275	347	n/a	0.89	0.000
HB42	NO_3^-	84	0.491	0.013	$4.99x10^{-5}$	254	555	n/a	0.97	0.000
	NH_4^+	56	0.491	0.204	$8.94x10^{-4}$	228	555	n/a	0.90	0.000
	C	84	0.491	1.186	$3.49x10^{-3}$	340	555	0.0023	0.97	0.000

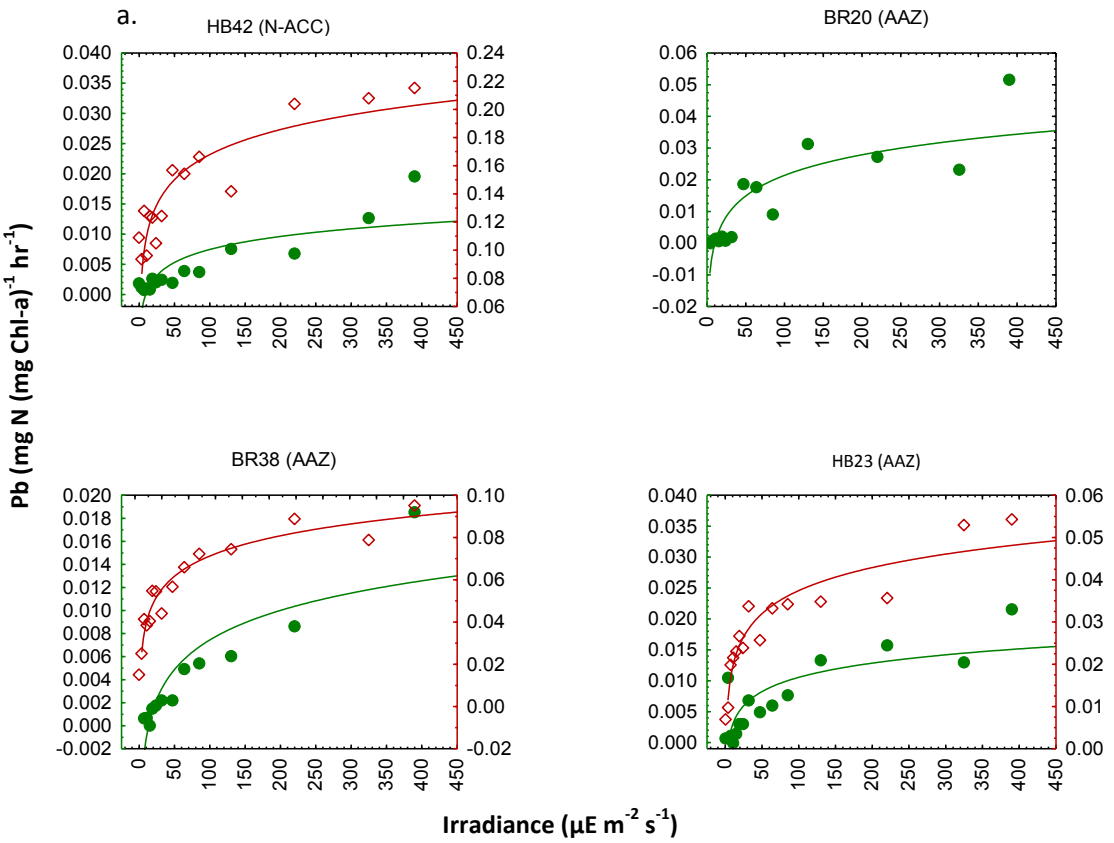

Figure 3.10a. P-E curves for NH_4^+ and NO_3^- assimilation at all 11 productivity stations. Red diamonds represent P^B for NH_4^+, green circles represent P^B for NO_3^-. Note the different scales on the y-axes where green represents P^B for NH_4^+ and red represents P^B for NO_3^-. BR = Buoy Run stations on Legs 2 and 3, HB = Homeward Bound stations on Leg 4, and zones are indicated in brackets.

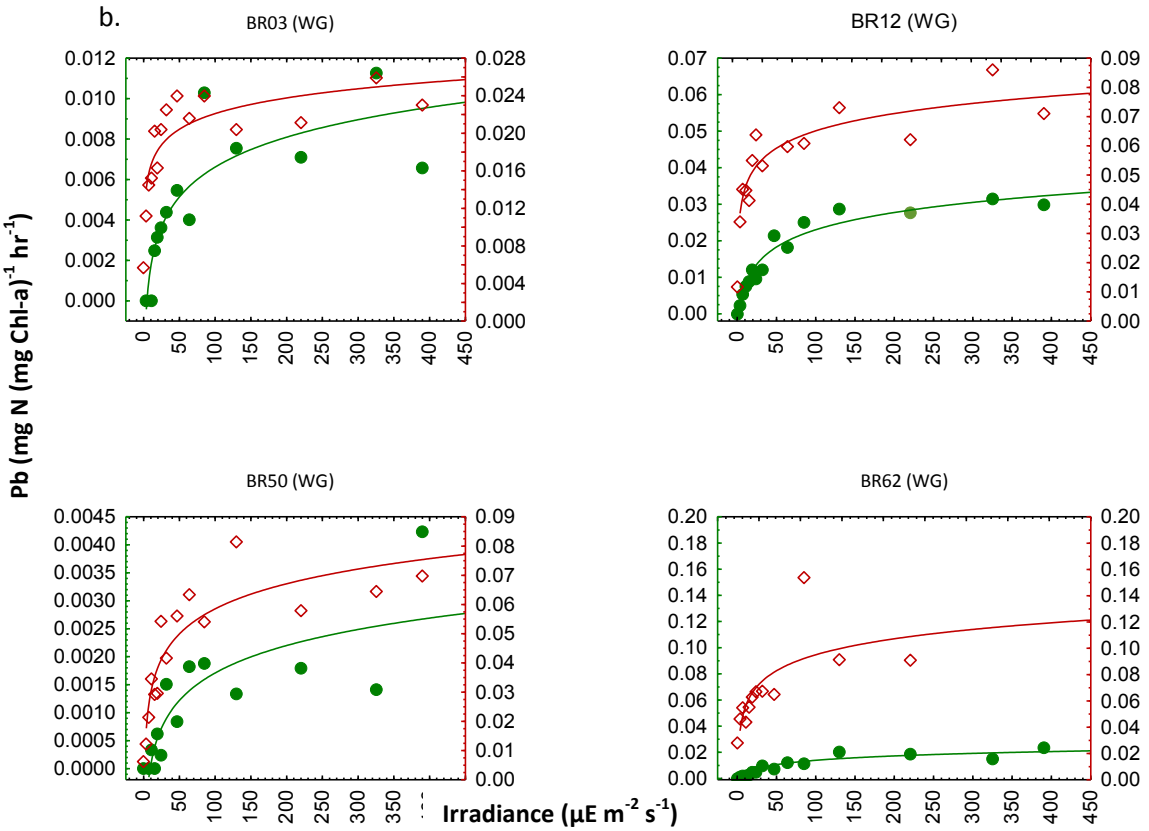

Figure 3.10b. P-E curves for NH_4^+ and NO_3^- assimilation at all 11 productivity stations. Red diamonds represent P^B for NH_4^+, green circles represent P^B for NO_3^-. Note the different scales on the y-axes where green represents P^B for NH_4^+ and red represents P^B for NO_3^-. BR = Buoy Run stations on Legs 2 and 3, HB = Homeward Bound stations on Leg 4, and zones are indicated in brackets.

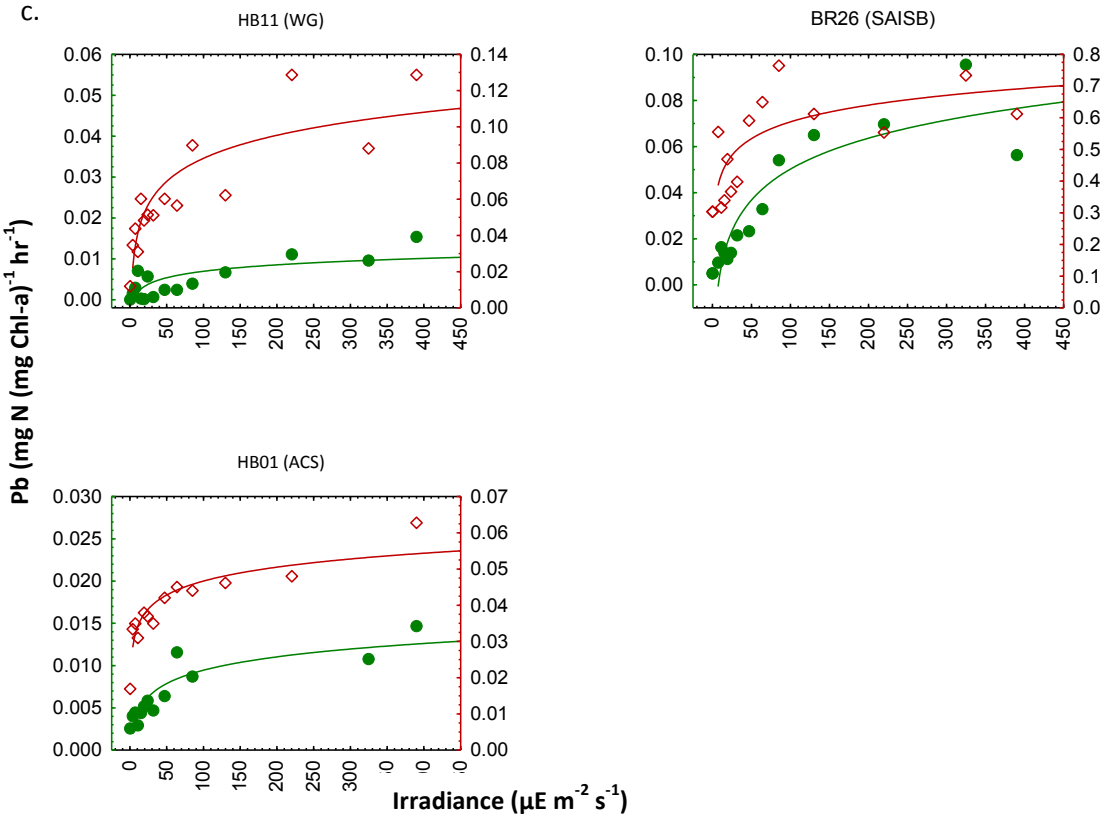

Figure 3.10c. P-E curves for NH_4^+ and NO_3^- assimilation at all 11 productivity stations. Red diamonds represent P^B for NH_4^+, green circles represent P^B for NO_3^-. Note the different scales on the y-axes where green represents P^B for NH_4^+ and red represents P^B for NO_3^-. BR = Buoy Run stations on Legs 2 and 3, HB = Homeward Bound stations on Leg 4, and zones are indicated in brackets.

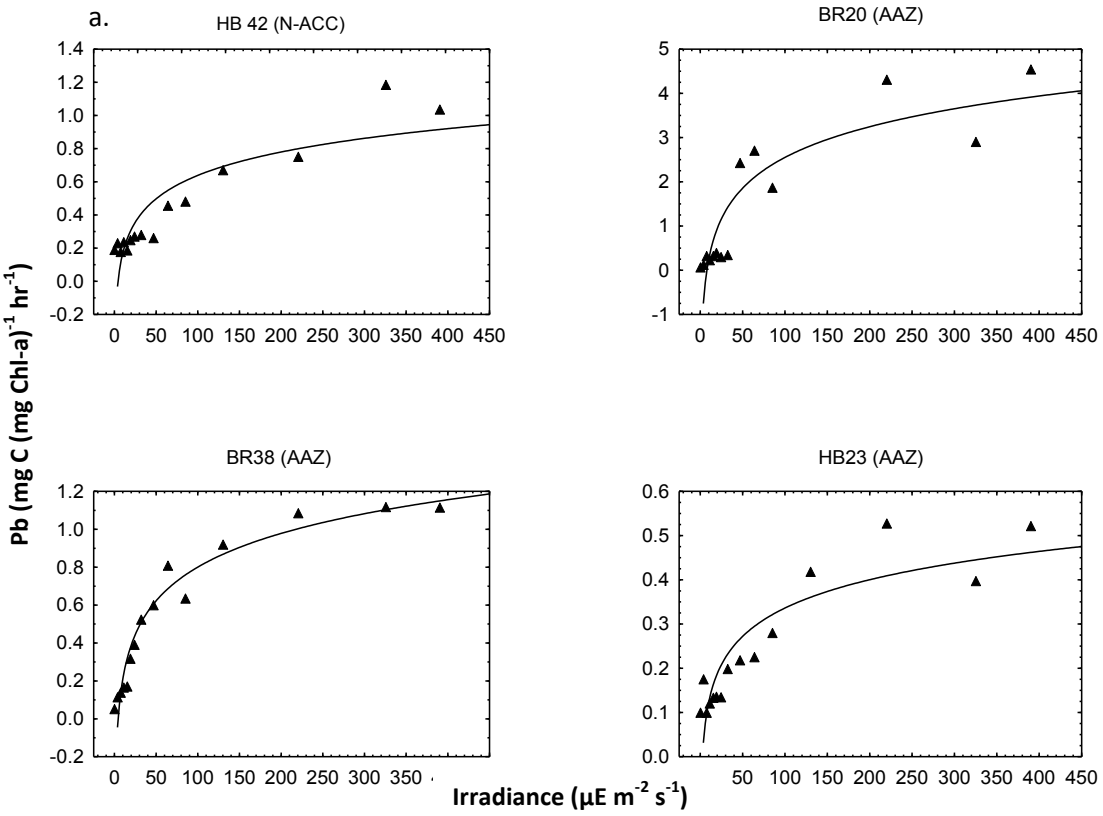

Figure 3.11a. P-E curves for all 11 productivity stations. Black triangles represent P^B for carbon fixation. BR = Buoy Run stations on Legs 2 and 3, HB = Homeward Bound stations on Leg 4, and zones are indicated in brackets.

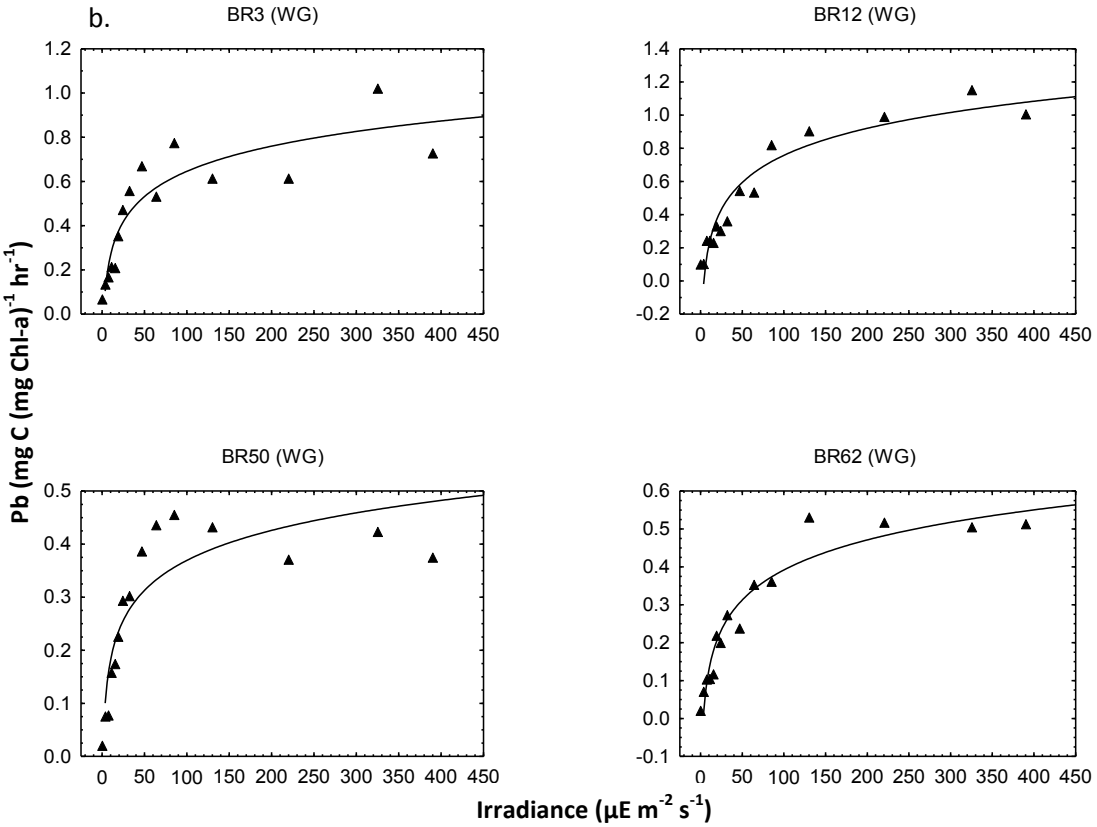

Figure 3.11b. P-E curves for all 11 productivity stations. Black triangles represent P^B for carbon fixation. BR = Buoy Run stations on Legs 2 and 3, HB = Homeward Bound stations on Leg 4, and zones are indicated in brackets.

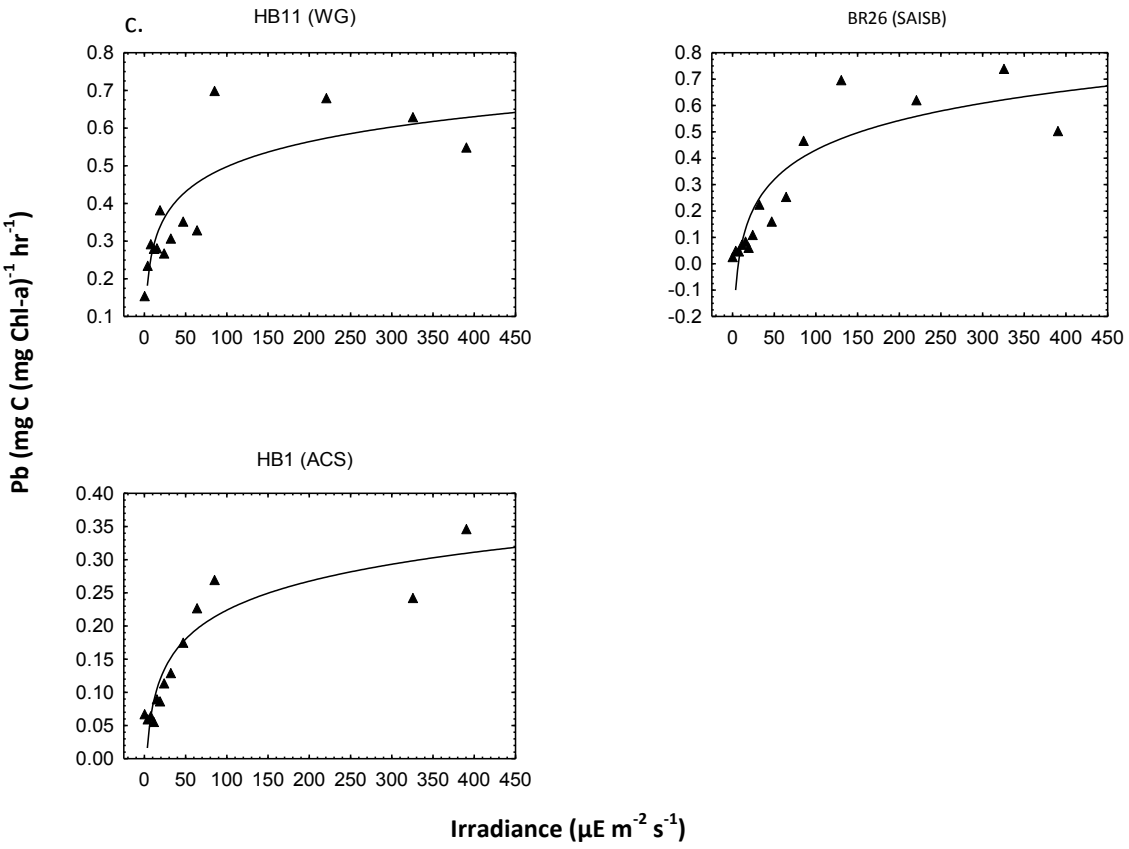

Figure 3.11c. P-E curves for all 11 productivity stations. Black triangles represent P^B for carbon fixation. BR = Buoy Run stations on Legs 2 and 3, HB = Homeward Bound stations on Leg 4, and zones are indicated in brackets.

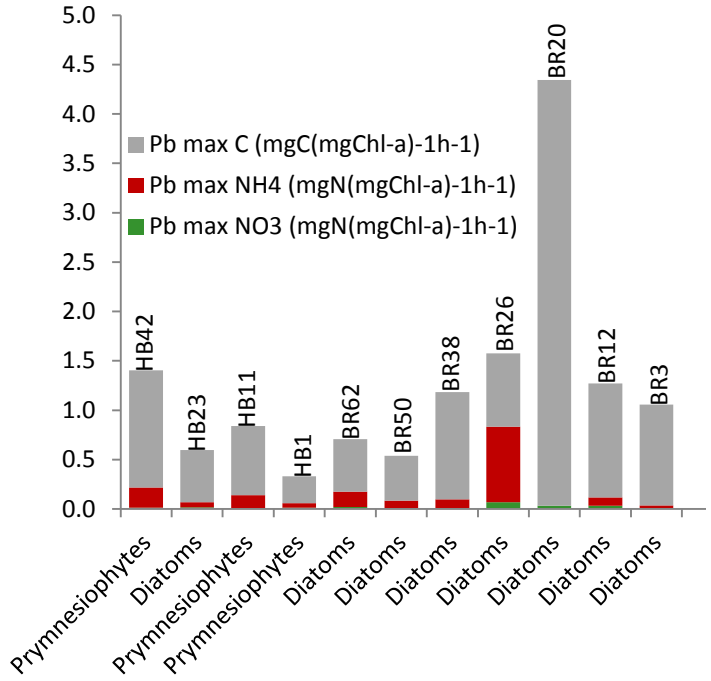

Figure 3.12 Relationship between dominant algal groups and P^{B}_{max} for C, NH_4^+ and NO_3^-. Grey columns represent proportion of P^{B}_{max} for C-fix, red columns NH_4^+ and green columns NO_3^-. Station numbers are indicated above the columns, BR = Buoy Run stations on Legs 2 and 3, HB = HomewardBound stations on Leg 4.

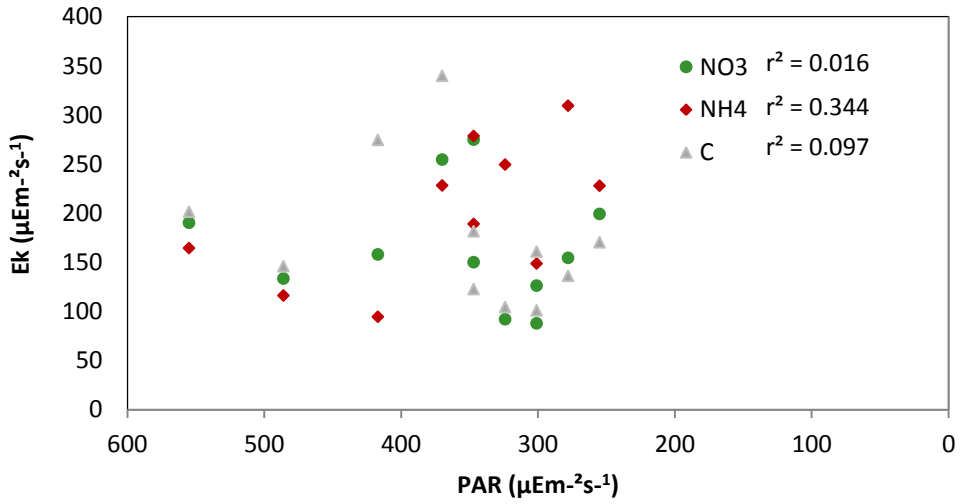

Figure 3.13 Scatter plot of E_k versus PAR for nitrate and ammonium uptake and carbon fixation at all 11 productivity stations. NO_3^- is represented by green circles, NH_4+ by red diamonds and C-fix by grey triangles.

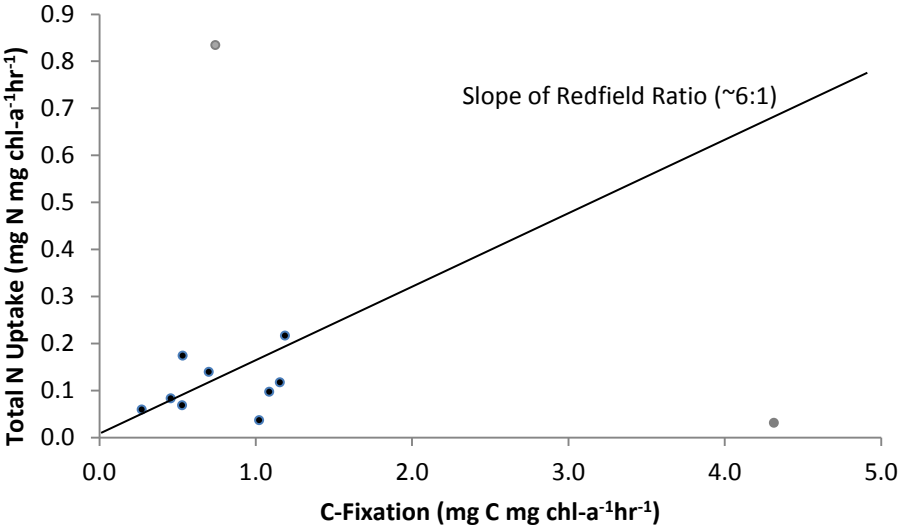

Figure 3.14 Scatter plot of total N uptake versus C-fixation for all 11 productivity stations. Two outliers (BR20 and BR26) are represented by grey dots and all other stations, black dots.

3.4 Discussion

This chapter's discussion is broken down by zones and firstly addresses the dominant phytoplankton groups according to how potential physical and chemical controls influence their regional distribution and how this pattern relates to observed productivity patterns. The latter part for each zone focuses on the role that light plays in phytoplankton nitrogen dynamics and explore regional distinctions in the factors influencing primary productivity.

Although fundamentally controlled by light and nutrient availability, variable phytoplankton primary production is often associated with differences in community structure. For example, larger cells such as diatoms usually exhibit higher production (Uitz et al. 2008, Barlow et al. 2010) while smaller cell sizes are often associated with lower productivity (Savidge & Gilpin 1999, Barlow et al. 2010). Diatoms and prymnesiophytes (=haptophytes; *Phaeocystis antarctica* in this case) that are well adapted to low temperatures have high nutrient requirements, and high maximal growth rates, and are known to dominate sporadic bloom events in the HNLC Southern Ocean provided that

dissolved iron is available (Arrigo et al. 1999, Poulton et al. 2007, Wright et al. 2010). Cryptophytes may also contribute significantly to blooms (Gabriotti et al. 2005, Wright et al. 2010). Relatively efficient food webs supported by diatom-dominated blooms export significant quantities of organic matter to the deep ocean (Blain et al. 2007, Pollard et al. 2009). Light-nutrient-iron interactions are therefore crucial determinants of phytoplankton community structure, as well as regulating overall productivity and C and N export via the biological carbon pump. However, unravelling the interplay between light and nitrogen metabolism in Southern Ocean phytoplankton communities has rarely been tackled (Cochlan 2008). Central to one part of this story is the ability of phytoplankton to harvest light, as determined by their photosynthetic pigments.

All phytoplankton have pigment-protein complexes within their light-harvesting antenna (in PSI & PSII), whose job it is to absorb light for photosynthesis. Absorption is influenced by both cellular pigment composition and pigment packaging, and varies with changes in phytoplankton community structure and photoacclimation (Barlow et al. 2010). Phytoplankton adapt well to changes in both light intensity and quality (Falkowski & La Roche 1991) and have evolved specific arrays of pigments to respond to diverse light conditions in different ecosystems (Barlow et al. 2010). Photosynthetic carotenoids are more pronounced in high-productivity ecosystems where large phytoplankton dominate (Barlow et al. 2002), making up ~80% of total carotenoids (Gibb et al. 2000, Barlow et al. 2010). Alternatively, photoprotective carotenoids prevail at the surface in low-chlorophyll waters where small cells are prominent and can contribute >70% to the entire carotenoid pool (Gibb et al. 2000, Barlow et al. 2010). These distinctions are correlated with changes in community structure and physiological responses to differences in environmental conditions (Barlow et al. 2010). On account of phytoplankton's development of taxon-specific suites of pigments, this fact can be used to instruct important chemotaxonomic information on community composition with certain key pigments being signatures for specific phytoplankton groups (Barlow et al. 1999, 2002, 2010). Although pigment biomarkers do not give any information to species level, pigment indices provide useful interpretation at the class level (Barlow et al. 2010). In the following discussion each zone will be addressed according to its community composition followed by a description of related productivity, light conditions and nitrogen dynamics. Before discussing the individual regional results from this study, some general observations that should be highlighted here

are as follows. Firstly, ammonium uptake was higher than nitrate uptake at all productivity stations (Figures 3.10a, b, c and 3.11a, b, c) which is expected in HNLC regions of the Southern Ocean where NH_4^+ utilisation is considered a more metabolically efficient strategy for assimilating N in Fe-limited conditions. Second, diatoms were the most dominant algal group followed by prymnesiophytes. When diatoms dominated community structure it was in association with higher C-fixation photosynthetic rates (P^B_{max}) and in some cases higher NH_4^+ assimilation rates (Figure 3.12). Finally, there was not a strong relationship between E_k values and PAR (Figure 3.13). One would expect E_k to decrease as PAR decreases southwards, however at higher latitudes you have less light over longer periods of time due to extended day length in summer, whereas at low latitudes there is higher light over less time which could help explain this poor relationship. In general E_k values were low as expected. Southern Ocean phytoplankton are known to have low E_k values, particularly diatoms (Dower et al. 1996, Saggiomo et al. 2002, Van Hilst and Smith 2002, Arrigo et al. 2010, Mills et al. 2010) indicating that they are adapted to low light and thus unlikely to be light limited.

The Subtropical Zone (STZ)

Pigments and Community Structure

In this zone, picoplanktonic prokaryotes, *Prochlorococcus spp.* and *Synechococcus spp.* (Gibb et al. 2001) dominate, as confirmed by the presence of the diagnostic pigments, zea and DV, biomarkers representing cyanobacteria and *Prochlorococcus spp.* (respectively; Figure 3.6, Table 3.1) (see also Uitz et al. 2006, Barlow et al. 2010). This community coincides with a low chl-*a* standing stock and low NO_3^- and PO_4^{3-} concentrations (Figures 2.10b & 2.8b, Chapter 2) characteristic of oligotrophic, Agulhas Current waters, which originate in the tropics. Low nutrient concentrations favour smaller celled pico-prokaryotes due to their ability to scavenge nutrients at low concentrations (Eppley et al. 1969). This type of community makes up the 'microbial loop', which recycles nitrogen but loses significant amounts of carbon to respiration, thus leaving little C for export to the deep sea (Poulton et al. 2006, Thomalla et al. 2011).

As a result of variable environmental conditions, phytoplankton pigment composition changes accordingly (Barlow et al. 2010). The most notable pigment adaptation in the STZ was the greater contribution of carotenoids, specifically PPC, as the community changed in response to oligotrophic conditions (Figure 3.7b, HB44 to HB48). Photo-protective carotenoids shifted from contributing ~10% throughout most other regions to ~20 to 30% in this zone. They play a more important role in oligotrophic waters where year round irradiances are generally higher and penetrate the water column to greater depths due to reduced biomass, thus necessitating photo-protective adaptations. Similar findings have been reported for the tropical Atlantic (Gibb et al. 2000), the Arabian Sea (Sathyendranath et al. 1999), and the eastern boundary of the Atlantic (Barlow et al. 2004).

Unfortunately, there were no productivity stations within this region, so comment on primary production, the light environment and nitrogen metabolism cannot be given.

The Northern-ACC Zone (N-ACC)

Pigments and Community Structure

Based on the HPLC data, the N-ACC region's phytoplankton community was dominated by prymnesiophytes which made up the greatest contribution (~57%) to chl-*a* standing stock (Figure 3.6). They were in the nano- size class (Figure 3.8) represented by the pigment Flag (Figure 3.15, HB42) and were most likely coccolithophores up to the SAF, at which point a shift to *Phaeocystis antarctica* was likely. One would expect to find coccolithophores in the nano- size class in subtropical to subpolar latitudes (McIntyre & Be 1967, Takahashi & Okada 2000, Alderkamp 2010, Boyd et al. 2010), but south of the APF where calcite saturation falls significantly (Holligan et al. 2010), prymnesiophytes would most likely be represented by *P. antarctica,* one of the dominant species in the Southern Ocean (Arrigo et al. 1999, DiTullio et al. 2003, Wright et al. 2010, Smith et al. 2010, Alderkamp et al. 2010, Boyd et al. 2010). While speculative because there is no microscopy data to identify these groups to species level, it is understood that coccoliths have expanded their range into subpolar waters due to warming trends, but remain absent in polar waters (Boyd et al. 2010). On the other hand, *P. antarctica* is only found at cooler high latitudes,

with a reported maximum temperature threshold of 10°C for their growth (Buma et al. 1991, Boyd et al. 2010). A change in temperature from 15°C at the STF to 10°C at the SAF (Figure 2.5b, Chapter 2) therefore suggests a temperature controlled shift in community structure.

Coccolithophores fix dissolved inorganic CO_2 into both POC and particulate inorganic carbon (PIC or calcite) forms, thus playing a critical role in the C cycle. Like all phytoplankton, C fixation sequesters CO_2, but coccolith calcification converts 2 mols of HCO_3^- to 1 mol each of CO_2 and $CaCO_3$. Therefore, it is uncertain whether coccolithophore blooms are net sinks or net sources of CO_2 to the atmosphere (Boyd & Trull 2007, Boyd et al. 2010). Nevertheless, the marine C cycle may also be indirectly influenced by calcite through its contribution to mineral ballasting of marine aggregates, resulting in rapid and efficient C export (Boyd et al. 2010). Additionally, like *Phaeocystis*, coccoliths are a major source of dimethyl sulphide (DMS) to the atmosphere. The Charlson-Lovelock-Andreae-Warren hypothesis (Charlson et al. 1987) argues that DMS fluxes from the surface ocean function as cloud condensation nuclei, whereby cloud formation helps regulate net incoming solar radiation and global temperatures (Boyd et al. 2010).

Closer to the APF, pymnesiophytes declined and diatoms as well as green flagellates (= prasinophytes) increased marginally and made up the greatest proportion of this region's relatively low biomass at this point (Figure 3.6).

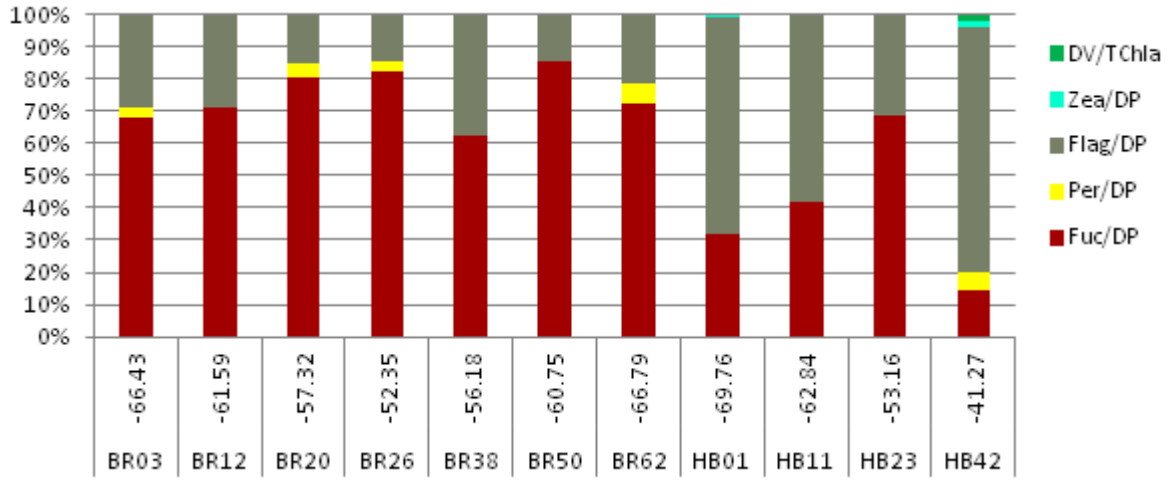

Figure 3.15 Diagnostic pigments for all productivity stations. Fuc (red) represents the diatom proportion of the total diagnostic pigment pool (DP) (All+But+Chlb+Fuc+Hex+Per+Zea). Per (yellow) represents the dinoflagellate proportion of DP. Flag (grey) represents a grouping of small flagellates including, cryptophytes, chrysophytes, prymnesiophytes, and chlorophytes in relation to total DP. Zea (aqua) represents the cyanobacteria proportion of DP. DV (green) represents a grouping of green flagellates and prochlorophytes in proportion to total chl-*a*.

Productivity and Biomass

Productivity in the N-ACC region was moderate (0.580 mg C m^{-3} hr^{-1}), which can be attributed to oligotrophic nitrate limited conditions at HB 42 which was at the northern extent of this region and in close proximity to the STF. A smaller, NH_4^+ recycling based community developed within a high surface irradiance environment, (abstracted from satellite composites; PAR ~555 µE m^{-2} s^{-1}, Figure 3.9d) but within a low nitrate environment (Table 3.3). Unsurprisingly, therefore, the light-saturated photosynthetic rate revealed far greater ammonium uptake relative to nitrate uptake (ρNH_4, P^B max = 0.204; $\rho N0_3$ = 0.013 mgC mgChl*a*$^{-1}$ h^{-1}, Table 3.6), yet still a relatively high rate of chl-*a* normalised carbon fixation (1.19 mgC mgChl*a*$^{-1}$ h^{-1}), indicating efficient photosynthesis per unit chlorophyll. Speculatively, one might therefore argue that there was sufficient dissolved iron (dFe) to satisfy the demands of PSII and PSI, particularly since dFe is not needed for nitrate assimilation. Resultant very low *f*-ratios for this region (*f* = 0.06) are indicative of a N recycling community where new production and carbon export is minimal.

P vs. E parameters

The light required to saturate photosynthesis (E_k), for the single experiment (HB42) on this leg in the N-ACC region, was relatively high (228 [nitrate], 254 [ammonium], and 340 [carbon] µE m^{-2} s^{-1}), as expected at lower latitudes (~41°S) in response to higher surface irradiances. Because of the higher energy cost in assimilating nitrate (and reducing it to ammonium) relative to assimilating ammonium, one might expect the E_k of nitrate to exceed that of ammonium. The assumption here is that more light-generated ATP is required to do this. But for this experiment, that was not the case. However, it seems more than likely that the E_k for ammonium and nitrate in this experiment were in practice indistinguishable, although this cannot be tested. For P^B_{max}, the values for nitrate, ammonium and carbon were, respectively, 0.013, 0.204 mgN mgChl*a*$^{-1}$ h^{-1} and 1.186 mgC mgChl*a*$^{-1}$ h^{-1}. When the P^B_{max} values for nitrate and ammonium are summed, this yields a combined value of 0.217 mgN mgChl*a*$^{-1}$ h^{-1}, which when multiplied by the approximate Redfield ratio of 6:1 becomes 1.302 mgC mgChl*a*$^{-1}$ h^{-1}. Happily, this is close to the expected and experimentally derived carbon-based P^B_{max} value of 1.19 mgC mgChl*a*$^{-1}$ h^{-1}. This provides

confidence in the experimental values, particularly since the P^B_{max} for nitrate is barely 15% of that for ammonium. One explanation for this is that the P^B_{max} for nitrate uptake is curtailed simply because of nitrate limitation in this N-ACC region, although ammonium inhibition and a lack of dFe cannot be excluded (Lucas et al. 2007, Cochlan 2008). For α, the maximum light utilisation coefficient, the slopes were all low, decreasing in the order C > NH_4 > NO_3, indicating that the quantum efficiency of nitrate utilisation was the poorest. This indicates that increasing light had less effect on nitrate assimilation relative to ammonium uptake, in keeping with either and/or nitrate and iron co-limitation of phytoplankton growth that was otherwise supported by ammonium.

In the N-ACC, and in all other regions, the photoinhibition parameters were negligible and can probably be considered an artefact when performing on-deck incubation experiments at fixed light levels. Not only are light levels constrained, but phytoplankton movement between different light levels is also confined within bottles. Furthermore, according to the literature, inhibition of light-saturated photosynthesis is not evident in nutrient-replete cells except when experimental irradiance exceeds actual growth irradiance by a factor of 10 (MacIntyre et al. 2002). Since experimental irradiances in this study never exceeded 400 μE m^{-2} s^{-1}, this should not be a problem. In the field, phytoplankton are often well mixed throughout the water column, so will experience varying light levels and for different periods of exposure. In the Southern Ocean in particular, it is unlikely that phytoplankton will experience consistently saturating (and higher) light intensities, so that photoinhibition is unlikely in the field during normal turbulent conditions.

The Antarctic Zone (AAZ)

Pigments and Community Structure

This region was crossed on all three legs (2, 3 & 4) and is characterised by the steep increase in Si concentrations upon crossing the APF (Figure 2.8b & 2.9, Chapter 2). Consequently, diatoms dominate phytoplankton community biomass at most stations south of the APF. Diatoms are cosmopolitan by nature and have a great impact on biogeochemical

cycles of C, Si, N and Fe in the open ocean (Boyd et al. 2010). Diatoms use Si to form their frustules and in the Southern Ocean, the sediments contain large deposits of biogenic silica that signify the importance of diatom bloom export (Treguer et al. 1995). In particular, chain-forming species produce large fast-sinking assemblages during the declining phase of blooms that results in significant POC export and sequestration into the deep ocean where DIC can remain for 100s to 10,000s of years (Lampitt 1985, Boyd et al. 2010).

Along the northbound transect from Antarctica to Cape Town (Leg 4), Fuc was the most dominant diagnostic pigment (Figure 3.21) and TChl*a* made up the greatest proportion of the pigment pool with PSC the next greatest (Figure 3.7). Diatoms therefore contributed greatest to the low chl-*a* standing stock, with prymnesiophytes contributing the next greatest amount (Figure 3.6). Along Legs 2 (Antarctica to South Georgia) and 3 (South Georgia to Antarctica) a similar pigment pattern was observed, and although biomass was slightly higher, prymnesiophytes were less important (Figures 3.4 & 3.5). Along Leg 4 between the sACCf and the SBdy, a deepening mixed layer and seasonal progression likely played a part in suppressing biomass, due to light limitation (Figure 2.10b, Chapter 2).

As microphytoplankton were the dominant size class in terms of biomass (Figure 3.8), even though this was relatively low throughout the AAZ region along all three transects, it is reasonable to suppose that whatever C fixation occurred in this group would ultimately settle below the seasonal thermocline because of Si ballasting by the diatom based structure of the community. Furthermore, in an Fe-limited HNLC environment, the Si:N ratio of diatom cells shifts from a more normal 1:1 ratio (when Fe replete) to ~3:1 or more (Moore et al. 2007), which facilitates rapid sedimentation.

Productivity and Biomass

There were three productivity stations within this zone, two of which were somewhat similar and the third (BR20) different, potentially due to its relatively close proximity to South Georgia and a source of dissolved Fe. This latter station exhibited exceptionally high productivity (3.260 mgC m^{-3} hr^{-1}) although chl-*a* biomass was only 0.659 mg m^{-3} and surface PAR was moderate (~347 µE m^{-2} d^{-1}). The macro-nutrient environment was non-limiting and chl-*a* normalised carbon fixation was high (P^B max 4.31 mgC mgChl*a*$^{-1}$

h^{-1}), indicating efficient light harvesting and energy synthesis by the photosystems; perhaps made so by available dFe, as was the case during CROZEX (Pollard et al. 2009).

Even so, chl-*a* normalised nitrate uptake (ρNO_3) was relatively low (0.031 mgNmgChl$a^{-1}h^{-1}$). But due to irreparable errors in the NH_4^+ experiment for this station, there are no ammonium uptake values. However, based on ρNO_3 / total C-fixation, a low *f*-ratio (*f* = 0.27) can be derived, suggesting once again that ρNH_4 dominated community N demands at this station. The implication here is that either ρNO_3 is Fe-limited, or it is suppressed by NH_4 inhibition (Lucas et al. 2007). Clearly, the arguments become speculative in the absence of dFe data, but arguing for sufficient dFe to efficiently drive C-fixation does not contradict any argument for *either* NH_4^+ inhibition of ρNO_3^- or Fe-limited ρNO_3^-. If in the latter case, whatever Fe is available can be used to support PSII and PSI, while N demands can be met by regenerated N uptake.

Low biomass, but a high rate of production suggests top down control by grazing, which keeps phytoplankton abundance in check (Bracher et al. 1991, Smetacek et al. 2004). Low nitrate uptake and consequently a low *f*-ratio indicate that overall productivity is sustained by regenerated N, where new production is perhaps Fe-limited. Here, the diatom community comprised medium sized species (*Fragilariopsis spp., Chaetoceros spp., Eucampia spp*. and *Nitszchia spp*. (from unpublished SEM data, Amy Harrington, *pers. com.*), which are more susceptible to grazing pressure than larger diatoms (Smetacek et al. 2004).

At the other two stations (BR38 and HB23) in this region, results were somewhat more typical of HNLC conditions in the open ocean areas of the Southern Ocean where macronutrients were readily available, biomass, chl-*a* normalised productivity and chl-*a* normalised N uptake of both substrates were all low at HB23 or moderate at BR38 (see Table 3.7, Laubsher et al. 1993 for a comparative study in the same region). Ammonium uptake always surpassed nitrate uptake and *f*-ratios at both stations were low (*f* = 0.16 and 0.31 respectively). Light was not limiting at BR38 (~486 µE m^{-2} s^{-1}) or at HB23 (~347 µE m^{-2} s^{-1}) so it is likely productivity was Fe-limited at these two stations.

Table 3.7 Absolute productivity measurements from this study relative to reported rates in the literature. Laubsher et al. (1993) were only 12 hour incubations so hourly rate has been multiplied by 12 to get daily rate.

Date	Location	Productivity (mg C m^{-3} d^{-1})	Authors
Jan/Feb	Atlantic sector of SO (41-70°S)	2.25 to 52.16	Kean 2012
Jan/Feb	Atlantic sector of SO (41-70°S)	4.2 to 69.9	Gibberd 2011
Nov/Jan	Crozet Islands (43-49°S)	2.8 to 38	Seeyave et al. 2007
Fe enrichment exp	Subantarctic Pacific (54°S)	3.5 to 82.9	Coale et al. 2004
Fe enrichment exp	Antarctic Pacific (66°S)	3.5 to 55.3	Coale et al. 2004
Jan/Feb	Atlantic Antarctic zone	~3 to 35 (from figure)	Laubsher et al. 1993
December	Pacific ACC	~1 to 45 (from figure)	Vaillancourt et al. 2003
Nov/Dec	Bellingshausen Sea (open ocean stns)	13.73 to 25.68	Bury et al. 1995
Jan/Feb	Atlantic sector of SO (34-70°S)	~0 to 18 (from figure)	Froneman et al. 2001

P vs. E parameters

E_k values were low at BR 20 (126 [NO_3] and 101 [C-fixation] µE m^{-2} s^{-1}), and at HB 23 (158 [NO_3], 94 [NH_4] and 275 [C-fixation] µE m^{-2} s^{-1}) which is a response to the lower irradiance field encountered in this higher latitude area and a (diatom based) community adapted to take full advantage of lower light conditions. Concurrently, the increase in PSCs indicates a shift to a community with more effective photosynthetic apparatus, which enhances their light harvesting capacity in such conditions. E_k values at station BR38 were moderate 199 [NO_3], 228 [NH_4] and 170 [C-fixation] while PAR was relatively high. Light was certainly not limiting here and the photosynthetic saturation point increased accordingly. PPCs did not increase which was unexpected within a higher light regime, but could be explained by greater productivity here, thus, an increase in PSCs enabled more effective utilization of available light (Figure 3.7a).

P^B_{max} for BR20 and BR38 were both high, BR20 being exceptionally high (4.3 mgC mgChl*a*$^{-1}$ h^{-1}). At BR38 the calculated Redfield ratio far surpasses expected values and evokes little confidence in the experimentally derived carbon-based P^B_{max} value. In further support of this, particularly in the case of BR20, the results far exceeded similar studies in the Southern Ocean (Table 3.8). Laubsher et al.'s (1993) maximum rate for the Atlantic Antarctic zone only reached 35 mg C chl-a^{-1} d^{-1} and even Seeyave et al.'s Crozet Island study

only reached a maximum of 14.76 mg C mg chl-a^{-1} d^{-1}, whereas daily rates for BR38 and BR20 were 17.92 mg C mg chl-a^{-1} d^{-1} and an alarming 68.96 mg C mg chl-a^{-1} d^{-1}, respectively (Table 3.8). For P^B_{max} at HB23, the values for nitrate, ammonium and carbon were, respectively, 0.016, 0.053 mgN mgChla^{-1} h^{-1} and 0.528 mgC mgChla^{-1} h^{-1}. When the P^B_{max} values for nitrate and ammonium are summed, this yields a combined value of 0.069 mgN mgChla^{-1} h^{-1}, which when multiplied by the approximate Redfield ratio of 6:1 equals 0.414 mgC mgChla^{-1} h^{-1}. This is close to the expected and experimentally derived carbon-based P^B_{max} value of 0.528 mgCmgChl$a^{-1}h^{-1}$. This elicits confidence in the experimental values, particularly since the P^B max for nitrate is barely 3% of that for ammonium. One possible explanation for this is that the P^B_{max} for nitrate uptake is diminished because of ammonium inhibition and/or a lack of dFe in this open ocean region (Lucas et al. 2007, Cochlan 2008). For α at all three stations, the slopes were all low, decreasing in the order C > NH_4 > NO_3, (except for BR20 for lack of an NH_4 experiment) indicating that the quantum efficiency of nitrate utilisation was the poorest, again supporting the idea that N demands were met by regenerated N uptake and enough dFe to support C-fixation.

Table 3.8 Table of production normalised to chl-*a* comparing this study to other studies in the Southern Ocean.

Season	Region	Type of measurement	P^B (mg C mg chl-a^{-1} d^{-1})	Authors
Late summer	Atlantic	P^B_{max}	5.28-19.55 (BR20 68.96)	Kean 2012
Late summer	Atlantic	P^B	10.2-34.9	Gibberd 2011
Late summer	Subpolar Pacific	P^B_{opt}	31.2±2.4	Hiscock et al. 2003
Early summer	Crozet Islands	P^B_{opt}	3.6-14.76	Seeyave et al. 2007
Late summer	Atlantic	∫ Water column	2 to 23	Froneman et al. 2001
Summer	South Pacific	Surface values	2.78±2.28 (hourly- daylight incubation)	DiTullio et al. 2003
Late summer	Atlantic AAZ	Surface values	1 to 35	Laubsher et al. 1993
Summer	Scotia Sea	P^B_{opt}	22.4±2.8 to 56.7±13.6	Korb et al. 2005

The Weddell Gyre (WG)

Pigments and Community Structure

There were no notable differences in community structure in this region compared to the AAZ. Diatoms again dominated the group, with prymnesiophytes playing a secondary role along Leg 4 (Antarctica to Cape Town). An exception to the general similarities occurred at ~61°S on Legs 2 and 3 (Antarctica to South Georgia and South Georgia to Antarctica, respectively) where chl-*a* values increased to 1.7 mg m^{-3} along Leg 2 and 2.4 mg m^{-3} along Leg 3, roughly a 37% increase on Leg 2 and a 47% increase on Leg 3 (Figure 2.11a & b, Table 2.2), and are in association with the low salinity feature discussed in Chapter 2. Macronutrient concentrations in this region were high (mean NO_3 22.4±2.3, 20.5±1.7 and mean Si 37.7 ±4.2, 30.6 ±8.3, Leg 2 and 3 for each, respectively) with a coincident decline in Si by ~29% at ~61°S on Leg 2 and 3 due to diatom silicification. Microplankton were the dominant size-class, with potential for enhanced C drawdown.

The TChl pool in this region was dominated by Chl*a*, *b* and *c*, making up 50-60% of the total pool, while PSCs made up ~30% and PPCs were often < 10% (Figure 3.7). It is arguable that the TChl*c* and PSC indices increased together with an increase in the microphytoplankton size class index, indicating that diatoms increased the proportion of Chl *c* and PSCs to optimize their light-harvesting capability (Barlow et al. 2004). This argument has previously been substantiated by Stuart et al. (1998) and Barlow et al. (2002) who revealed that absorbtion at 440nm in diatom-dominated communities is due to chlorophylls *a* and *c*, and at 490nm to photosynthetic carotenoids (Barlow et al. 2004).

Similar to BR20 in the AAZ, the size class data for this station indicates a dominant microphytoplankton size class, however, it is more likely that smaller diatoms in the nanoplankton size range made up a greater portion than demonstrated. Uitz et al. (2006) draw attention to the limitations in assigning size classes based on the proportion of taxonomic pigments, which may be represented across a wide size-spectrum. Two parallel studies (Amy Harrington, MJ Gibberd, *pers. comm.*) found that nano- sized diatoms (~5-40 µm, *Fragilariopsis spp., Chaetoceros spp., Eucampia spp*. and *Nitszchia spp.*) were the dominant group in the WG region.

Productivity and Biomass

Five productivity stations were sampled in this region (BR3, BR12, BR50, BR62, and HB11) and the prominent pattern was quintessential HNLC conditions. Productivity and biomass was very low at four of the five stations (PP < 0.42 mgC m^{-3} h^{-1}) while BR50 exhibited relatively high biomass (1.14 mg m^{-3}) as well as a marginal increase in productivity (0.5 mgC m^{-3} h^{-1}) (Table 3.5), albeit still a very moderate value. This station is in the vicinity of the low salinity feature (~61°S) described in Chapter 2, where perhaps melt-water flowing eastwards from the Antarctic Peninsula as part of the northern branch of the Weddell Gyre circulation, is made up of fresher and most likely Fe-enriched water (de Baar et al. 1995) and potentially escapes Fe-limiting concentrations for nitrate uptake considered by Cochlan (2008) to be 0.03–0.04 nM, thus giving one explanation for the higher biomass, which of course can only be realised if productivity exceeds grazing rates. *f*-ratios were low at all five stations, ranging from 0.03 to 0.30, as nitrate uptake became more light-limited than reduced N uptake. Furthermore, the size-structure of the community was also important, with small cells better able to scavenge Fe at low concentrations exhibiting higher *f*-ratios than larger cells, which consequently exhibited lower *f*-ratios. This is similar to findings by Lucas et al. (2007).

P vs. E Parameters

P^{B}_{max} was relatively high at BR3 and BR12 (1.02 and 1.15 mgC mgChl*a*$^{-1}$ h^{-1} [C-fixation]) and low for nitrate and ammonium assimilation (BR3 0.011 mgN mgChl*a*$^{-1}$ h^{-1}, 0.026 mgN mgChl*a*$^{-1}$ h^{-1} and BR12 0.0315 and 0.086 mgN mgChl*a*$^{-1}$ h^{-1}, respectively). Redfield stoichiometry is unrealistic for BR3 (27:1), but acceptable for BR12 (10:1), although the latter is on the high side. However, the remaining three stations in this region exhibited relatively moderate P^{B}_{max} values (Table 3.6) and corresponding Redfield ratios for BR50 and HB11 were close to 6:1 while BR62 was lower than expected at ~3:1. PAR ranged from 255 to 417 µE m^{-2} s^{-1} (Table 3.6, Figure 3.9a-d) and while somewhat low at BR62, it was not limiting. Decreases in PAR coincided with increases in latitude as well as a seasonal progression to less light and a lower sun angle. E_k mimicked this pattern where the lowest photosynthetic saturation rate occurred at BR62 (133, 116, and 146 µE m^{-2} s^{-1} for [NO_3], NH_4 and [C-fix], respectively). However, E_k variability was generally high and at high latitudes has been coupled with variability in P^{B}_{max}, which was associated with temperature effects in

similar, albeit older, studies (Dower et al. 1996). For α, at each station the slopes were all low, decreasing in the order C > NH_4 > NO_3, indicating that the quantum efficiency of nitrate utilisation was the weakest. This indicates that increasing light had less effect on nitrate assimilation relative to ammonium uptake.

A comparison between BR3 and BR62 (that share a similar lat. and long.) and BR12 and BR50 (that share a similar lat. and long.), stations in close proximity to one another within the same region, highlights the variability experienced in this region. Over the approximately 7 to 11 days time difference between sampling periods, a noticeable shift in biomass and P-E parameters from BR3 to BR62 and from BR12 to BR50 occurred. BR3 and BR12 exhibit low biomass (0.41 and 0.27 mg m^{-3} respectively), low productivity (0.42 and 0.31 (mgC m^{-3} hr^{-1}) respectively) and a high photosynthetic rate (1.02 and 1.15 mg C mg chl-$a^{-1}hr^{-1}$ respectively) with a moderate to high POC:Chl-*a* ratio (474 and 358 respectively) suggesting Fe is not a limiting factor. One suspects that grazing may be influencing the cap on biomass. Move one week forward in time and conditions changed. At BR50 and BR62, productivity was still low (0.5 and 0.25 mg C m^{-3} hr^{-1}), P^B_{max} was low (0.45 and 0.51 mgC mg chl-a^{-1} hr^{-1}), and at BR50, biomass was unusually high (1.14 mg m^{-3}), while biomass at BR62 remained low (~0.5 mg m^{-3}). The POC:Chl-*a* ratio decreased at both stations (62 and 113 respectively).

The light environment decreased substantially, but was still not limiting, so what was happening? Without dFe, grazing or MLD data, it is difficult to speculate with any certainty, but it may be that mesozooplankton grazing pressure subsided, allowing biomass accumulation to occur in close proximity to the South Sandwich Islands and in the previously described salinity feature - both being potential sources of dFe. Extending this argument, an increased biomass depleted any available Fe, so the photosynthetic rate slowed accordingly. This was driven by a diatom-based recycling community where available NH_4 increased (BR3 and BR12, both 0.88, BR62, 1.13 and BR50, 1.09 µmol NH_4 l^{-1}) concurrently with chl-*a* normalised NH_4 uptake (BR3, 0.03; BR12, 0.08; BR62, 0.15 and BR 50, 0.08 mgN mgChl*a*$^{-1}$ h^{-1}). This is a feasible scenario where ammonium concentrations increase due to bacterial activity and microzooplankton grazing, which in turn increase ammonium uptake that is not Fe dependant. The fact that ammonium concentrations increase means that ammonium regeneration exceeds ammonium uptake rates. Decreasing C-fixation due to Fe limitation is not at odds with the N cycling as outlined.

The variability in P-E parameters experienced throughout this region emphasises the highly dynamic Weddell Gyre region, and points to the need for more frequent *in situ* sampling to gain a better understanding of the factors influencing such variability. Indeed, previous studies in the region described P vs. E experimental results as, 'polar waters exhibit "bewildering variability"!' (Dower et al. 1996).

The Subantarctic Islands and Shallow Bathymetry Region (SAISB)

Pigments and Community Structure

Diatoms made up an even greater proportion (~85%) of the elevated biomass in this region. Although both dinoflagellates and prymnesiophytes made an appearance, they made just a small contribution (~15%) to total biomass (Figure 3.4). This pattern was also evident in the diagnostic pigment proportions for BR26, where Fuc (diatoms) was ~80%, Per (dinoflagellates) ~5%, and Flag (prymnesiophytes) ~15% (Figure 3.15). Size class structure was dominated by microplankton, with nanoplankton playing a secondary role (Figure 3.8).

Pigment indices differed slightly for BR26 from the previous trend. Tchl*a* increased while Chl*bc*, PSC and PPC all decreased at BR26 (Figure 3.7). These surface pigment adaptations were probably associated with the nutrient regime in this area, which was characterized by high nitrates and biomass, diatom dominance, a high proportion of chlorophylls and a low PPC index. Diatoms are opportunistic organisms able to respond rapidly to nitrate enrichment (Fogg 1991) provided that sufficient light and Fe are available, and chlorophyll molecules contain nitrogen atoms while carotenoids do not (Porra et al. 1997, Barlow et al. 2004).

Productivity and Biomass

Productivity and biomass for the only productivity station in this region were high (2.18 mgC m^{-3} hr^{-1} and 2.94 mg Chl-*a* m^{-3} respectively). The station was situated downstream (northwest) of South Georgia, an area influenced by the island and its shelf, so was likely to be Fe replete (Ward et al. 2005). Comparable measurements of integrated water column productivity were found in Subantarctic island HNLC regions by Korb and Whitehouse (2004) to the northwest (downstream) of South Georgia (2505 mgCm^{-2} d^{-1}) and by Seeyave et al. (2007) north of the Crozet Islands (2998 mgC m^{-2} d^{-1}), compared to the 3270 mgC m^{-2} d^{-1}

recorded in this study. Additionally, a similar pattern between the three studies around the islands was found in the north-south chl-*a* concentration gradient (Korb et al. 2004, Seeyave et al. 2007). The low *f*-ratio at this station (0.18) was likely due to the high NH_4^+ concentration (1.9 µmol l^{-1}) that satisfied phytoplankton N requirements.

P vs. E Parameters

For station BR26, P^B_{max} for C-fixation was also high (0.74 mg C mg chl-a^{-1} hr^{-1}), which translates to 11.11 mgC mg Chl-a^{-1} d^{-1} assuming a 15 hr day. This is towards the high end of the P^B_{opt} range (3.6-14.76 mgC mgChl-a^{-1} d^{-1}) recorded by Seeyave et al. (2007) for the Crozet study. *In situ* PAR at this station derived from an 8-day satellite composite (Fig 3.9a-d) roughly approximates 324 µE m^{-2} s^{-1}, while Ek values were 154 [NO_3], 309 [NH_4], 136 [C-fix] µE m^{-2} s^{-1}. Thus the Ek values were close to or about 50% lower than measured PAR. This discrepancy should not be surprising on the basis of highly variable regional PAR (see Figure 3.8a-d) and experimental error, not to mention the previous and immediate light history of the phytoplankton. In summary, the approximate correspondence is good. α exhibited the same pattern as the previous stations which affirms that the photosynthetic process is more efficient in the order C > NH_4 > NO_3, a testament to the success of 'regenerated' versus 'new' production based communities in an HNLC environment.

The Antarctic Continental Shelf (ACS)

Pigments and Community Structure

Community structure was remarkably different and variable in this region. In early summer on leg 3 (68-70°S), diatoms were most abundant followed closely by prymnesiophytes (Figure 3.5). Later in summer along leg 4, prymnesiophytes peaked when diatoms were low in abundance (68-70°S) (Figure 3.6). Dinoflagellates contributed a small proportion to phytoplankton community structure at 68°S, and chrysophytes also made a very small contribution (Figure 3.6). Chrysophytes are predominantly a fresh water species, but there are well known marine species, and interestingly, some species that occur in snow (del Campo et al. 2011). However, it is possible that the Uitz et al. (2006) method misclassified this group according to size as they are predominantly pico- sized

phytoplankton, but have the same pigment content as prymnesiophytes. The community was primarily made up of nano- sized phytoplankton (Figure 3.8). TChla and Chlb&c make up 58% of the pigment pool, PSC contributes 32% and PPC ~10% (Figure 3.7) indicating that the chlorophylls were the key light-harvesting pigments. This pattern is more common in high productivity regions compared to oligotrophic regions where PPCs would make up a greater proportion of the total pigment pool.

There appeared to be a pattern of alternating abundance between diatoms and prymesiophytes (most likely *P. antarctica*) (Figures 3.5 & 3.6). It is plausible that in this region potentially high dFe concentrations (from ice melt, icebergs, and shelf sediments, Klunder et al. 2011, Johnson et al. 1999, Tagliabue et al. 2011) fuel a diatom specific response in a nutrient replete environment, but as Si is depleted and dFe concentrations decline, prymnesiophytes take over and more readily respond to a lower light regime due to (diatom) self-shading and a preference for regenerated N when iron starts to decline.

P. antarctica are known to outcompete diatoms because of their higher rates of photosynthesis and growth at lower light levels (Kropuenske et al. 2009). Ammonium uptake was indeed higher than nitrate uptake at HB1 (Table 3.4) which supports a recycling community at this station. *P. antarctica* has a complex life cycle and is found as single cells or in gelatinous colonies. Colonies are believed to be grazer resistant (Schoemann et al. 2005) and can store Fe within the mucilage for use during later Fe-limiting conditions. Success of the species is therefore intrinsic with their ability to form colonies when sufficient Fe allows them to do so.

Productivity and Biomass

While biomass in this region reached highest values of ~3.0 mg chl-*a* m^{-3}, more than in any other region, productivity was only measured at one station (HB1) and was rather low (0.28 mgC m^{-3} hr^{-1}) commensurate with only a moderate biomass (0.85 mg chl-*a* m^{-3}).

High variability in primary productivity is not uncommon in continental shelf regions. A recent study in the western Antarctic Peninsula reported average primary production rates could vary by an order of magnitude, from ~250 to ~1100 mgC m^{-2} d^{-1} (Vernet et al. 2008), with a strong inshore–offshore gradient of higher production inshore. This study's

daily rate (448 mgC m^{-2} d^{-1}) was within Vernet et al.'s (2008) reported range (see above), but comment can only be limited with just one offshore station to report on for the region. Once again, a low *f*-ratio (*f* = 0.2) confirmed the dominance of reduced N uptake, implying very limited new production and carbon export.

P vs. E Parameters

P^B_{max} was also low (0.269 mgC mg chl-$a^{-1}hr^{-1}$) suggesting that primary production was limited despite a shallow MLD of ~50m (Figure 2.10b, Ch. 2) that most likely provided a favourable nutrient and light environment. When P^B_{max} values for ammonium and nitrate are summed and multiplied by the approximate Redfield ratio (6:1) this becomes 0.36 mgC mgChl-$a^{-1}hr^{-1}$ which is close to, and evokes confidence in the experimental carbon-based P^B_{max} value, 0.27 mgC mgChl-$a^{-1}hr^{-1}$. It is possible that high light attenuation due to glacial till outwash which would increase the sediment load at this station (which was in close proximity to the ice shelf, bay ice and ice bergs) could explain moderate biomass, low production, and a low photosynthetic rate, but there is no data or significant observation to support this theory in this case. For this station, E_k was 92 [NO_3], 249 [NH_4], and 104 [C-fix] µE m^{-2} $s^{-1}$and declined with PAR (278 µE m^{-2} s^{-1}) compared to lower latitude stations (HB42 for example). This was a more typical relationship between E_k and PAR and is indicative of the shorter day length (~13 hrs) and lower sun angle late in the summer season. α was low for all three substrates and followed the same pattern as all of the previous stations (C > NH_4 > NO_3), illustrating that the quantum efficiency of nitrate utilisation was the weakest, again supporting the idea that N requirements were satisfied by regenerated N uptake and sufficient dFe to support C-fixation.

3.5 Conclusions

North of the STF in the Subtropical zone picoplanktonic prokaryotes dominated community structure, upon crossing the STF community structure shifted to prymnesiophytes as the greatest contributor to chl-*a* standing stock, presumably coccolithophores while still in subtropical to subpolar waters. After crossing the APF any presence of prymnesiophytes would most likely be *P. antarctica*, a prevalent colonial species in the Southern Ocean. Diatoms dominated south of the APF, particularly where dFe

introduced into the water column is suggested to have stimulated 'blooms'. When these organisms are in the micro-size class they are well equipped to exploit silification as a defence mechanism to grazing pressure and when they are smaller (nano-) are efficient scavengers of limiting Fe at low ambient concentrations, as well as effective in utilising regenerated N to boost productivity. Two exceptions to prevailing community structure occurred at two different locations, one station (HB11) in the Weddell Gyre and one (HB1) in the Antarctic Continental Shelf region where prymesiophytes replaced diatoms as the dominant group. This shift is unlikely due to photosynthetic responses as both groups are well adapted to low irradiance conditions and is more likely from a complex series of controls including trace metal effects, vertical mixing, differentiated grazer communities and other factors.

Southern Ocean phytoplankton are well adapted to low light environments. Relatively low irradiances were required to saturate NO_3^- and NH_4^+ uptake and C fixation at all stations. The maximal light saturation photosynthetic rate often occurred at 50% or less of surface irradiance. NH_4^+ uptake always exceeded NO_3^- uptake, but often reached its maximal rate at a higher saturation point than NO_3^-, unlike results from an older study in the Indian sector of the Southern Ocean (Slawyk 1979). Indeed only a few N uptake versus irradiance experiments have been run in the Southern Ocean and like this study, variability between sampling stations and regions is high. Some of these differences might be explained by differences in species composition of the assemblages (diatom versus prymnesiophyte blooms), the stage of the bloom development, or the sampling time during the season (Cochlan 2008).

Production in the open ocean regions of the Southern Ocean has been well defined as limited by dFe in the late summer. In this study, production was predominantly low, dominated by micro- and nanoplankton that rely on reduced N substrates (NH_4^+) to quench their N requirements. Recognising due vigilance in the concept of 'new' production to infer export, community *f*-ratios from this study (0.03 to 0.31) suggest that very little production (3 to 31%) was potentially available for export. These low values are consistent with Fe-limited nitrate assimilation (ρNO_3^-) and are comparable to similar findings in the Southern Ocean (e.g. Lucas et al. 2007, Joubert et al. 2011, Thomalla et al. 2011a). However, because much of the micro- and nanoplankton were diatoms, sinking rates abetted by their silica

ballasting were increased and C was likely to be drawn down to depth. In particular, the community sampled downstream of South Georgia demonstrated prime conditions for atmospheric CO_2 'draw-down'. Here, interactions of the ACC with the shallow shelf region surrounding the island introduces dFe (as well as Si) to surface waters which is suggested to drive increased new production rates and microplankton production. Reoccurring bloom conditions around South Georgia are believed to account for the largest carbon sink in the Southern Ocean (Schlitzer et al. 2002) and Subantarctic island regions in general, are known to contribute significantly to the sequestration of carbon in the Southern Ocean (Arrigo et al. 2008).

Chapter 4. Concluding Remarks and Thesis Summary

The Southern Ocean is comprised of several well defined provinces that differ physically and chemically including parameters such as temperature, micro and macro nutrient concentrations, light availability, sea ice formation, currents and vertical mixing (Jacques 1989, Boyd 2002, Van Oijen et al. 2004). Frontal systems, like the Antarctic Polar Front, are generally characterized by high phytoplankton biomass whereas in other regions, like the Antarctic Circumpolar Current away from the influence of frontal systems, biomass is low (Lutjeharms et al. 1985, Laubscher et al. 1993, Bracher et al. 1999, Van Oijen et al. 2004). Understanding how marine phytoplankton productivity is controlled is valuable because algal carbon fixation in the ocean is a link between the atmospheric and oceanic compartment of the global carbon cycle (Falkowski et al. 1998, Van Oijen et al. 2004). Specifically, diatom blooms in the Southern Ocean are assumed to be followed by a significant export flux of carbon out of the euphotic zone and carbon dioxide (CO_2) drawdown (De Baar & Boyd 2000, Van Oijen et al. 2004).

This study investigated facets of the biological carbon pump in the south Atlantic sector of the Southern Ocean. Surface phytoplankton communities were sampled and analyses attempted to ascertain the role of light in limiting phytoplankton productivity to explain:

I. Spatial variability in phytoplankton biomass,
II. Nitrogen assimilation rates and what they reveal about light as a limiting factor,
III. Community composition and size based community structure in terms of iron stress and ultimately, CO_2 sequestration,
IV. What P vs. E curves reveal about regional differences in the light dependant uptake of new versus regenerated production

in relation to the physical and chemical environments encountered throughout the region.

High phytoplankton biomass occurred in the SAISB, sections of the WG, and in the ACS, and corresponded with shallow coastal and shelf waters, shallow bathymetric features, or in the case of the seasonal ice zone (which includes the ACS, WG, and a portion of the

AAZ), recent melting of sea ice in its different forms. Albeit speculative, this suggests the introduction of Fe to stimulate phytoplankton growth in addition to a more stratified water column and an improved light regime, as well as longer light exposure due to increased day length in summer. In regions of low biomass (STZ, N-ACCZ, AAZ) NO_3^- limitation, presumably iron and light co-limitation, and light limitation (respectively) prevent phytoplankton production. While frontal positions previously have been aligned with the spatial distribution of increased chl-*a* biomass along the fronts, this study's results exhibit a more recent understanding of how fronts define boundaries to distinct zones with similar characteristics and elevated or depleted biomass. These regionally dependent boundaries were evident when crossing the STF from the STZ to the N-ACC in terms of temperature, salinity and biomass or when crossing the APF from the N-ACC to the AAZ in terms of the steep increases in the macro nutrient environment, particularly Si, for example.

Across all regions P-E parameters were variable, but displayed a few prominent trends that were characteristic of the HNLC condition. Regenerated ammonium uptake always exceeded nitrate uptake and supports findings that Southern Ocean phytoplankton are photo-physiologically well adapted to low light regimes and are able to exploit the more energetically efficient NH_4^+ uptake when Fe is limiting. E_k values and *in situ* PAR derived from 8 day satellite composites indicate that light was not a limiting factor across all regions. Along Legs 1 and 4 where MLD data was available recent deeper vertical mixing was implicated in areas of low production (in the AAZ and the N-ACC for example), in which case light would play a limiting role. In the Subantarctic island and shallow bathymetry region where sufficient light and presumably Fe were available, as well as potentially reduced grazing pressure primary productivity and carbon based P^B_{max} increased substantially. Productivity was low in all other regions and the maximal photosynthetic rate was variable across regions. However, there was a noticeable decline in P^B_{max} towards the end of summer when comparing rates measured on Leg 1 (January) to Leg 4 (February). This seasonal signal was most apparent in the WG where more stations were sampled over a relatively longer period of time.

Community composition in the STZ was comprised of picoplanktonic prokaryotes, *Synechoccoccus spp. and Prochlorococcus spp.,* south of the STF prymnesiophytes, most likely made up of coccolithophores were the dominant group. At the SAF where polar

waters replace warmer subpolar and subtropical waters and macronutrients (Si and NO3-) increase, presence of prymnesiophytes was presumably *P. antarctica*. Southwards of the APF diatoms dominated community composition, except for in the ACS region where prymnesiophytes once again contributed significantly to chl-*a* standing stock. Diatoms were primarily in the micro size range across all regions south of the APF except for in the WG where nano sized diatoms were more abundant. Where high productivity and biomass coincided with a larger size-classed diatom community C export was potentially considerable due to increased sinking rates of heavily silicified diatoms. This was evident in the SAISB region (BR26), downstream of South Georgia where significant atmospheric CO_2 'drawdown' is known to occur. Another area for potential C export to depth was at BR50 in the WG region where a low salinity feature (~61°S) persisted through the sampling period. It is hypothesised that this stream originates from the Antarctic Peninsula to the west of the study region and forms part of the eastward flowing, northern limb of the Weddell Gyre circulation. The reduced salinity stream demonstrates that it came from melt waters, and the favourable biological responses exhibited (increased biomass, moderate productivity, and large diatoms) suggest elevated dFe concentrations and the potential for C export. All other regions exhibited characteristic HNLC conditions in the Southern Ocean where low *f*-ratios, regenerated production, and nano- to micro size phytoplankton communities were suggestive of an Fe stressed environment with limited potential for export of C to the deep ocean.

References

Alderkamp AC, de Baar HJW, Visser RJW, Arrigo KR (2010) Can photoinhibition control phytoplankton abundance in deeply mixed water columns of the Southern Ocean? Limnology and Oceanography 55(3): 1248-1264

Allanson BR, Hart RC, Lutjerharms JRE (1981) Observations on the nutrients, chlorophyll and primary production of the Southern Ocean south of Africa. South African Journal of Antarctic Research 10/11: 3-14

Alves PL da CA, Magalhaes ACN, Barja PR (2002) The phenomenon of photoinhibition of photosynthesis and its importance in reforestation. The Botanical Review 68(2): 193-208

Ansorge IJ, Speich S, Lutjeharms JRE, Goni J, Rautenbach CJ, Froneman W, Rouault M, and Garzoli S (2004) Monitoring the oceanic flow between Africa and Antarctica. S. Afr. J. Sci. 101: 29–35

Armstrong RA, Lee C, Hedges JI, Honjo S, Wakeham S (2002) A new, mechanistic model for organic carbon fluxes in the ocean based on the quantitative association of POC with ballast material. Deep-Sea Research II 49: 219–236

Arrigo, KR, Robinson DH, Worthen DL, Dunbar RB, DiTullio GR, Van Woert M, Lizotte MP, (1999) Phytoplankton community structure and the drawdown of nutrients and CO_2 in the Southern Ocean. Science 283:365–367

Arrigo KR, van Dijken GL (2004) Annual changes in sea-ice, chlorophyll a, and primary production in the Ross Sea, Antarctica, Deep-Sea Res. Pt. II 51:117–138

Arrigo KR, Van Dijken GL, Bushinsky S (2008) Primary production in the Southern Ocean, 1997–2006. Journal of Geophysical Research 113: 1-27

Arrigo KR, Mills MM, Kropuenske LR, van Dijken GL, Alderkamp AC, Robinson DH (2010) Photophysiology in two major Southern Ocean phytoplankton taxa: photosynthesis and growth of *Phaeocystis antarctica* and *Fragilariopsis cylindrus* under different irradiance levels. Integrative and Comparative Biology 50:950–966

Atkinson A, Whitehouse MJ, Priddle J, Cripps GC, Ward P, Brandon MA (2001) South Georgia, Antarctica: a productive, cold water, pelagic ecosystem. Mar. Ecol. Prog. Ser. 216: 279–308

Bakker DCE, Hoppema M, Schröder M, Geibert W, de Baar HJW (2008) A rapid transition from ice covered CO_2-rich waters to a biologically mediated CO_2 sink in the eastern Weddell Gyre. Biogeosciences 5: 1373-1386

Barlow RG, Cummings DG, Gibb SW (1997) Improved resolution of mono- and divinyl chlorophylls *a* and *b* and zeaxanthin and lutein in phytoplankton extracts using reverse phase C-8 HPLC. Mar Ecol Prog Ser 161:303–307

Barlow RG, Aiken J, Holligan PM, Cummings DG, Maritorena S, Hooker S (2002) Phytoplankton pigment and absorption characteristics along meridional transects in the Atlantic Ocean. Deep-Sea Research I 49: 637–660

Barlow RG, Mantoura RFC, Cummings DG (1999) Monsoonal influence on the distribution of phytoplankton pigments in the Arabian Sea. Deep-Sea Research II 46:677–699

Barlow R, Stuart V, Lutz V, Sessions H, Sathyendranath S, Platt T, Kyewalyanga M, Clementson L, Fukasawa M, Watanabe S, Devred E (2007) Seasonal pigment patterns of surface phytoplankton in the subtropical southern hemisphere. Deep-Sea Research I 54:1687–1703

Barlow R, Kyewalyanga M, Sessions H, van den Berg M, Morris T (2008) Phytoplankton pigments, functional types, and absorption properties in the Delagoa and Natal Bights of the Agulhas ecosystem. Estuarine, Coastal and Shelf Science 80:201–211

Barlow R, Lamont T, Kyewalyanga M, Sessions H, Morris T (2010) Phytoplankton production and physiological adaptation on the southeastern shelf of the Agulhas ecosystem. Continental Shelf Research 30:1472-1486

Banse K (1995) Zooplankton: Pivotal role in the control of ocean production. ICES Journal of Marine Science 52: 265-277

Behrenfeld MJ and Falkowski PG (1997) Photosynthetic rates derived from satellite-based chlorophyll concentration. Limnology and Oceanography 42(1): 1-20

Behrenfeld MJ (2010) Abandoning Sverdrup's critical depth hypothesis. Ecology 91: 977–989

Bengtsson L (2010) Climate change as a political problem – input to a hearing at the Swedish Parliament 24 of March 2010. By Prof. Lennart Bengtsson, Director Emeritus, Max-Planck Institute for Meteorology, Hamburg, e-mail lennart.bengtsson@zmaw.de

Blain S et al. (2007) Effect of natural iron fertilization on carbon sequestration in the Southern Ocean. *Nature* 446*:*1070–1074

Blain S, Treguer P, Belviso S, Bucciarelli E, Denis M, Desabre S, Fiala M, Martin-Jezequel V, Le Fevre J, Mayzaud P, Marty J-C, Razouls S (2001) A biogeochemical study of the island mass effect in the context of the iron hypothesis: Kerguelen Islands, Southern Ocean. Deep-Sea Research I 48: 163–187

Blain S, Queguiner B, Armand L, Belviso S, Bombled B, Bopp L, Bowie A, Brunet C, Brussaard C, Carlotti F, Christaki U, Corbiere A, Durand I, Ebersbach F, Fuda J-L, Garcia N, Gerringa L, Griffiths B, Guigue C, Guillerm C, Jacquet S, Jeandel C, Laan P, Lefevre D, Lomonaco C, Malits A, Mosseri J, Obernosterer I, Park Y-H, Picheral M, Pondaven P, Remeny T, Sandroni V, Sarthou G, Savoye N, Scouarnec L, Souhaut M, Thuiller D, Timmermans K, Trull T, Uitz J, van-Beek P, Veldhuis M, Vincent D, Viollier E, Vong, Wagener T (2007) Impacts of natural iron fertilization on the Southern Ocean. Nature 446: 1070–1074

Blain S, Sarthou G, Laan P (2008) Distribution of dissolved iron during the natural iron fertilization experiment KEOPS (Kerguelen Plateau, Southern Ocean). Deep-Sea Research II 55: 559–565

Booth BC (1987) Size classes and major taxonomic groups of phytoplankton at two locations in the subarctic Pacific Ocean in May and August, 1984. Mar. Biol. 97:275–286

Bopp L, Monfray P, Aumont O, Dufresne J-L, Le Treut H, Madec G, Terray L, Orr J C (2001) Potential impact of climate change on marine export production. Global Biogeochemical Cycles 15(1):81-99

Bopp L, Aumont O, Cadule P, Alvain S, and Gehlen M (2005) Response of diatoms distribution to global warming and potential implications: A global model study. Geophys. Res. Lett. 32:L19606

Bouman HA, Platt T, Sathyendranath S, Stuart V (2005) Dependence of light-saturated photosynthesis on temperature and community structure. Deep-Sea Res. I 52: 1284–1299

Boyd PW (2002) Review: Environmental factors controlling phytoplankton processes in the Southern Ocean. J. Phycol. 38: 844–861

Boyd PW, Watson AJ, Law CS, Abraham ER, Trull T, Murdoch R, Bakker DCE, Bowie AR, Buesseler KO, Chang H, Charette M, Croot P, Downing K, Frew R, Gall M, Hadfield M, Hall J, Harvey M, Jameson G, La Roche J, Liddicoat M, Ling R, Maldanado MT, Mckay RM, Nodder S, Pickmere S, Pridmore R, Rintoul S, Safi K, Sutton P, Strzepek R, Tanneberger K, Turner ST, Waite A, Zeldis J (2000) A mesoscale phytoplankton bloom in the polar Southern Ocean stimulated by iron fertilization. Nature 407:695-702

Boyd PW, Jickells T, Law CS, Blain S, Boyle EA, Buesseler KO, Coale KH, Cullen JJ, De Baar HJW, Follows M Harvey M, Lancelot C, Levasseur M, Owens NPJ, Pollard R, Rivkin RB, Sarmiento J, Schoemann V, Smetacek V, Takeda S, Tsuda A, Turner S, Watson AJ **(**2007) Mesoscale iron enrichment experiments 1993–2005, Synthesis and future directions. Science 315: 612–617

Boyd PW, Trull TW (2007) Understanding the export of biogenic particles in oceanic waters: Is there consensus? Progress in Oceanography 72:276–312

Boyd PW, Strzepek R, Fu F, Hutchins DA (2010) Environmental control of open-ocean phytoplankton groups: Now and in the future. Limnol. Oceanogr. 55(3):2010, 1353–1376 doi:10.4319/lo.2010.55.3.1353

Bracher A (1999) Photoacclimation of phytoplankton in different biogeochemical provinces of the Southern Ocean and its significance in estimating primary production. Ber. Polarforsch 341 ISSN0176 – 5027

Bidigare RR, Frank TJ, Zastrow C, Brooks JM (1986) The distribution of algal chlorophylls and their degradation products in the Southern Ocean. Deep-Sea Research 33: 923-937

Buma AGJ, Bano N, Veldhuis MJW, Kraay GW (1991) Comparison of the pigmentation of two strains of the prymnesiophyte Phaeocystis sp. Neth. J. Sea Res. 27:173–182 doi:10.1016/0077-7579(91)90010-X

Bury SJ, Owens NJP, Preston T (1995) C-13 and N-15 uptake by phytoplankton in the marginal ice-zone of the Bellingshausen Sea. Deep-Sea Research II 42:1225–1252

Busalacchi AJ (2004) The role of the Southern Ocean in global processes: An earth system science approach. Antarctic Science 26(4): 363-368

Brzezinski MA, Dickson ML, Nelson DM, and Sambrotto R (2003) Ratios of Si, C and N uptake by microplankton in the Southern Ocean. Deep-Sea Res. Pt. II 50: 619–633

Caldiera K, and Duffy P (2000) The role of the Southern Ocean in uptake and storage of anthropogenic carbon dioxide. Science 287: 620-622

Campbell NA, Reece JB (2002) Biology (6th Edition) Benjamin Cummings, San Francsico, CA ISBN 0-8053-6624-5

Cassar N, Bender ML, Barnett BA, Songmiao F, Moxim WJ, Levy II H, Tilbrook B (2007) The Southern Ocean biological response to Aeolian iron deposition. Science 317: 1067–1070

Cavalieri D, Thorsten M, Comiso J (2004) updated daily. *AMSR-E/Aqua Daily L3 25 km Brightness Temperature and Sea Ice Concentration Polar Grids V002*, 1 Nov 2008 to 15 Feb 2009. Boulder, Colorado USA: National Snow and Ice Data Center. Digital media.

Charlson RJ, Lovelock JE, Andreae MO, Warren SG (1987) Oceanic phytoplankton, atmospheric sulphur, cloud albedo and climate. Nature 326:655–61

Claustre H (1994) The trophic status of various oceanic provinces as revealed by phytoplankton pigment signatures. Limnol. Oceanogr. 39(5):1206–1210

Coale KH, Johnson KS, Chavez FP, Buesseler KO, Barber RT, Brzezinski MA, Cochlan WP, Millero FJ, Falkowski PG, Bauer JE, Wanninkhof RH, Kudela RM, Altabet MA, Hales BE, Takahashi T, Landry MR, Bidigare RR, Wang X, Chase Z, Strutton PG, Friederich GE, Gorbunov MY, Lance VP, Hilting AK, Hiscock MR, Demarest M, Hiscock WT, Sullivan KF, Tanner SJ, Gordon RM, Hunter CN, Elrod VA, Fitzwater SE, Jones JL, Tozzi S, Koblizek M, Roberts AE, Herndon J, et al. (2004) Southern ocean iron enrichment experiment: Carbon cycling in high- and low-Si waters. Science 304: 408-414

Cochlan WP, Price NM, Harrison PJ (1991) Effects of irradiance on nitrogen uptake by phytoplankton: Comparison of frontal and stratified communities. Mar. Ecol. Prog. Ser 69: 103–116

Cochlan WP (2008) Nitrogen in the marine environment: A review. In Capon et al. Chapter 12: Nitrogen Uptake in the Southern Ocean (2008) Elsevier Inc. doi: 10.1016/B978-0-12-372522-6.00012-8

Collos Y, Slawyk G (1986) 13C and 15N uptake by marine phytoplankton—IV. Uptake ratios and the contribution of nitrate to the productivity of Antarctic waters (Indian Ocean sector). Deep-Sea Research 33: 1039–1051

Comiso JC, McClain CR, Sullivan C W, Ryan JP, and Leonard CL (1993) Coastal Zone Color Scanner pigment concentrations in the Southern Ocean and relationships to geophysical surface features. J. Geophys. Res. 98: 2419–2451

Cullather RI, Bromwich DH, and Van Woert ML (1996) Interannual variations in Antarctic precipitation related to El Nino-Southern Oscillation. Journal of Geophysical Research 101, 19,109-19,118 (don't have)

Cullen JJ (1991) Hypotheses to explain high-nutrient conditions in the open sea. Limnol. Oceanogr. 36(8): 1578-1599

de Baar HJW, de Jong JTM, Bakker DCE, Loscher BM, Veth C, Bathmann U, Smetacek V (1995) Importance of iron for plankton blooms and carbon dioxide drawdown in the Southern Ocean. Nature 373: 412–415

de Baar HJW, Boyd PW, Coale KH, Landry MR, Tsuda A, Assmy P, Bakker DCE, Bozec Y, Barber RT, Brzezinski MA, Buesseler KO, Boye M, Croot PL, Gervais F, Gorbunov MY, Harrison PJ, Hiscock WT, Laan P, Lancelot C, Law CS, Levasseur M, Marchetti A, Millero FJ, Nishioka J, Nojiri Y, Van Oijen T, Riebesell U, Rijkenberg MJA, Saito H, Takeda S,

Timmermans K, Veldhuis MJW, Waite A, Wong C-S (2005) Synthesis of iron fertilization experiments, From the iron age in the age of enlightenment. Journal of Geophysical Research 110: 1-24

de Boyer CM, Madec G, Fischer AS, Lazar A and Ludicone D (2004) Mixed layer depth over the global ocean: An examination of profile data and a profile based climatology. JOURNAL OF GEOPHYSICAL RESEARCH 109: C12003 doi:10.1029/2004JC002378

de Mora S, Demers S, Vernet M (2000) The effects of UV radiation in the marine environment. Cambridge Univ. Press, Cambridge 324

del Campo J, Massana R (2011) Emerging diversity within chrysophytes, choanoflagellates and bicosoecids based on molecular surveys. Protist 162:435–448

Demidov AB, Vedernikov VI, Sheberstov SV (2007) Spatiotemporal Variability of Chlorophyll-a in the Atlantic and Indian Sectors of the Southern Ocean during February–April of 2000 according to satellite and expeditionary data. Oceanology 47(4): 507–518 ISSN 0001-4370

Denman KL, Brasseur G, Chidthaisong A, Ciais P, Cox PM, Dickinson RE, Hauglustaine D, Heinze C, Holland E, Jacob D, Lohmann U, Ramachandran S, da Silva Dias PL, Wofsy SC, Zhang X (2007) Couplings Between Changes in the Climate System and Biogeochemistry. In: Climate Change 2007: The Physical Science Basis. Contribution of Working Group I to the Fourth Assessment Report of the Intergovernmental Panel on Climate Change [Solomon S, Qin D, Manning M, Chen Z, Marquis M, Averyt KB, Tignor M and Miller HL (eds.)]. Cambridge University Press, Cambridge, United Kingdom and New York, NY, USA.

DiTullio GR, Geesey ME, Jones DR, Daly KL, Campbell L, Smith WO (2003) Phytoplankton assemblage structure and primary production along 170 W in the South Pacific Ocean. Marine Ecology Progress Series 255:55-80

Doney SC, Balch WM, Fabry VJ, and Feely RA (2009a) Ocean acidification: A critical emerging problem for the ocean sciences. Oceanography 22(4):16-25

Dower KM, Lucas MI (1993) Photosynthesis-irradiance relationships and production associated with a warm-core ring shed from the Agulhas Retroflection south of Africa. Marine Ecology Progress Series 95:141-154

Dower KM, Lucas MI, Phillips R, Dieckmann G, Robinson D H (1996) Phytoplankton biomass, P-I relationships and primary production in the Weddell Sea, Antarctica, during the austral autumn. Polar Biology 16:41-52

Dugdale RC, Goering JJ (1967) Uptake of new and regenerated forms of nitrogen in primary productivity. Limnol. Oceanogr. 12:196–206

Eppley RW (1972) Temperature and phytoplankton growth in the sea. Fisheries Bulletin 70: 1063-1085

Eppley RW, Peterson BJ (1979) Particulate organic matter flux and planktonic new production in the deep ocean. Nature 282:677–680

Eppley RW, Rogers JN, McCarthy JJ (1969) Half-saturation constants for uptake of nitrate and ammonium by marine phytoplankton. Limnology and Oceanography 14:912-920

Falkowski PG (1992) Molecular ecology of phytoplankton photosynthesis. *In* Falkowski PG, Woodhead AD [Eds] Primary productivity and biogeochemical cycles in the sea. Plenum Press, New York, 47-68

Falkowski PG and La Roche J (1991) Acclimation to spectral irradiance in algae. J. Phycol. 27:8-14

Falkowski PG, Barber RT, Smetacek V (1998) Review: Biogeochemical Controls and Feedbacks on Ocean Primary Production Science 281:200-206

Falkowski PG, et al. (2008) Biogeochemical cycles: The microbial engines that drive earth's biogeochemical cycles. Science 320:1034 doi: 10.1126/science.1153213

Falkowski PG, Raven JA (2007) Aquatic Photosynthesis (2nd edition). Princeton University Press Princeton, New Jersey, USA

Fasham MJR, Ducklow HW, McKelvie SM (1990) A nitrogen based model of plankton dynamics in the oceanic mixed layer. J. Mar. Res. 48:591-639

Feely RA, et al. (2004) Impact of anthropogenic CO2 on the CaCO3 system in the oceans. Science 305:362 doi: 10.1126/science.1097329

Fenton N, Priddle J, Teit P (1994) Regional variations in bio-optical properties of the surface waters in the Southern Ocean. Antarctic Science 6(4):443-448

Fielding S, Ward P, Pollard RT, Seeyave S, Read JF, Hughes JA, Smith T, Castellani C (2007) Community structure and grazing impact of mesozooplankton during late spring/early summer 2004/2005 in the vicinity of the Crozet Islands (Southern Ocean). Deep-Sea Research II 54: doi:10.1016/j.dsr2.2007.07.016

Figueroa FL (2002) Bio-optical characteristics of Gerlache and Bransfield Strait waters during an Antarctic summer cruise. Deep-Sea Research II 49: 675–691

Finkel ZV, Beardall J, Flynn KJ, Quigg A, Alwyn T, Rees V, Raven JA (2010) Phytoplankton in a changing world: cell size and elemental stoichiometry. Journal of Plankton Research 32:119-137

Fogg GE (1991) The phytoplanktonic ways of life. New Phytol. 118:191–232

Franck VM, Brzezinski MA, Coale KH, Nelson DM (2000) Iron and silicic acid concentrations regulate Si uptake north and south of the Polar Frontal Zone in the Pacific Sector of the Southern Ocean. Deep-Sea Res. II 47:3315–3338

Froneman PW, Perissinotto R (1996a) Microzooplankton grazing and protozooplankton community structure in the South Atlantic and in the Atlantic sector of the Southern Ocean. Deep-Sea Research I 43: 703-721

Froneman P, Perissinotto R (2008) Microzooplankton grazing in the Southern Ocean: Implications for the carbon cycle. Marine Ecology 17: 1-3: 99-115 (Published Online: 13 May 2008)

Froneman PW, Laubscher RK, McQuaid CD (2001) Size-fractionated primary production in the south Atlantic sectors of the Southern Ocean. Journal of Plankton Research 23: 611-622

Gao Y, Fan S, and Sarmiento J L (2003) Aeolian iron input to the ocean through precipitation scavenging: A modeling perspective and its implication for natural iron fertilization in the ocean. J. Geophys. Res. 108: 4221, doi:10.1029/2002JD002420

Garibotti IA, Vernet M, Ferrario ME (2005a) Annually recurrent phytoplanktonic assemblages during summer in the seasonal ice zone west of the Antarctic Peninsula (Southern Ocean). Deep-Sea Research I 52:1823–1841

Geider RJ, LaRoche J, Greene RM, Olaizola M (1993) Response of the photosynthetic apparatus of *Phaeodactylum tricornutum* (Baccilariophyceae) to nitrate, phosphate or iron starvation. Journal of Phycology 29:755–766

Gervais F, Riebesell U, Gorbunov MY (2002) Changes in primary productivity and chlorophyll *a* in response to iron fertilization in the Southern Polar Frontal Zone. Limnology and Oceanography 47:1324-1335

Gibbs RJ (1979) Chlorophyll b interference in the fluorometric determination of chlorophyll a and phaeo-pigments. Aust. J. Mar. Freshwater Res. 30:597–606

Gibb SW, Barlow RG, Cummings DG, Rees NW, Trees CC, Holligan P, Suggett D (2000) Surface phytoplankton pigment distributions in the Atlantic Ocean: an assessment of basin scale variability between 501N and 501S. Progress in Oceanography 45:339–368

Gieskes WWC, Kraay GW, Nontji A, Setiapermana D, Sutomo (1988) Monsoonal alternation of a mixed and a layered structure in the phytoplankton of the euphotic zone of the Banda Sea (Indonesia): A mathematical analysis of algal pigment fingerprints. Neth. J. Sea Res. 22(2):123–137

Gloor M, et al. (2003) A first estimate of present and preindustrial air-sea CO2 flux patterns based on ocean interior carbon measurements and models. Geophys. Res. Lett. 30(1):1010 doi:10.1029/2002GL015594

Goldman JC, Carpenter EJ (1974) A kinetic approach to the effect of temperature on algal growth. Limnology and Oceanography 19:756-766

Goldman JC (1977a) Biomass production in mass cultures of marine phytoplankton at varying temperatures. Journal of Experimental Biology and Ecology 27: 161-169

Goldman JC (1977b) Temperature effects on phytoplankton growth in continuous culture. Limnology and Oceanography 22:932-936

Grotti M, Francesco S, Carmela I, and Roberto F (2005) Trace metals distributions in coastal sea ice of Terra Nova Bay, Ross Sea, Antarctica, Antarct. Sci. 17: 290–300

Gurney KR, et al. (2002) Towards robust regional estimates of CO2 sources and sinks using atmospheric transport models. Nature 415(6872): 626–630

Harrison WG, Platt T (1986) Photosynthesis–irradiance relationships in polar and temperate phytoplankton populations. Polar Biol 5:153–164

Hart TJ (1934) On the phytoplankton of the Southwest Atlantic and the Bellingshausen Sea 1929–1931. Disc. Rep. 8:1–268

Hiscock MR, Marra J, Smith WO, Goericke R, Measures C, Vink V, Olson RJ, Sosik HM, Barber RT (2003) Primary productivity and its regulation in the Pacific Sector of the Southern Ocean. Deep-Sea Research II 50:533–558

Hiscock MR, Lance VP, Apprill AM, Bidigare RR, Johnson ZI, Mitchell BG, Smith Jr WO, and Barber RT (2007) Photosynthetic maximum quantum yield increases are an essential component of the Southern Ocean phytoplankton response to iron. PNAS 105:12 4775-4780

Hogg AM and Blundell JR (2006) Interdecadal variability of the Southern Ocean. J. Phys. Oceanogr. 36: 1626–1645

Holligan PM, Charalampopoulou A, Hutson R (2010) Seasonal distributions of the coccolithophore, *Emiliania huxleyi*, and of particulate inorganic carbon in surface waters of the Scotia Sea. Journal of Marine Systems 82:195–205

Hoppema M, Fahrbach E, Schröder M (1997) On the total carbon dioxide and oxygen signature of the Circumpolar Deep Water in the Weddell Gyre. Oceanologica Acta 20: 783–798

Hoffmann LJ, Peeken I, Lochte K, Assmy P, Veldhuis M (2006) Different reactions of Southern Ocean phytoplankton size classes to iron fertilization. Limnology and Oceanography 51:1217-1229

Honjo S, Manganini SJ, Kirshfield RA, Francois R (2008) Particulate organic carbon fluxes to the ocean interior and factors controlling the biological pump: A synthesis of global sediment trap programs since 1983. Progress in Oceanography 76: 217-285

Hutchins DA, Sedwick PN, DiTullio GR, Boyd PW, Queguiner B, Griffiths FB, Crossley C (2001) Control of phytoplankton growth by iron and silicic acid availability in the subantarctic Southern Ocean: experimental results from the SAZ project. J. Geophys. Res. C: Oceans 106: 31559–31572

Indermuhle A, Stocker TF, Joos F, Fischer H, Smith HJ, Wahlen M, et al. (1999). Holocene carbon-cycle dynamics based on CO2 trapped in ice at Taylor Dome, Antarctica. Nature 398(6723):121-126

IPCC (2007) 4th Assessment Report, Climate Change 2007: The Physical Science Basis. Contribution of Working Group I to the Fourth Assessment Report of the Intergovernmental Panel on Climate Change [Solomon S, D Qin, M Manning, Z Chen, M Marquis, KB Averyt, M Tignor and HL Miller (eds.)]. Cambridge University Press, Cambridge, United Kingdom and New York, NY, USA.

Irigoien X, Flynn KJ and Harris RP (2005) Phytoplankton blooms: a 'loophole' in microzooplankton grazing impact? Journal of Plankton Research 27 (4): 313–321

Ito T, Follows MJ (2003) Upper ocean control on the solubility pump of CO_2. Journal of Marine Research 61:465–489

Jeffrey SW, Vesk M (1997) Introduction to marine phytoplankton and their pigment signatures. In: Jeffrey SW, Mantoura RFC, Wright, SW (eds) Phytoplankton pigments in oceanography. UNESCO, Paris, p 37–84

Johnson K S, Chavez F P, and Friederich G E (1999) Continental shelf sediment as a primary source of iron for coastal phytoplankton. Nature 398: 697–700

Joint I, Groom SB (2000) Estimation of phytoplankton production from space: current status and future potential of satellite remote sensing. Journal of Experimental Marine Biology and Ecology 250:233–255

Joubert WR, Thomalla SJ, Waldron HN, Lucas MI (2011) Nitrogen uptake by phytoplankton in the Atlantic sector of the Southern Ocean during late austral summer. Biogeosciences Discussion 8:4917-4952

Kang S-H, Kang J-S, Lee S, Chung K H, Kim D, Park M G (2001) Antarctic phytoplankton assemblages in the marginal ice zone of the Northwestern Weddell Sea. Journal of Plankton Research 23(4):333-352 doi: 10.1093/plankt/23.4.333

Klein P, and G Lapeyre (2009) The oceanic vertical pump induced by mesoscale and submesoscale turbulence. Annu. Rev. Mar. Sci. 1:351–375 doi:10.1146/annurev.marine.010908.163704

Klunder MB, Laan P, Middag R, De Baar HJW, van Oiijen J (2011) Dissolved iron in the Southern Ocean (Atlantic sector). Deep-Sea Research II.

Knox GA (1994) Phytoplankton and primary production. In: studies in Polar Research; the biology of the Ocean. Cambridge University Press, London. Pp. 13-39

Kohfeld KE, Le Que´re´ C, Harrison SP, Anderson RF (2005) Role of marine biology in glacial-interglacial CO_2 cycles. Science 308:74– 78

Korb RE, Whitehouse M (2004) Contrasting primary production regimes around South Georgia, Southern Ocean: large blooms versus high nutrient, low chlorophyll waters. Deep-Sea Research II 51: 721-738

Korb RE, Whitehouse MJ, Thorpe SE, Gordon M (2005) Primary production across the Scotia Sea in relation to the physico-chemical environment. Journal of Marine Systems 57: 231-249

Kokkinakis S A, Wheeler P A (1987) Nitrogen uptake and phytoplankton growth in coastal upwelling regions. Limnol. Oceanogr. 32: 1112–1123

Krause GH (1994) Photoinhibition induced by low temperatures. Pp. 331-348 in NR Baker & JR Bowyer (eds.), Photoinhibition of photosynthesis: From molecular mechanisms to the field. Bios Scientific Publishers, Oxford

Krause GH, Virgo A, Winter K (1995) High susceptibility to photoinhibition of young leaves of tropical forest trees. Planta 197:583-591

Kreutz KJ, Mayewski PA, Meeker LD, Twickler MS, Whitlow SI, and Pittalwala II (1997) Bipolar changes in atmospheric circulation during the little ice age. Science 277:1294-1296

Kropuenske LR, Mills MM, van Dijken GL, Bailey S, Robinson DH, Welschmeyer NA, Arrigo KR (2009) Photophysiology in two major Southern Ocean phytoplankton taxa: photoprotection in *Phaeocystis antarctica* and *Fragilariopsis cylindrus*. Limnology and Oceanography 54:1176–96

Kudela RM, Cochlan WP (2000) Nitrogen and carbon uptake kinetics and the influence of irradiance for a red tide bloom off southern California. Aquatic Microb. Ecol. 21:31–47

Laing WA, Greer DH, Schnell T (1995) Photoinhibition of photosynthesis causes a reduction in vegetative growth rates of dwarf bean (Phaseolus vulgaris) plants. Austral. J. Pl. Physiol. 22:511-520

Lampitt RS (1985) Evidence for seasonal deposition of detritus to the deep-sea floor and its subsequent resuspension. Deep-Sea Res. 32:885–897

Lancelot C, Hannon E, Becquevort S, Veth C, De Baar HJW (2000) Modeling phyto-plankton blooms and carbon export production in the Southern Ocean: dominant controls by light and iron of the Atlantic sector in austral spring 1992. Deep-Sea Research I 47:1621–1662

Lannuzel D, Schoemann V, De Jong JTM, Chou L, Delille B, Becquevort S, Tison J-L (2008) Iron study during a time series in the western Weddell pack ice. Marine Chemistry 108: 85–95

Laubscher RK, Perisinotto R, and Mcquaid CD (1993) Phytoplankton production and biomass at frontal zones in the Atlantic sector of the Southern Ocean. Polar Biol. 13: 471–481

Le Quéré C, Rödenbeck C, Buitenhuis ET, Conway TJ, Langenfelds R, Gomez A, Labuschagne C, Ramonet M, Nakazawa T, Metzl N, Gillett N, Heimann M (2007) Saturation of the Southern ocean CO2 sink due to recent climate change. Science 316:1735–1738

Le Quére C, et al. (2009) "Global Carbon Project" Trends in the sources and sinks of carbon dioxide. Nature Geoscience 2:831-836 [www.globalcarbonproject.org, 26 September 2008]

Levitus S, Conkright ME, Reid JL, Najjar RG, Mantyla A (1993) Distribution of nitrate, phosphate and silicate in the world oceans. Progress in Oceanography 31:245–73

Lévy M, Klein P, and Treguier A-M (2001) Impact of sub-mesoscale physics on production and subduction of phytoplankton in an oligotrophic regime. J. Mar. Res. 59: 535–565 doi:10.1357/002224001762842181

Lévy M, Shankar D, André J-M, Shenoi S S C, Durand F, and de Boyer Montégut C (2007) Basin-wide seasonal evolution of the Indian Ocean's phytoplankton blooms. J. Geophys. Res. 112: C12014 doi:10.1029/2007JC004090

Lévy M, Klein P, and Jelloul M B (2009) New production stimulated by high-frequency winds in a turbulent mesoscale eddy field. Geophys. Res. Lett. 36: L16603 doi:10.1029/2009GL039490

Lévy M, Klein P, Tréguier A-M, Iovino D, Madec G, Masson S, and Takahashi K (2010) Modifications of gyre circulation by sub-mesoscale Physics. Ocean Modell. 34: 1–15 doi:10.1016/j.ocemod.2010.04.001

Lizotte, MP (2001) The contributions of sea ice algae to Antarctic marine primary production. Amer. Zool. 41:57–73

Long SP, Humphries S, Falkowski PG (1994) Photoinhibition of photosynthesis in nature. Annual Rev. Pl. Physiol. Pl. Molec. Biol. 45:633-662

Lovenduski NS, Gruber N, Doney SC, Lima ID (2007) Enhanced CO_2 outgassing in the Southern Ocean from a positive phase of the Southern Annular Mode. Global Biogeochemical Cycles 21: GB2026

Lucas M, Seeyave S, Sanders R, Moore CM, Williamson R, Stinchcombe M (2007) Nitrogen uptake responses to a naturally Fe-fertilised phytoplankton bloom during the 2004/2005 CROZEX study. Deep Sea Research II 54:2138-2173

Lutjeharms JRE (1985) Location of frontal systems between Africa and Antarctica; some preliminary results. Deep-Sea Research 32: 1499-1509

Lutjeharms JRE (2006) The Agulhas Current. Springer-Verlag, Heidelberg 329 pp.

Macedo MF, Duarte P, Mendes P and Ferreira G (2001) Annual variation of environmental variables, phytoplankton species composition and photosynthetic parameters in a coastal lagoon. Journal of Plankton Research 23:719-732

Machua E, Biastochb A, Oschliesb A, Kawamiyab M, Lutjeharms JRE, Garc-ona V (2005) Phytoplankton distribution in the Agulhas system from a coupled physical–biological model. Deep-Sea Research I 52: 1300–1318

Mac Intyre HL, Kana TM (2002) Photoacclimation of photosynthesis irradiance response curves and photosynthetic pigments in microalgae and cyanobacteria. J. Phycol. 38:17-38

MacIsaac JJ, Dugdale RC (1972) Interactions of light and inorganic nitrogen in controlling nitrogen uptake in the sea. Deep-Sea Res. 19:209–232

Mantoura RFC, Barlow RG, Head EJH (1997) Simple isocratic HPLC methods for chlorophylls and their degradation products, in Phytoplankton Pigment in Oceanography: Guidelines to Modern Methods, edited by SW Jeffrey, RFC Mantoura, SW Wright pp. 383– 428 UNESCO, Paris

Marinov I, Gnanadesikan A, Toggweiler JR, Sarmiento JL (2006) The Southern Ocean biogeochemical divide. 441 doi:10.1038/nature04883

Matthews AJ, Meredith MP (2004) Variability of Antarctic circumpolar transport and the Sothern Annular Mode associated with the Madden-Julian Oscillation. Geophysical Research Letters 31: L23412

McIntyre A, Bé AWH (1967) Modern coccolithophoridae of the Atlantic Ocean- I. Placoliths and cyrtoliths. Deep-Sea Res. 14: 561–597

Mills MM*,* Kropuenske LR*,* Van Dijken GL*,* Alderkamp A-C*,* Berg GM*,* Robinson DH*,* Welschmeyer NA, Arrigo KR *(*2010*)* Photophysiology in two major Southern Ocean phytoplankton taxa: photosynthesis and growth of *Phaeocystis antarctica (Prymnesiophyceae)* and *Fragilariopsis cylindrus (Bacillariophyceae)* under simulated mixed layer irradiance*.* J. Phycol. 46*:*1114–27

Mikaloff Fletcher SE, et al. (2006) Inverse estimates of anthropogenic CO2 uptake, transport, and storage by the ocean. Global Biogeochem. Cycles 18: doi:10.1029/2005GB002530

Minas HJ, Minas M, Packard TT (1986) Productivity in upwelling areas deduced from hydrographic and chemical fields. Limnol. Oceanogr. 31:1182–1206

Mitchell BG, Holm-Hansen 0 (1991) Observations and modeling of the Antarctic phytoplankton crop in relation to mixing depth. Deep Sea Res. 38:981-1007

Moore J K, Abbott M, Richman J (1999) Location and dynamics of the Antarctic Polar Front from satellite sea surface temperature data. Journal of Geophysical Research 104: 3059–3073

Moore JK and Abbott MR (2000) Phytoplankton chlorophyll distributions and primary production in the Southern Ocean. Journal of Geophysical Research 105(C12): 28: 709 –28, 722

Moore JK, Abbott MR (2002) Surface chlorophyll concentrations in relation to the Antarctic Polar Front: seasonal and spatial patterns from satellite observations. Journal of Marine Systems 37:69–86

Moore CM, Hickman AE, Poulton AJ, Seeyave S, Lucas MI (2007a) Iron-light interactions during the CROZet natural iron bloom and EXport experiment (CROZEX) II: taxonomic responses and elemental stoichiometry. Deep-Sea Research II, this issue doi:10.1016/j.dsr2.2007.06.015

Moore CM, Seeyave S, Hickman AE, Allen JT, Lucas MI, Planquette HF, Pollard RT, Poulton A J (2007b) Iron-light interactions during the CROZet natural iron bloom and Export experiment (CROZEX) I: phytoplankton growth and photophysiology. Deep-Sea Research II, this issue doi:10.1016/j.dsr2.2007.06.011

Moore J K, Abbott MR, and Richman JG (1999) Location and dynamics of the Antarctic Polar Front from satellite sea surface temperature data. J. Geophys. Res. 104: 3059–3073

Moore K and Doney SC (2006) Remote sensing observations of ocean physical and biological properties in the region of the Southern Ocean Iron Experiment (SOFeX). Journal of Geophysical Research 111: XXXXXX doi:10.1029/2005JC003289

Nelson DM, Smith WO (1991) Sverdrup re-visited: critical depths, maximum chlorophyll levels, and the control of Southern Ocean productivity by the irradiance-mixing regime. Limnology and Oceanography 36: 1650-1661

Nelson DM, Brzezinski MA, Sigmon DE, Franck VM (2001) A seasonal progression of Si limitation in the Pacific sector of the Southern Ocean. Deep- Sea Research II 48: 3973-3995

Nydahl F (1976) On the optimum conditions for the reduction of nitrate to nitrite by cadmium: Talanta 23: 349-357

Olbers D, Borowski D, Volker C and Wolff J-O (2004) The dynamical balance, transport and circulation of the Antarctic Circumpolar Current. Antarctic Science 16 (4): 439–470 DOI: 10.1017/S0954102004002251439

Osmond CB (1994) What is photoinhibition? Some insights from comparisons of shade and sun plants. pp. 1-24 in Baker NR & Bowyer JR (eds.), Photoinhibition of photosynthesis: From molecular mechanisms to the field. Bios Scientific Publishers, Oxford

Orr JC, Fabry VJ, Aumont O, Bopp L, Doney SC, Feely RA, Gnanadesikan A, Gruber N, Ishida A, Joos F, Key RM, Lindsay K, Maier-Reimer E, Matear R, Monfray P, Mouchet A, Najjar RG, Plattner G-K, Rodgers KB, Sabine CL, Sarmiento JL, Schlitzer R, Slater RD, Totterdell IJ, Weirig M-F, Yamanaka Y, Yool A (2005) Anthropogenic ocean acidification over the twenty-first century and its impact on calcifying organisms 18:437 doi:10.1038/nature04095

Orsi A H, Whitworth III T W, Nowlin Jr. WD (1995) On the meridional extent and fronts of the Antarctic Circumpolar Current. Deep Sea Research Part I 42: 641– 673

Park J, Oh I, Kim H, and Yoo S (2010) Variability of SeaWiFs chlorophyll-a in the southwest Atlantic sector of the Southern Ocean: Strong topographic effects and weak seasonality. Deep-Sea Res. Pt. I 57: 604–620

Pendall E, Markgraf V, White JWC, and Dreier M (2001) Multiproxy record of Late Pleistocene-Holocene climate and vegetation changes from a peat bog in Patagonia. Quaternary Research 55:168-178

Planquette, HF, Statham P, Fones GR, Charette MA, Moore CM, Salter I, Nédélec FH, Taylor SL, French M, Baker AR, Mahowald N, Jickells TD (2007) Dissolved iron in the vicinity of the Crozet Islands, Southern Ocean. Deep-Sea Research II 57: 1999-2019

Platt T, Sathyendranath S, Caverhill CM, Lewis MR (1988) Ocean primary production and available light: further algonthms for remote sensing. Deep Sea Res. 35(6):855-879

Platt T, Sathyendranath S (1988) Oceanic primary production: Estimation by remote sensing at local and regional scales. Science 241:1613−1620

Platt T, Sathyendranath S, Forget M-H, White III GN, Caverhill C, Bouman H, Devred E, Son S-H (2008) Operational estimation of primary production at large geographical scales. Remote Sensing of Environment 112:3437–3448

Pollard R T, Lucas MI, Read JF (2002) Physical controls on biogeochemical zonation in the Southern Ocean. Deep Sea Research Part II 49: 3289– 3305

Pollard RT, Venables HJ, Read JF, Allen JT (2007) Large-scale circulation around the Crozet Plateau controls an annual phytoplankton bloom in the Crozet Basin. Deep Sea Research Part II 54: 1915 – 1929

Pollard R, Sanders R, Lucas M, Statham P (2007) The Crozet natural iron bloom and export experiment (CROZEX). *Deep Sea Res. II* 54:1905–1914 doi:10.1016/j.dsr2.2007.07.023

Pollard RT, Salter I, Sanders R J, Lucas MI, Moore CM, Mills RA, Statham PJ, Allen JT, Baker A R, Bakker DCE, Charette MA, Fielding S, Fones GR, French M, Hickman AE, Holland RJ, Hughes JA, Jickells TD, Lampitt RS, Morris PJ, Nedelec FH, Nielsdottir M, Planquette H, Popova EE, Poulton AJ, Read JF, Seeyave S, Smith T, Stinchcombe M, Taylor S, Thomalla S, Venables HJ, Williamson R, Zubkov MV (2009) Southern Ocean deep-water carbon export enhanced by natural iron fertilization. Nature 457: 577–580

Porra RJ, Pfündel EE, Engel N (1997) Metabolism and function of photosynthetic pigments. In: Jeffrey SW, Mantoura RFC, Wright, SW (eds) Phytoplankton pigments in oceanography. UNESCO, Paris, p 85–126

Poulton AJ, Sanders R, Holligan PM, Sinchcombe MC, Adey TR, Brown L, Chamberlain K (2006) Phytoplankton mineralisation in the tropical and subtropical Atlantic Ocean. Global Biogeochemical Cycles 20: GB4002

Poulton AJ, Moore CM, Seeyave S, Lucas MI, Fielding S, Ward P (2007) Phytoplankton community composition around the Crozet Plateau, with emphasis on diatoms and *Phaeocystis*. Deep-Sea Research II 2085-2105

Prentice C, et al. in Climate Change (2001) The Scientific Basis, Contribution of Working Group I to the Third Assessment Report of the Intergovernmental Panel on Climate Change, Houghton J, et al. Eds. Cambridge Univ. Press, New York (2001) pp. 183–238

Preston T, Owens NJP (1983) Interfacing an automatic elemental analyser with an isotope ratio mass spectrometer: the potential for fully automated total nitrogen and ^{15}N analysis. Analyst 108:971-977

Priddle J, Smetacek V, Bathman U (1992) Antarctic marine primary production, biogeochemical carbon cycles and climatic change. Biological Sciences, Antarctica and Environmental Change 338 (1285): 289-297

Prince SD and Goward SN (1995) Global Primary Production: A Remote Sensing Approach. Journal of Biogeography 22(4/5) in Terrestrial Ecosystem Interactions with Global Change, 2: 815-835 (Jul. - Sep., 1995)

Priscu JC (1989) Photon dependence of inorganic nitrogen transport by phytoplankton in perennialy ice-covered Antarctic lakes. In High Latitude Limnology Vincent WF and Ellis-Evans JC, eds. Hydrobiologia 172:173–182

Probyn T A, Lucas M I (1987) Ammonium and phosphorus flux through the microplankton community in Agulhas Bank waters. In: Payne A I L, Gulland J A, Brink K H (eds.) The Benguela and comparable ecosystems. S. Afr. J. Mar. Sci. 5: 209-221

Raven JA (1988) The iron and molybdenum use efficiencies of plant growth with different energy, carbon and nitrogen sources. New Phytologist. 109:279–288

Raven JA (1990) Predictions of Mn and Fe use efficiencies of phototrophic growth as a function of light availability for growth and of C assimilation pathway. New Phytologist 116: 1–18

Raven JA and Falkowski PG (1999) Ocean sinks for atmospheric CO2. Plant, Cell and Environment 22: 741-756

Read JF, Lucas MI, Holley SE, Pollard RT (2000) Phytoplankton, nutrients and hydrography in the frontal zone between the Southwest Indian Subtropical gyre and the Southern Ocean Deep-Sea Research I 47: 2341-2368

Roy T, Rayner P, Matear R and Francey R (2003) Southern hemisphere ocean CO2 uptake: reconciling atmospheric and oceanic estimates. Tellus 55B(2): 701–710

Sabine CL, et al. (2004) in The Global Carbon Cycle: Integrating Humans, Climate, And The Natural World. SCOPE 62, Field CB, Raupach MR Eds. Island Press, Washington, DC pp 17–46

Sabine CL, Feely RA, Gruber N, Key RM, Lee K, Bullister J L, Wanninkhof R, Wong C S, Wallace DWR, Tilbrook B, Millero FJ, Peng T-H, Kozyr A, Ono T, Rios AF (2004) The Oceanic Sink for Anthropogenic CO_2. Science 305: 16 July

Saggiomo V, Catalano G, Mangoni O, Budillon G Carrada GC (2002) Primary production processes in ice-free waters of the Ross Sea (Antarctica) during the austral summer 1996. Deep-Sea Research II 49:1787–801

Sakshaug E, Bricaud A, Dandonneau Y, Falkowski PG, Kiefer DA, Legendre L, Morel A, Parslow J, Takahashi M (1997) Parameters of photosynthesis: definitions, theory and interpretation of results. Journal of Plankton Research 19: 1637–1670

Sarmiento JL and Bender M (1994) Carbon biogeochemistry and climate change. Photosynthesis Research 39:209-234

Sarmiento JL, Hughes TMC, Stouffer RJ, Manabe S (1998) Simulated response of the ocean carbon cycle to anthropogenic climate warming. Nature 393: 245-249

Sarmiento J L, Gruber N, Brzezinski M A, and Dunne J P (2004) High-latitude controls of thermocline nutrients and low latitude biological productivity. Nature 427: 56–60 doi:10.1038/nature02127

Savidge G, Gilpin L (1999) Seasonal influences on size-fractionated chlorophyll a concentrations and primary production in the north-west Indian Ocean. Deep-Sea Research II 46:701–723

Savidge G, Priddle J, Gilpin LC, Bathmann U, Murphy EJ, Owens NJP, Pollard RT, Turner DR, Veth C, Boyd P (1996) An assessment of the role of the marginal ice zone in the carbon cycle of the Southern Ocean. Antarctic Science 8(4): 349-358

Sathyendranath S, Stuart V, Irwin BD, Maass H, Savidge G, Gilpin L, Platt T (1999) Seasonal variations in bio-optical properties of phytoplankton in the Arabian Sea. Deep-Sea Res Part II 46:633–653

Schlitzer R (2002) Carbon export fluxes in the Southern Ocean: results from inverse modelling and comparison with satellite-based estimates. Deep-Sea Research II 49: 1623–1644

Schoemann V, De Baar HJW, De Jong JTM, and Lancelot C (1998) Effects of phytoplankton blooms on the cycling of manganese and iron in coastal waters. Limnol. Oceanogr. 43: 1427–1441

Schoemann V, Becquevort S, Stefels J, Rousseau V, Lancelot C (2005) *Phaeocystis* blooms in the global ocean and their controlling mechanisms: a review. Journal of Sea Research **53:**43–66

Sedwick P N and DiTullio GR (1997) Regulation of algal blooms in Antarctic shelfwater by the release of iron from melting sea ice. Geophys. Res. Lett. 24: 2515–2518

Seeyave S, Lucas M, Moore CM, and Poulton AJ (2007) Phytoplankton productivity and community structure in the vicinity of Crozet Plateau during austral summer 2004/2005. Deep-Sea Res. Pt. II 54: 2020–2044

Sieburth JM (1979) Sea Microbes. Oxford University Press,New York 491pp.

Sigman DM and Boyle E A (2000) Glacial/interglacial variations in atmospheric carbon dioxide. Nature 407: 859-869

Slawyk G (1979) 13C and 15Nuptake by phytoplankton in the Antarctic upwelling area: Results from Antiprod I cruise in the Indian Ocean sector. Aust. J. Mar. Freshwater Res. 30: 431–448

Slawyk G, L'Helgijen S, Collosa Y, Frewe H (1988) Quantitative determination of particulate organic N and C in marine-phytoplankton samples using mass-spectrometer signals from isotope-ratio analysis in 15N and llC-tracer studies. J. Exp. Mar. Biol. Ecol. 115:187-195

Smith Jr WO, Dinniman MS, Tozzi S, DiTullio GR, Mangoni O, Modigh M, Saggiomo V (2010) Phytoplankton photosynthetic pigments in the Ross Sea: Patterns and relationships among functional groups. Journal of Marine Systems 82:177-185

Smetacek V, Scharek R, Nöthig E-M (1990) Seasonal and regional variation in the pelagial and its relationship to the life history cycle of krill. *In* KERRY, K.R. & HEMPEL, G., *eds*. *Antarctic ecosystems: ecological change and conservation*. Berlin: Springer 103–114

Smetacek V, Assmy P, Henjes J (2004) The role of grazing in structuring Southern Ocean pelagic ecosystems and biogeochemical cycles. Antarctic Science 16: 541–558

Smith Jr WO and Lancelot C (2004) Bottom-up versus top-down control in phytoplankton of the Southern Ocean. Antarctic Science 16(4):531–539 DOI:10.1017/S0954102004002305531

Smith Jr W O and Nelson D M (1986) Importance of ice edge phytoplankton production in the Southern Ocean. BioScience 36:251–257

Smith Jr WO and Sakshaug E (1990) Polar phytoplankton. In Polar Oceanography, Part B: Chemistry, Biology, and Geology, Academic Press, New York. pp 477–525

Sokolov S, Rintoul SR (2002) Structure of Southern Ocean fronts at 140°E. Journal of Marine Systems 37: 151–184

Sokolov S, Rintoul SR (2007) On the relationship between fronts of the Antarctic Circumpolar Current and surface chlorophyll concentrations in the Southern Ocean. Journal of Geophysical Research 112: C07030

Sokolov S and Rintoul S R (2007a) Multiple Jets of the Antarctic Circumpolar Current South of Australia. J. Phys. Oceanogr. 37:1394–1412

Sokolov S, Rintoul SR (2009) Circumpolar structure and distribution of the Antarctic Circumpolar Current fronts: Mean circumpolar paths. Journal of Geophysical Research 114: C11018

Strass VH, Garabato ACN, Bracher AU, Pollard RT, Lucas MI (2002) A 3-D mesoscale map of primary production at the Antarctic Polar Front: Results of a diagnostic model. Deep-Sea Research II 49 (18): 3813-3834

Strass VH, Garabato ACN, Pollard RT, Fischer HI, Hense I, Allen JT, Read JF, Leach H, Smetacek V (2002) Mesoscale frontal dynamics: shaping the environment of primary production in the Antarctic Circumpolar Current. Deep-Sea Res. Pt. II 49: 3735–3769

Stuart V, Sathyendranath S, Platt T, Maass H, Irwin BD (1998) Pigments and species composition of natural phytoplankton populations: effect on the absorption spectra. J Plankton Res 20:187–217

Sunda WG, Huntsman SA (1997) Interrelated influence of iron, light and cell size on marine phytoplankton growth. Nature 390:389-392

Sverdrup HU (1953) On conditions for the vernal blooming of phytoplankton. Journal du Conseil International pour l'Exploration de la Mer 18:287–295

Swart S, Speich S, Ansorge IJ, Goni GJ, Gladyshev S, Lutjeharms JRE (2008) Transport and variability of the Antarctic Circumpolar Current south of Africa. Journal of Geophysical Research 113: C09014

Swart S, Speich S, Ansorge IJ, and Lutjeharms JRE (2010) An altimetry-based gravest empirical mode south of Africa: Development and validation. Journal of Geophysical 115: C03002 doi:10.1029/2009JC005299

Swart S, Thomalla SJ, Monteiro PMS, Ansorge IJ (2011) Oceanography and primary production in the south-east Atlantic Ocean during the 2010-2011 South African National Antarctic Expedition: Continuing results from the GoodHope program eight years on. AJMS *in press*

Tagliabue A, Mtshali T, Bowie AR, Swart S (2011) A global compilation of over 13,000 dissolved iron measurements: focus on distributions and processes in the Southern Ocean. Biogeosciences Discuss. 8:11489–11527

Takahashi K, Okada H (2000) Environmental control on the biogeography of modern coccolithophores in the southeastern Indian Ocean offshore of Western Australia. Marine Micropaleontology 39 (1–4):73–86

Takahashi T, et al. (2002) Global sea-air CO2 flux based on climatological surface ocean pCO2, and seasonal biological and temperature effects. Deep-Sea Res. II 49(9–10): 1601–1622

Taucher J and Oschlies A (2011) Can we predict the direction of marine primary production change under global warming? Geophysical Research Letters 38: L02603 doi:10.1029/2010GL045934

Talley L, Chereskin T, Dickson A, Fine R, Farias L, Ulloa O, Sloyan B (2008) AIW formation in the southeast Pacific http://www-pord.ucsd.edu/~ltalley/aaiw/ Updated October 23 2008

Thomalla S (1999) Phytoplankton Distribution and Nitrogen Dynamics in the Southwest Indian Subtropical gyre and Southern Ocean Waters MSc. Thesis under the supervision of M I Lucas, Department of Zoology, University of Cape Town, RSA

Thomalla SJ, Fauchereau N, Swart S, and Monteiro PMS (2011) Regional scale characteristics of the seasonal cycle of chlorophyll in the Southern Ocean. Biogeosciences 8: 2849–2866 doi:10.5194/bg-8-2849

Tilzer M M, Elbrachter M, Gieskes WW, Besse B (1986) Light–temperature interactions in the control of photosynthesis in Antarctic phytoplankton. Polar Biol. 5:105–111

Toggweiler JR, Murnane R, Carson S, Gnanadesikan A, Sarmiento JL (2003) Representation of the carbon cycle in box models and GCMs: 2. Organic pump, Global Biogeo chem. Cycles 17(1):1027 doi:10.1029/2001GB001841

Treguer P, Jacques G (1992) Dynamics of nutrients and phytoplankton, and fluxes of carbon, nitrogen and silicon in the Antarctic Ocean. PolarBiology 12:149-162

Treguer P, Nelson DM, Van Bennekom AJ, Demaster DJ, Leynart A, Queguiner B (1995) The silica balance in the world ocean: A re-estimate. Science 268:375–379

Tremblay JE, Lucas MI, Kattner G, Pollard R, Strass VH, Bathman U, Bracher A (2002) Significance of the Polar Frontal Zone for large-sized diatoms and new production during summer in the Atlantic sector of the Southern Ocean. Deep-Sea Research II 49: 3793-3811

Trull TW, Bray SG, Manganini SJ, Honjo S, and Francois R (2001)
Moored sediment trap measurements of carbon export in the subantarctic and polar frontal zones of the southern ocean, south of Australia. J. Geophys. Res. 106(C12): 31,489

Uitz J, Claustre H, Morel A, Hooker SB (2006) Vertical distribution of phytoplankton communities in open ocean: An assessment based on surface chlorophyll. Journal of Geophysical Research 111:C08005

Uitz J, Huot Y, Bruyant F, Babin M, Claustre H (2008) Relating phytoplankton photophysiological properties to community structure on large scales. Limnol. Oceanogr. 53(2):614–630

Vaillancourt RD, Sambrotto RN, Green S, Matsuda A (2003) Phytoplankton biomass and photosynthetic competency in the summertime Mertz Glacier region of east Antarctica. Deep-Sea Research 50:1415-1440

Van Hilst CM, Smith WO (2002) Photosynthesis / irradiance relationships in the Ross Sea, Antarctica, and their control by phytoplankton assemblage composition and environmental factors. Marine Ecology Progress Series 226:1–12

Van Oijen T, Van Leeuwe MA, Granum E, Weissing FJ, Bellerby RGJ, Gieskes WWC,
and De Baar HJW (2004) Light rather than iron controls photosynthate production and allocation in Southern Ocean phytoplankton populations during austral autumn. Journal of Plankton Research 26:8:885-900

Venables H and Moore CM (2010) Phytoplankton and light limitation in the Southern Ocean: Learning from highnutrient, high-chlorophyll areas. J. Geophys. Res. 115: C02015
doi:10.1029/2009JC005361

Venables HJ, Pollard RT, Popova EE (2007) Physical conditions controlling the development of a regular phytoplankton bloom north of the Crozet Plateau, Southern Ocean. Deep-Sea Research II 54:1949-1965

Vernet M, Martinson D, Iannuzzi R, Stammerjohn S, Kozlowski W, Sines K, Smith R, Garibotti I (2008) Primary production within the sea-ice zone west of the Antarctic Peninsula: I—Sea ice, summer mixed layer, and irradiance. Deep-Sea Research II 55: 2068-2085

Vidussi F, Claustre H, Manca BB, Luchetta A, Marty JC (2001) Phytoplankton pigment distribution in relation to upper thermocline circulation in the eastern Mediterranean
Sea during winter. J Geophys Res 106:19939–19956

Villafañe VE, Sundbäck K, Figueroa FL, Helbling EW (2003) Photosynthesis in the aquatic environment as affected by UVR. In: Helbling EW, Zagarese HE (eds) UV effects in
aquatic organisms and ecosystems. The Royal Society of Chemistry, Cambridge p 357–397

Villafañe VE, Marcoval MA, Helbling EW (2004) Photosynthesis versus irradiance characteristics in phytoplankton assemblages off Patagonia (Argentina): temporal variability and solar UVR effects. Marine Ecology Progress Series 284:23–34

Volk T and MI Hoffert (1985) Ocean Carbon Pumps: Analysis of relative strengths and efficiencies in ocean-driven atmospheric CO2 changes, from The Carbon Cycle and Atmospheric CO2: Natural Variations Archean to Present, Geophysical Monograph 32, American Geophysical Union.

Wagener T, Guieu C, Losno R, Bonnet S, and Mahowald N (2008) Revisiting atmospheric dust export to the Southern Hemisphere ocean: Biogeochemical implications. Global Biogeochem. Cycles 22: GB2006
doi:10.1029/2007GB002984

Ward P, Shreeve R, Whitehouse M, Korb B, Atkinson A, Meredith M, Pond D, Watkins J, Goss C, Cunningham N (2005) Phyto- and zooplankton community structure and production around South Georgia (Southern Ocean) during Summer 2001/02. Deep-Sea Research I 52: 421–441

Ward P, Meredith MP, Whitehouse MJ, Rothery P (2008) The summertime plankton community at South Georgia (Southern Ocean): Comparing the historical (1926/1927) and modern (post 1995) records Progress in Oceanography 78: 241–256

Waters R, Van Den Enden R, Marchant H (2000) Summer microbial ecology off East Antarctica (80–150 degrees E): protistan community structure and bacterial abundance. Deep-Sea Research II 47:2401–2435

Welschmeyer NA (1994) Fluorometric analysis of chlorophyll a in the presence of chlorophyll b and phaeopigments. Limnology and Oceanography 39(8): 1985-1992

Wheeler PA, Kokkinakis SA (1990) Ammonium recycling limits nitrate use in the oceanic subarctic Pacific. Limnol. Oceanogr. 35: 1267–1278

Whitehouse MJ, Korb RE, Atkinson A, Thorpe SE, Gordon M (2008) Formation, transport and decay of an intense phytoplankton bloom within the High-Nutrient Low- Chlorophyll belt of the Southern Ocean. Journal of Marine Systems 70: 150-167

Whitworth T III (1980) Zonation and geostrophic flow of the Antarctic Circumpolar Current at Drake Passage. Deep-Sea Research 21:497-507

Williams CA, Hanan NP, Neff JC, Scholes RJ, Berry JA, Denning AS and Baker DF (2007) Review: Africa and the global carbon cycle. Carbon Balance and Management 2(3): 1-13 doi:10.1186/1750-0680-2-3

Watson AJ and Orr JC (2003) Carbon dioxide fluxes in the global ocean. Ocean Biogeochemistry Unpublished Manuscript 1-45

Wright SW, Van Den Enden RL, Pearce I, Davidson AT, Scott FJ, Westwood KJ (2010) Phytoplankton community structure and stocks in the Southern Ocean (30–80°E) determined by CHEMTAX analysis of HPLC pigment signatures. Deep-Sea Research II 57:849-862

Yoder JA, Bishop SS (1985) Effects of mixing-induced irradiance fluctuations on photosynthesis of natural assemblages of coastal phytoplankton. Mar Biol 90:87–93

Yool A, Martin AP, Fernández C, Clark DR (2007) The significance of nitrification for oceanic new production. Nature 447:999-1002 doi:10.1038/nature05885